The impact of climate change effects on the planform of a headland-bay beach on the southern coast of South Africa

by
Pierre-Malan Hugo

Thesis presented in fulfilment of the requirements for the degree of Master of Science in the Faculty of Engineering at Stellenbosch University

Supervisor: Mr. Geoff Toms

March 2013

Declaration

By submitting this thesis electronically, I declare that the entirety of the work contained therein is my own, original work, that I am the sole author thereof (save to the extent explicitly otherwise stated), that reproduction and publication thereof by Stellenbosch University will not infringe any third party rights and that I have not previously in its entirety or in part submitted it for obtaining any qualification.

8 February 2013

Abstract

The various consequences of climate change pose a significant threat to developments near the coast. These threats include saltwater intrusion, coastal erosion and flooding. In the coastal context, the climate change effect often raising the most concern is that of sea-level rise. Much work has therefore been done on the linear setback caused by a rise in sea-level. In order to get the full picture of possible changes caused by sea-level rise, the secondary effects of a rising sea-level also need to be considered. Sea-level rise could cause changes to the nearshore wave climate and could have impacts such as coastal erosion and changes to the coastline shape. The primary objective of this study was therefore to investigate the effects of sea-level rise on the nearshore wave climate and, consequently, the coastline stability.

Other consequences of climate change considered in this study include increasing average wave heights and a rotation of offshore wave directions. The many headland-bay beaches on the South African coastline are generally in a state of dynamic equilibrium and find their planforms based on the local wave climate. Changes to the wave climate may therefore disrupt the equilibrium shapes of these bays. This study was therefore also aimed at investigating the effects of the changes to the wave climate on the stability of headland-bay beaches.

The three consequences of climate change expected to affect the nearshore wave climate were identified as (1) sea-level rise; (2) an increased wave height; and (3) changing offshore wave angles. Although changes to storm frequency and intensity are also possible, the impacts of these changes were not studied.

In order to assess the impacts of the three considered changes on a typical headland-bay beach, two numerical models were set up for Mossel Bay – a headland-bay beach on the southern coast of South Africa. The modelling approach included a wave transformation model to calculate nearshore wave climates from offshore data and a coastline model to assess the stability of the bay under the changed nearshore wave climates.

The model results indicated that the rising sea-level alone would cause changes in the nearshore wave direction. These changes were shown to alter the longshore sediment transport regime such that rotations are expected in the south-western corner and eastern end of Mossel Bay. These rotations do not include the cross-shore effects of inundation and erosion, as suggested by models such as the Bruun Model.

The results for an increased offshore wave height were inconclusive. The southerly rotation in offshore wave angles was shown to affect the nearshore wave angles. These changes affected the

longshore transport regime such that the outward sediment transports were reduced. A minor accretion resulted in the centre of the bay for a 1° southerly rotation in offshore wave angles. For a 2° rotation, the extent of accretion increased and shifted towards the eastern end of the bay, primarily due to the dominance of south-westerly waves in the local wave climate.

A valuable observation was made regarding the current stability of Mossel Bay. Inter-tidal reefs are present along three sections of the bay. These reefs protect the coastline such that the current bay shape contains sharp bends between the reefs. Under a rising sea-level, however, the effect of the reefs will become less pronounced. If a water level should be reached where these reefs become less significant, the planform of the bay is expected to smooth out through a significant redistribution of sediment. This smoothing effect was shown to cause erosion of the coastline in the order of 80m near the town of Klein Brak River.

Opsomming

Die verskeie gevolge van klimaatsverandering bied ‘n merkwaardige bedreiging vir ontwikkelings naby die kus. Hierdie bedreigings sluit die versouting van varswaterbronne, kuserosie en oorstromings in. Vir kusgebiede is seevlakstyging gereeld die effek van klimaatsverandering wat die meeste kommer wek. Dus is heelwat navorsing rakende die direkte erosie as gevolg van seevlakstyging reeds gedoen. Om die volle beeld van die gevolge van ‘n stygende seevlak te verkry, is dit egter nodig om ook die sekondêre effekte hiervan in ag te neem. Seevlakstyging kan veranderinge in die golfklimaat naby die kus veroorsaak, en kan impakte soos kuserosie en veranderende baaivorms tot gevolg hê. Die primêre doel van hierdie studie is dus om die effek van seevlakstyging op die golfklimaat by die kus en gevolglik die stabiliteit van die kuslyn, te ondersoek.

Benewens die styging van die seevlak word die effekte van groter gemiddelde golfhoogtes en die rotasie van diepsee golfrigtings ook in hierdie studie ondersoek. Die vele landpunt-baaie (headland-bay beaches) op die Suid-Afrikaanse kus is meestal in ‘n dinamiese ekwilibriumtoestand, waarvan die vorm deur die lokale golfklimaat bepaal word. Veranderinge aan dié golfklimaat mag dus die ekwilibrium vorms van sulke baaie versteur. Hierdie studie het dus ook die stabilititeit van landpunt-baaie onder ‘n veranderende golfklimaat ondersoek.

Die drie gevolge van klimaatsverandering wat verwag word om die golfklimaat naby die kus te beïnvloed is geïdentifiseer as (1) seevlakstyging; (2) vergrote golfhoogtes; en (3) veranderende diepsee golfhoeke. Veranderinge aan die frekwensie en intensiteit van storms is ook moontlike gevolge van klimaatsverandering, maar die impakte hiervan is nie in die studie ondersoek nie.

Twee numeriese modelle is toegepas om die impak van die drie bogenoemde gevolge op Mosselbaai – ‘n tipiese landpunt-baai aan die suidkus van Suid-Afrika – te ondersoek. ‘n Golfmodel is ingespan om die golfklimaat naby die kus te bepaal waarna ‘n kuslynmodel gebruik is om die stabiliteit van die baai onder die veranderde golfklimaat te ondersoek.

Die resultate van die studie dui daarop dat die golfhoeke naby die kus beïnvloed word deur seevlakstyging. Daar is aangetoon dat dié veranderinge die langsstroomvervoer sodanig sal verander dat kuslynrotasies in die suid-westelike hoek asook die oostelike rand van Mosselbaai verwag word. Hierdie rotasies sluit nie die lineêre landwaartse verplasing van die kuslyn as gevolg van erosie en oorstroming in nie.

Die effek van vergrote golfhoogtes kon nie met akkuraatheid ondersoek word nie. Daar is wel gevind dat die suidwaartse rotasie van diepsee golfhoeke rotasies in die golfklimaat naby die kus veroorsaak. Hierdie rotasies verander die langsstroom sedimentvervoer sodanig dat die uitwaartse

sedimentvervoer verminder word en ‘n klein opbou van sediment in die middel van die baai vir ‘n 1° diepsee rotasie verwag word. Vir ‘n 2° suidwaartse rotasie is daar ‘n groter opbou van sediment wat verder ooswaarts veplaas is. Die ooswaartse veplasing is primêr ‘n gevolg van die oorheersing van suid-westelike golftoestande in die golfklimaat.

‘n Waardevolle gevolgtrekking rakende die huidige stabiliteit van Mosselbaai is ook gemaak. Langs drie gedeeltes van die Mosselbaaise kus word riwwe in die gebied tussen hoog- en laagwater aangetref. Hierdie riwwe beskerm die kus sodanig dat skerp kinkels in die vorm van die baai tussen die riwwe gesien kan word. Wanneer die seevlak styg, word die beskermende effek van die riwwe egter minder doeltreffend. Indien ‘n watervlak bereik word waar dié effek genoegsaam verminder is, word daar verwag dat die baai deur ‘n merkwaardige verplasing van sediment die kinkels sal uitstryk. Deur hierdie proses word erosie in die orde van 80m naby die dorp van Klein Brakrivier verwag.

Acknowledgements

The financial assistance of the National Research Foundation (NRF) towards this research is hereby acknowledged. Opinions expressed and conclusions arrived at, are those of the author and are not necessarily to be attributed to the NRF.

The financial assistance of the University of Stellenbosch is also acknowledged and much appreciated.

I would like to thank the South African National Hydrographic Office (SANHO), the Transnet National Ports Authority (TNPA), Prestedge Retief Dresner Wijnberg (PRDW), the South African Weather Service (SAWS) and the Council for Scientific and Industrial Research (CSIR) for providing me with data essential to this study. Furthermore, I would like to thank the CSIR for granting me the use of UNIBEST without which this study could not have been completed.

I would like to thank SAVUSA (South Africa – VU University Amsterdam – Strategic Alliances) and the Delft University of Technology (TU Delft) for the opportunity and funding to study at TU Delft for three months during which I attended courses presented by some of the world's leading scientists in the field of coastal engineering. The experience gained has contributed significantly to this study.

Much gratitude is extended to Mr Andre Theron for taking an interest in my work, for significant help in understanding the complexities of sediment transport modelling and for words of encouragement. I would also like to thank Mr Laurie Barwell for early guidance and sharing his knowledge of the site and the important processes present and Mr Marius Rossouw for conceptual help with the wave modelling.

My supervisor, Mr Geoff Toms is gratefully acknowledged for his guidance, encouragement and constant willingness to assist where needed.

My great friend, Sterrenberg Schoombee is thanked for his accompaniment and assistance on the site visit to Mossel Bay.

I would like to thank my family, and close friends for their continual support and encouragement.

Lastly, I would like to thank the Lord for the opportunity and the means to finish this project.

Contents

List of Figures

List of Tables

Nomenclature

Symbol	Description
a	Reference level for suspended load sediment transport [m]
a	Constant in hyperbolic bay shape equation [m]
B	Berm height [m]
b	Constant in hyperbolic bay shape equation [-]
C_0, C_1, C_2	Constants in the parabolic bay shape equation [-]
c	Wave celerity [m/s]
c	Sediment concentration [kg/m^3]
CD	Chart datum [-]
c_f	Friction coefficient [-]
D	Particle diameter [m]
D_*	Dimensionless particle diameter [-]
D_{50}	Median particle diameter [m]
D_B	Berm height [m]
D_C	Depth of closure [m]
D_w	Energy dissipation through wave breaking [J]
d	Water depth [m]
d	Active profile height [m]
d_1	Closure depth [m]
E	Wave energy [J]
F	Fetch [km]
F_D	Drag force [N]
F_L	Lift force [N]
F_x, F_y	Forces due to radiation stresses [N]
f	Wave frequency [Hz]
$G(f)$	JONSWAP peak enhancement function
g	Gravitational acceleration [m/s^2]
H	Wave height [m]
$H_{0_{max}}$	Maximum deep water wave height [m]
$H_{1/3}$	Significant wave height calculated from time series [s]
H_b	Wave height at breaking [m]

H_{bs}	Significant wave height at breaking [m]
H_e	Significant wave height exceeded 12 hours per year [m]
H_{max}	Maximum wave height in shallow water [m]
H_{m0}	Significant wave height from wave spectrum [m]
H_S	Significant wave height [m]
HAT	Highest astronomical tide [m]
h	Water depth [m]
h_*	Closure depth [m]
h_b	Water depth at breaking [m]
k	Wave number [rad/m]
L	Wave length [m]
L_*	Cross-shore distance to closure depth [m]
L_0	Deep water wavelength [m]
LAT	Lowest astronomical tide [m]
MHWN	Mean high water neap [m]
MHWS	Mean high water springs [m]
ML	Mean level [m]
MLWN	Mean low water neap [m]
MLWS	Mean low water springs [m]
m	Constant in hyperbolic bay shape equation [-]
m_0	Zeroth order moment of wave spectrum [m^2]
n	Ratio of wave speed over group velocity [-]
p	Porosity [-]
Q	Sediment transport rate [m^3/year]
q	Momentum under a harmonic wave [kg.m/s]
$q_{b,c}$	Current-related bed load transport [m^3/m/year]
q_{drift}	Momentum due to Stokes' drift [kg.m/s]
q_{roller}	Momentum due to breaking wave [kg.m/s]
$q_{s,c}$	Current-related suspended load transport [m^3/m/year]
$q_{t,c}$	Current-related total load transport [m^3/m/year]
R	Shoreline retreat [m]
R, R_1, R_2, R_0	Radii for headland bay beach models [m]

S	Sediment transport rate [m^3/year]
S	Sea-level rise [m]
$S_{xx}, S_{yy}, S_{xy}, S_{yx}$	Radiation stresses [N/m^2]
S'_{yx}	Turbulent shear stress [N/m^2]
s_{max}	Maximum wave steepness [-]
T	Wave period [s]
T	Dimensionless bed-shear parameter for bed load sediment transport
$T_{1/3}$	Significant wave period calculated from time series [s]
T_e	Period of wave condition exceeded 12 hours per year [s]
U_{10}	Wind speed at 10m elevation [m/s]
u	Current velocity [m/s]
$u_{*,cr}$	Critical bottom shear velocity [m/s]
V	Longshore current velocity [m/s]
x	Alongshore distance [m]
y	Cross shore distance [m]
α	Angle in logarithmic spiral model [rad]
α_k	Beach slope angle to breaker line [rad]
β	Angle of obliquity in the parabolic bay shape equation [rad]
γ	JONSWAP peak enhancement factor [-]
γ	Wave breaker index [-]
η	Water surface elevation [m]
θ	Wave angle [rad]
θ_b	Incident wave angle at breaking [rad]
ν_T	Turbulent eddy viscosity [Pa.s]
ρ	Mass density of water [kg/m^3]
ρ_s	Relative mass density of sediment [kg/m^3]
$\tau_{b,cr}$	Critical bottom shear stress [N/m^2]
$\bar{\tau}_{b,y}$	Time-averaged bed-shear stress [N/m^2]
φ	Wave incidence angle [rad]
ω	Angular frequency [rad.Hz]

1 Introduction and background

Currently, more than 160 million people live within 1m of mean sea level (Allison et al., 2009). When faced with sea-level rise predictions in the order of 1.0m within the next century, obvious concern arises. Predicted increases in wave height and changes in wave direction are also causes for concern. Not only loss of infrastructure, but also damage and destruction of sensitive environments (such as mangrove forests and estuaries) and saltwater intrusion into inland freshwater reservoirs are issues to be considered.

It is therefore important that long-term management decisions regarding the response to sea-level rise and other effects of climate change be made at an early stage. To enable decision-makers to employ the best response strategies, it is imperative to be able to gauge the impacts of these effects.

The beach is often an area of high economic value. On the southern coast of South Africa, many beaches are located within bays of which the shape is determined by the presence of headlands and the angle of wave attack. These curvilinear bays containing sandy beaches bounded by headlands are called headland-bay beaches.

The planforms of headland-bay beaches are heavily dependent on the direction of waves. As the sea-level rises, in addition to inundation, the refraction of waves may be affected, causing a change in the incident wave angle. Furthermore, a rotation of offshore wave directions causes a change in the mean direction of waves attacking the coastline. Consequently, the planform of headland-bay beaches may become unstable and rotate. When considering the large scale of headland-bay beaches found in South Africa, even small rotations may cause significant displacements in the shoreline position.

The superposition of the rotation-related displacements and the retreat caused by sea-level rise could have dire implications for valuable infrastructure and environments located where both these effects result in erosion. If significant rotation occurs, it could be possible for some parts of the headland-bay beach to experience accretion. The prior knowledge of these effects can therefore be employed in the evaluation of future scenarios involved in decision-making by local authorities.

Much work has been done on the linear setback caused by a risen sea-level on a soft coastline, while little attention has been given to the changing wave climate and its effect on the stability of the shoreline. This study is therefore aimed at filling this gap by investigating the effect of sea-level rise

and a changing wave climate on the long-term stability and planform of a headland-bay beach on the South African coast.

1.1 Objective

The objective of this study is to investigate the impact of a changing wave climate caused by sea-level rise and other climate change effects on a typical headland-bay beach on the southern coast of South Africa by means of numerical modelling.

1.2 Chapter overview

The study will commence with a review of literature aimed at identifying the processes important in shaping coastlines. Some aspects regarding the numerical modelling of shoreline change will also be discussed. The literature review is found in Chapter 2.

In Chapter 3, a study site is selected and described. Hypotheses are formulated based on the site characteristics. The modelling approach is presented in Chapter 4, followed by a summary of the available data.

Chapters 5 and 6 present the numerical modelling process, as set out in the methodology. The results of the study are discussed in Chapter 7. The study is concluded in Chapter 8 where recommendations are also made.

2 Literature review

The review of literature to follow will primarily be focused on the formation and description of headland-bay beaches, some effects of climate change, and how these two interact. The formation of bays relies heavily on erosion caused by coastal processes. In order to fully understand the mechanisms of coastal erosion, some basic concepts relating to wave dynamics need to be clarified. Some aspects of wave generation and the evolution of the wave state are also discussed, as this becomes important in the modelling of wave transformation to the nearshore.

Figure 2.1 illustrates the propagation of deep water wave spectra towards a headland-bay beach. In Chapter 2.1, the dominant processes in the generation of these wave spectra are discussed. Subsequently, Chapter 2.2 addresses the processes affecting the propagation of these wave spectra into a headland-bay beach.

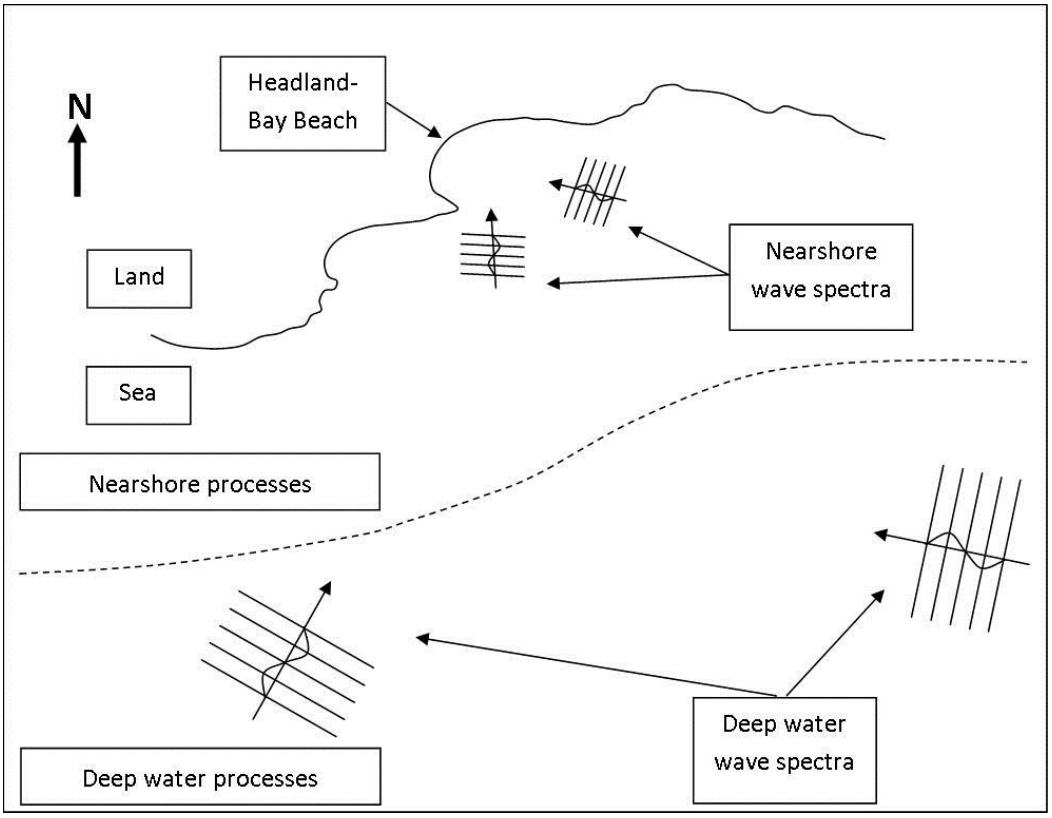

Figure 2.1: Introduction to wave generation and propagation

2.1 Wind-wave generation and wave spectra in deep water

When wind blows across a water body, small, short waves appear. These waves influence the flow of air over the ocean surface such that the resulting wind-induced pressure feeds back into the growth of the waves. Although the initial generation of waves is not well understood, this has little effect on

the evolution of the wave state, since small waves are almost always present to trigger wave growth (Holthuijsen, 2007).

With the initial small waves present, the factors affecting the idealised generation of waves are the fetch (F), duration (t), wind speed (generally taken to be at 10m height, U_{10}) and gravitational acceleration (g). The growth of waves does not carry on infinitely, but is often limited by the fetch or duration. This is referred to as a young sea state, since the growth of the waves is interrupted before the waves are fully developed. When the growth is neither fetch-limited nor duration-limited, a logical limit is reached when the wave speed approaches the wind speed and the energy transferred from the wind to the waves is balanced by dissipation through wave breaking. This is referred to as a fully developed sea state.

The balancing effect of wave breaking in deep water occurs through a very complex hydrodynamic process called white-capping. Theoretically, if the horizontal particle velocity in the crest of a wave is higher than the velocity of the wave itself, the wave becomes unstable and breaks. In deep water, this relates to a maximum wave steepness (s_{max}) of about (Holthuijsen, 2007):

$$s_{max} = {H_{0_{max}}}/{L_0} \approx 0.14 \tag{2.1}$$

where $H_{0_{max}}$ is the deep water wave height at breaking and L_0 is the corresponding deep water wave length. White-capping thus serves as a physical limit to the steepness of waves generated in deep water.

The basic parameters describing a stationary wave state are the significant wave height (H_s) and its corresponding wave period (T_s). When a time series of waves is considered, H_s and T_s are calculated as the average of the highest one third of the observations, and are also denoted as $H_{1/3}$ and $T_{1/3}$. At any given time, the surface elevation of the ocean is the sum of a vast number of wave components of varying heights, frequencies and directions. In order to accurately reflect such a random sea state, a more detailed description is often needed. This is found in the wave spectrum, which is representative of all the wave components present.

The one-dimensional wave spectrum is expressed as the mean variance of each wave component plotted against its frequency. The variance is used rather than the amplitude since it is statistically

more relevant and easily translates to wave energy[1] (Holthuijsen, 2007). The significant wave height (H_{m0}) is calculated from wave spectra as:

$$H_{m0} \approx 4\sqrt{m_0} \tag{2.2}$$

where m_0 is the zeroth-order moment of the variance density spectrum. Although H_{m0} is closely related to $H_{1/3}$, these parameters are not equal[2]. The wave period interpreted from the spectrum is calculated as the inverse of the frequency located at the spectral energy peak and is denoted as T_P. An example of the one-dimensional continuous variance density spectrum is shown in Figure 2.2.

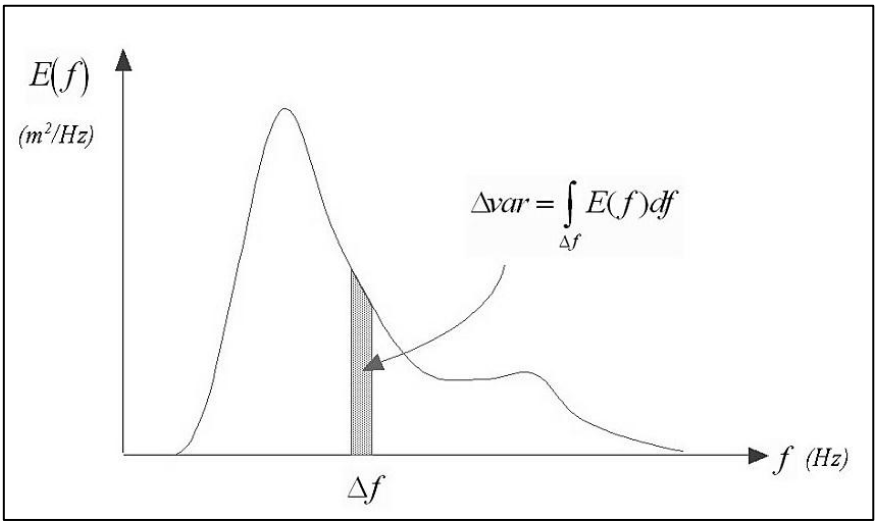

Figure 2.2: The one-dimensional variance density spectrum (Holthuijsen, 2007)

A wide spectrum (such as the one in Figure 2.2) is representative of a random wave field with wave components covering a wide range of frequencies – as is often found during a storm. On the other hand, swell conditions are characterised by long period waves within a limited number of frequencies. During pure swell conditions, fewer components are present and the spectrum may therefore be significantly narrower.

The above spectrum only considers the distribution of waves over a range of frequencies, while the characteristic sea state is also distributed over a range of directions. In order to represent directional distribution, a two-dimensional spectrum can be constructed or a function describing the directional spreading for each frequency can be prescribed to the one-dimensional spectrum.

The evolution of the wave spectrum under near-idealised conditions was studied in detail under the Joint North Sea Wave Project (JONSWAP; Hasselmann et al. (1973)). It was concluded that the wave

[1] From linear wave theory, the wave energy is proportional to the variance of a wave, such that:
$E = \frac{1}{2}\rho g a^2 = \rho g \cdot var$

[2] $H_{1/3}$ is 5%-10% lower than H_{m0} (Holthuijsen, 2007).

spectrum maintained its shape with varying fetch lengths and that the high-frequency range matched the spectrum observed by Pierson and Moskowitz (1963) (known as the PM spectrum) for a fully developed sea state. This observation can be explained by the presence of nonlinear wave-wave interactions.

Nonlinear wave-wave interactions refer to the processes through which energy is transferred amongst wave components through wave resonance. When two wave components with different directions, speeds and wave lengths cross, a third wave component with its own direction, speed and wave length is generated. If a wave component with the same properties as the generated wave exists, the condition of resonance is satisfied. Energy is thus transferred through resonance from the two original components to the third while maintaining the balance of energy of the whole system. This process is termed *triad wave-wave interactions*. The resonance conditions for triad interactions are only met in very shallow water (Holthuijsen, 2007). In deep water, however, the generated waves from two pairs of wave components can have the same direction, speed and wave length, thereby resulting in or transferring energy to a fifth wave component. This process is termed *quadruplet wave-wave interactions*.

The effect of quadruplet interactions on wave growth in deep water is to redistribute energy amongst wave frequencies. Energy is moved from mid-range frequencies to the lower range, and a small fraction to the high range where it is dissipated by white-capping (Holthuijsen, 2007). The resulting effect is thus to shift the peak of the spectrum to a lower frequency and to smooth the tail of the spectrum. Under stormy conditions, the waves are steep and the quadruplet interactions are strong. These interactions tend to stabilise the spectrum into the shape observed during JONSWAP (commonly referred to as the JONSWAP spectrum). Under swell conditions, however, lower wave steepness reduces the strength of quadruplet interactions. The spectrum is then not expected to stabilise into the JONSWAP shape. However, local winds may generate a secondary peak at a higher frequency which follows the general shape of a JONSWAP spectrum. The spectrum presented in Figure 2.2 contains a secondary peak.

The JONSWAP spectra were also observed to have sharper peaks than those of the PM spectra. The derivation of the JONSWAP spectrum was thus to modify the PM spectrum with the following peak enhancement function:

$$G(f) = \gamma^{\exp\left[-\frac{1}{2}\left(\frac{1}{\sigma}\left\{\left(f/f_{peak}\right)-1\right\}\right)\right]^2} \tag{2.3}$$

where γ is known as the peak enhancement factor and σ is a peak-width parameter. For the South African wave climate, Rossouw (1989) proposed and average value of 2.2 for the peak enhancement factor, when JONSWAP spectra were applied to design wave conditions.

After being generated by winds, waves propagate through the ocean and are transformed by a number of processes prevalent in shallower water. These processes are described in Chapter 2.2.

2.2 Wave dynamics in coastal waters

The wave field generated by a storm is initially random, with wave components in a wide range of frequencies. The dispersion relation, which follows from linear wave theory, implies that waves propagate at speeds inversely proportional to their frequencies, such that:

$$c = \frac{g}{\omega} \tanh kd \tag{2.4}$$

where c is the wave celerity, g is the gravitational acceleration, $\omega = 2\pi f$ is the angular frequency, $k = 2\pi/L$ is the wave number and d is the water depth.

Since the wave components travel at different speeds, a certain component will reach a point in the ocean while some components with lower frequencies have already passed and some components with higher frequencies have yet to arrive. The wave field at that location is no longer random and can be said to only have waves within a certain frequency range[3]. This effect is called *frequency-dispersion*. Similarly, the occurrence of waves within a directional sector is termed *direction-dispersion*. The effect of wave dispersion is thus that only a fraction of the initial wave energy generated by the storm is present at any given location, without any dissipation of energy.

When waves reach the shallower waters on the continental shelf, dissipation through bottom friction occurs. The particle motions caused by waves create a thin turbulent boundary layer on the bed. Bottom friction refers to the transfer of energy and momentum from the water particles to the boundary layer, the rate of which is dependent on the particle velocity and the shear stress directly above the boundary layer (Holthuijsen, 2007). The shear stress is also dependent on the characteristics of the bed – such as the presence of ripples – and is represented by the coefficient of bed friction.

As waves approach the coastline and the water depth becomes limited, a depth is reached where the waves are affected by the bottom. From this point, wave celerity will change as a result of bottom friction or the presence of currents.

[3] This is true if only one storm is present in the entire ocean. In actual fact, wave components from various meteorological events including far away storms and local winds will meet at the considered location.

Shoaling is the phenomenon whereby the group velocity of waves is affected by the limited water depth. As a wave group approaches a shallow area, the group velocity is reduced, resulting in a slower propagation of wave energy. Wave energy is bunched up causing an increase in wave amplitude (Holthuijsen, 2007). In the same way, shoaling may also be caused by the presence of a current flowing against the direction of wave propagation, slowing down the propagation of wave energy.

When a wave reaches a depth contour at an angle, there will be a lateral difference (along the wave crest) in the celerity of each wave, resulting in a change in direction of the wave crest towards the shallower water. This process is referred to as wave refraction and can best be seen when lines are drawn orthogonally to the wave crests (referred to as wave rays). Figure 2.3 is an idealised plot of wave rays approaching a headland and bay system. The bottom contours are also indicated.

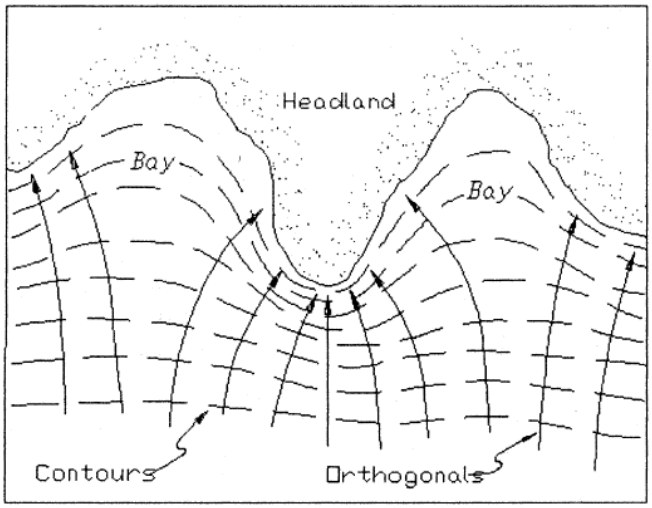

Figure 2.3: Idealised plot of wave rays approaching a headland (CEM, 2003)

The law of refraction is also known as Snell's law which is expressed as:

$$\frac{\sin\theta_1}{d_1} = \frac{\sin\theta_2}{d_2} = k \tag{2.5}$$

where θ is the angle between the wave direction and the normal to the bottom contour, d is the water depth and the ratio k remains constant. Positions 1 and 2 refer to positions along the path travelled by the wave.

The occurrence of waves behind obstacles is due to the process of diffraction. When waves are confronted by an obstruction such as a breakwater or headland, a large initial variation of wave height along the wave crest occurs. Diffraction is the process by which energy is spread along the

wave crest leading to the presence of waves in the shadow zone of the obstruction (Bosboom & Stive, 2012). The process of diffraction around the head of a breakwater is depicted in Figure 2.4.

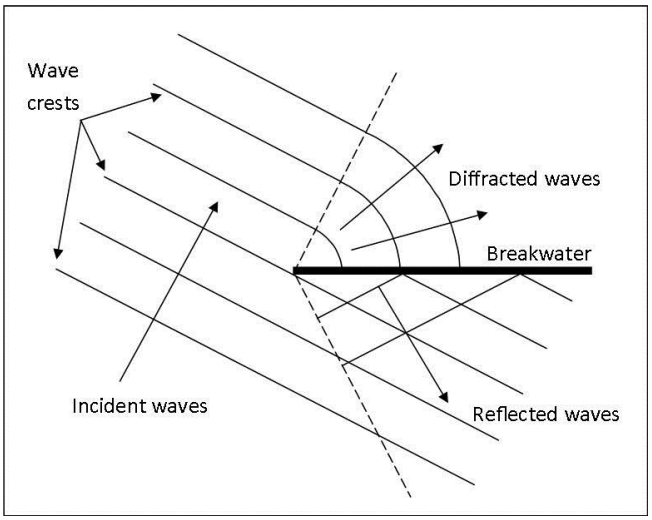

Figure 2.4: Diffraction behind a breakwater (adapted from Chadwick et al (2004))

In very shallow water, the effect of triad wave-wave interactions (see Chapter 2.1) also affects the energy in the wave spectrum. The triad interactions generate secondary peaks at higher multiples of the peak frequency. As the waves propagate deeper into the surf-zone, however, the same triad interactions remove these peaks and transform the tail back into a smooth shape (Holthuijsen, 2007).

As waves propagate into ever shallower waters, the wave height continuously increases through shoaling. Consequently, the wave steepness increases accordingly. In analogy to the limit of wave steepness in deep water (described in Chapter 2.1), the wave becomes unstable and breaks when the particle velocity in the crest exceeds the propagation speed of the wave. The point of depth-induced breaking defines the seaward edge of the surf zone. The wave height reached at this limit is referred to as the wave height at breaking, or H_b. From linear wave theory, the shallow water equivalent to the limit of wave steepness presented in Equation 2.1 is (Bosboom & Stive, 2012):

$$\frac{H_{max}}{L} \approx 0.88\frac{h}{L} \tag{2.6}$$

or:

$$\gamma = \left[\frac{H}{h}\right]_{max} = \frac{H_b}{h_b} \approx 0.88 \tag{2.7}$$

where L is the wave length, h is the water depth and the subscript b denotes the condition at breaking. Gamma (γ) is referred to as the breaker index. From solitary wave theory – a theory which

is more applicable to shallow water – a preferred value of the breaker index is found to be (Bosboom & Stive, 2012):

$$\gamma \approx 0.78 \tag{2.8}$$

According to the processes described above, significant changes to the wave spectrum have occurred by the time the wave energy has reached the shore. The resulting local wave climate near the coast is then responsible for the generation of various coastal processes. These processes are instrumental in the movement of sediment and therefore also the stability of the beach, and are discussed further in Chapter 2.3.

2.3 Coastal processes

The main contributing factor to shaping coastlines is the erosion driven by nearshore coastal processes such as waves, currents and wind. In order to understand the morphology of soft coastlines, it is imperative to clarify the mechanisms of coastal erosion. Hence, this section will briefly cover a few of the primary mechanisms of the erosion of sandy beaches.

The orbital motion of water particles under the crest of a wave in the nearshore area causes a movement of sediment on the bed. Also, the turbulence generated by wave breaking brings sediment into suspension which is then transported by a combination of currents. The transport of sediment by any of these mechanisms causes short-term changes in the beach profile and causes the beach to erode, accrete or remain stable in the long-term. In order to grasp the transport of sediment in the coastal zone, it is therefore important to understand the generation of these currents under the effect of waves.

As waves propagate, a mass of water is carried shoreward due to the orbital motion of the water particles between the crest and trough of a wave. The momentum produced by this transport of mass is commonly referred to as Stokes' drift. For non-breaking waves, the momentum is represented by the mass density multiplied by the particle velocity. Integrated over depth and averaged over time, the total momentum under a harmonic wave is calculated as (Bosboom & Stive, 2012):

$$q = \overline{\int_{-h}^{\eta} \rho u \, dz} = \frac{1}{c} E \tag{2.9}$$

where ρ is the mass density, u is the particle velocity, E is the wave energy and c is the wave group velocity. The surface elevation is denoted by η and h is the water depth. When wave breaking occurs, rollers are generated which significantly enhance the amount of mass transported shoreward. For the sake of brevity, the expression for the momentum generated by the roller is not

included in this review. The total momentum produced by the shoreward transfer of mass by a breaking wave then becomes:

$$q = q_{drift} + q_{roller} \tag{2.10}$$

The presence of a beach interrupts the flow created by the onshore mass transport. A return flow is therefore needed to maintain mass equilibrium. This flow is termed a *cross-shore current* (Dean & Dalrymple, 2002). The return flow can take the form of the undertow below waves in the surf zone or in rip currents.

The transport of momentum by waves can be seen as a stress in the direction of wave propagation called momentum flux or *radiation stress* (Chadwick et al., 2004). The momentum flux occurs in two parts: (1) through the horizontal particle velocity and; (2) through the wave-induced pressure force as indicated in Figure 2.5:

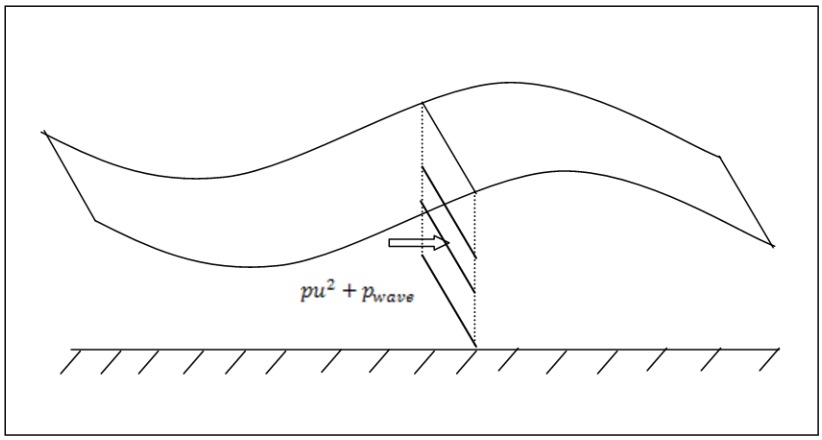

Figure 2.5: Momentum flux under a wave (Adapted from Bosboom & Stive (2012))

If a wave propagates at an angle to the coast, the following nonzero components of the radiation stress are present (Bosboom & Stive, 2012):

$$S_{xx} = \left(n - \frac{1}{2} + n\cos^2\theta\right)E \tag{2.11}$$

$$S_{yy} = \left(n - \frac{1}{2} + n\sin^2\theta\right)E \tag{2.12}$$

$$S_{xy} = S_{yx} = n\cos\theta\sin\theta\,E \tag{2.13}$$

where S_{xx} and S_{yy} are normal stresses in the cross-shore and longshore directions and S_{xy} and S_{yx} are shear stresses acting in the cross-shore and longshore directions. The angle of the incident wave to the coast is θ and n is the ratio of the group velocity over phase speed.

From Equations 2.11 to 2.13, it can be seen that variations in the radiation stresses are caused by changes in wave direction, wave energy and the velocity ratio. When a cross-shore gradient in the radiation stress exists, a net force can be said to act on the water body. Considering an alongshore uniform coast, this cross-shore oriented force can be derived from the balance of momentum as (Bosboom & Stive, 2012):

$$F_x = -\frac{\partial S_{xx}}{\partial x} \tag{2.14}$$

where S_{xx} is the radiation normal stress acting in the onshore direction. In the surf zone, dissipation through breaking reduces the wave energy, resulting in a shoreward oriented force. In order to counteract the force, a pressure gradient is generated by a rise in the sea-level shoreward of the point of breaking (Komar, 1998). This phenomenon is called *wave set-up*. Similarly, the bunching up of energy through shoaling causes an increase in radiation stress and, consequently, an offshore directed force. This force is counteracted by a drop in the sea-level directly seaward of the edge of the surf zone, called *wave set-down*. These phenomena are illustrated in Figure 2.6.

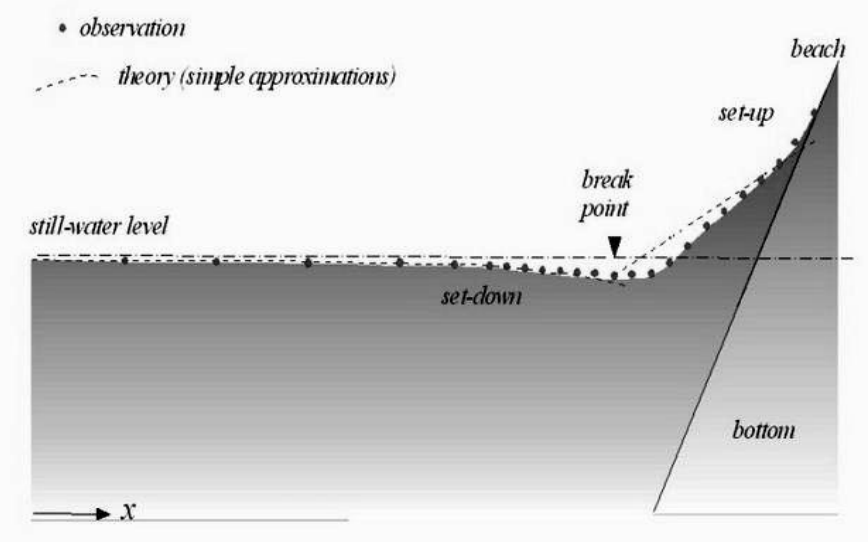

Figure 2.6: Wave set-up and set-down (Holthuijsen, 2007)

Although very important to the overall sediment balance in the surf zone, the cross-shore sediment transport due to the above-mentioned processes primarily causes short term morphological changes in the surf zone. For this specific study, the cross-shore processes are not expected to significantly influence the long-term coastline trends, which are mostly caused by gradients in longshore sediment transport. However, cross-shore processes are important to the sediment budget and consideration needs to be given to the increase in the volume of sediment available for longshore transport resulting from cross-shore dune erosion. Cross-shore processes are not discussed in further detail in this study.

Under the same assumptions as for the cross-shore direction, a longshore net force is generated by the cross-shore gradient in the longshore radiation shear stress, S_{yx}, such that (Fredsoe & Deigaard, 1992):

$$F_y = -\frac{\partial S_{yx}}{\partial x} = \frac{\sin\theta}{c} D_w \tag{2.15}$$

where the longshore radiation shear stress (S_{yx}) refers to the cross-shore transfer of alongshore momentum and D_w is the energy dissipated through wave breaking. According to Snell's refraction law, the ratio $\sin\theta/c$ remains constant. From Equation 2.15, it can be seen that the force only exists where wave energy is dissipated. Since the most prominent form of energy dissipation in the nearshore is wave breaking, the longshore current is primarily confined to the surf zone (Bosboom & Stive, 2012).

In the longshore direction there is no coast against which a water level gradient can be built up. In this case, the balancing force is found in the bed shear stress generated by the longshore current (Longuet-Higgins, 1970). The time-averaged bed shear stress ($\bar{\tau}_{b,y}$) in the alongshore direction required to counteract the alongshore driving force (F_y) is calculated as (Bosboom & Stive, 2012):

$$\bar{\tau}_{b,y} = \frac{1}{\pi}\rho c_f \sqrt{gh}\frac{H}{h}V \tag{2.16}$$

where c_f is the coefficient of friction, g is the gravitational acceleration, h is the water depth, H is the wave height and V is the velocity of the longshore current.

The gradient in the longshore component of radiation stress is not the only driver of longshore currents. In the surf zone, turbulent motions become very important to the lateral dispersion of momentum. The turbulent shear stresses (S'_{yx}) caused by these motions are related to the flow velocity gradients through the eddy viscosity (ν_T), such that (Bosboom & Stive, 2012):

$$S'_{yx} = h\rho\nu_T \frac{dV}{dx} \tag{2.17}$$

The balance of the above stresses in the longshore direction thus leads to the longshore momentum equation:

$$\frac{\sin\theta}{c} D_w + \frac{\partial}{\partial x}\left(h\rho\upsilon_T \frac{\partial V}{\partial x}\right) = \bar{\tau}_{b,y} \tag{2.18}$$

which describes the velocity of the longshore current as a function of the cross-shore position. This equation leads to the cross-shore velocity distribution presented in Figure 2.7.

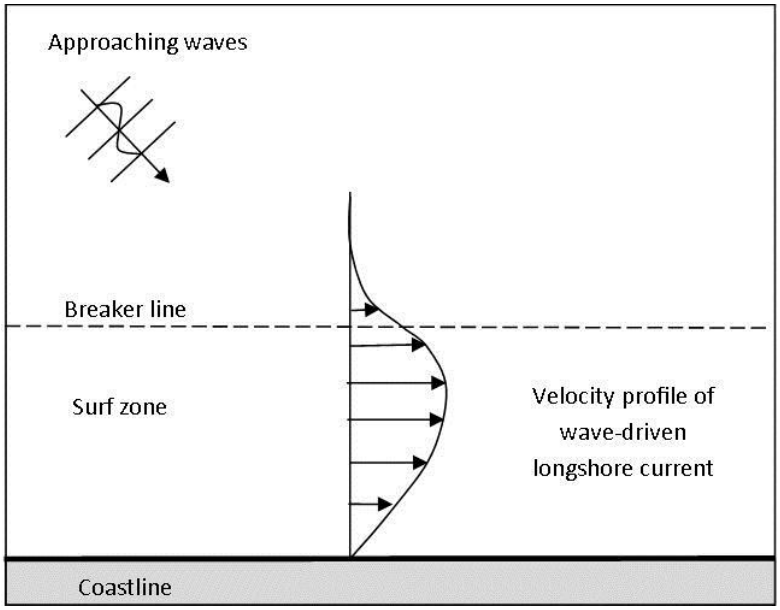

Figure 2.7: Velocity profile of a longshore current (adapted from Bosboom & Stive (2012))

Longshore currents can also be generated or enhanced by a longshore variation in the wave set-up. An obstruction such as a reef or headland may cause local sheltering from the wave energy which leads to a smaller wave height in the shadow area. Consequently, the wave set-up in the sheltered area is also lower, causing a lateral variation in the wave set-up. A flow is then generated by the longshore pressure gradient resulting from this water-level variation (Komar, 1998).

2.4 Sediment transport and coastal erosion

Considering the basic processes present in the coastal zone, the mechanisms through which beach erosion takes place can be described. For sediment transport in the surf zone, the most pronounced mechanism is through the currents described above. This section will therefore deal with the transport of sediment by currents in the surf zone.

In the surf zone, a flow of water is caused by the wave orbital motions as well as ambient currents. The motion of the water particles exerts a force on sediment particles. If this force is large enough, sediment is brought into motion. The transport of sediment occurs through three main modes (Fredsoe & Deigaard, 1992):

- Bed load transport;
- Suspended load transport;
- Wash load transport

Bed load transport refers to the part of the total transport which occurs very close to the bed such that the particles are almost continuously in contact with the bed. The transport can therefore be

expected to occur due to the bed shear stress acting on the sand surface (Fredsoe & Deigaard, 1992). In this mode of transport, particles can be seen to roll, shift or jump along the direction of the flow (Bosboom & Stive, 2012).

Suspended load transport refers to the sediment particles which are sufficiently agitated such that they are entrained into suspension and are carried forward by the current. The agitation is usually reached through turbulent motions in the flow (Fredsoe & Deigaard, 1992).

The wash load is the transport of very fine sediment particles in the water, which are usually always in suspension. These particles are therefore not represented in the bed and the total transport refers to the sum of the bed load and suspended load transports.

The initiation of motion of sediment particles can be explained by an analysis of the forces acting on a particle on the bed. Figure 2.8 presents the forces acting on a sediment particle in the presence of a nonzero horizontal current with velocity, u. The driving forces are the drag force (F_D) acting with the direction of the flow and lift force (F_L) acting upwards. The stabilising force is the gravity force (F_G).

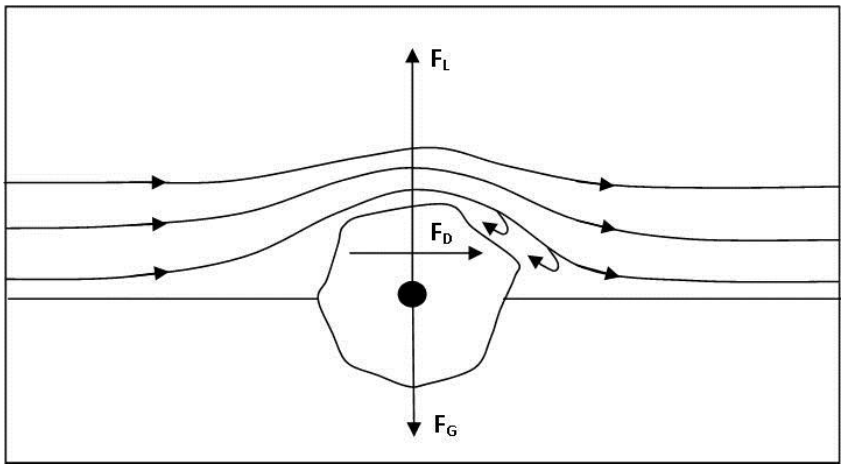

Figure 2.8: Initiation of motion of sediment particle (Adapted from Komar (1998))

The drag force occurs as a result of the skin friction on the surface of the particle as well as the pressure difference between the upstream and downstream sides of the particle. The drag force is related to the current magnitude (u) and particle size (D) such that (Bosboom & Stive, 2012):

$$F_D \propto u^2, D^2 \tag{2.19}$$

The lift force is caused by both the flow separation and the flow contraction, and is also proportional to the squares of the current velocity and particle diameter. From an equilibrium equation, the velocity at which the particle starts to move – the critical current velocity (u_{cr}) – is obtained. This

velocity is also termed the critical bottom shear velocity, denoted as $u_{*,cr}$, and is related to the critical bottom shear stress ($\tau_{b,cr}$) through:

$$\tau_{b,cr} = \rho {u_{*,cr}}^2 \tag{2.20}$$

where ρ is the density of the water.

The critical bed shear stress represents the driving forces on the particle and therefore determines the threshold of motion. The ratio between the driving and stabilising forces is constant and is referred to as the Shields parameter, according to the author of the work (Fredsoe & Deigaard, 1992).

The hydrodynamic interaction with sediment is poorly understood (Bosboom & Stive, 2012). The mathematical formulations describing the movement of sediment are therefore still largely based on empirical formulations. Consequently, there is considerable uncertainty in the results of sediment transport computations. It is not uncommon for the predicted transport rates to be inaccurate by a factor of two to five, when compared to measured data (Bosboom & Stive, 2012).

The mathematical formulations describing the movement of sediment in the nearshore can be divided into two groups. These are bulk transport formulae which calculate a total annual transport for a given wave condition based on empirical relations or dimensional analysis and detailed formulae which calculate the suspended and bed load transports locally in detail.

From a study of over 50 bulk and detailed transport formulae, Schoonees (1996) found the Kamphuis bulk formula to be the most universally applicable by comparing predicted longshore transports to a field data set of measured longshore sediment transport rates (Schoonees & Theron, 1993). Schoonees and Theron (1996) modified the Kamphuis formula according to the results of the study. The modified Kamphuis formula for sites where the breaking wave height usually exceeds 0.3m is presented as (Schoonees & Theron, 1996):

$$S = 63\,433\, X_{Kamphuis}\ (m^3/year) \tag{2.21}$$

where

$$X_{Kamphuis} = \frac{1}{(1-p)\rho_S} . \frac{\rho}{T_p} L_0^{1.25} H_{bs}^2 (\tan \alpha_k)^{0.75} . \left(\frac{1}{D_{50}}\right)^{0.25} (\sin 2\theta_b)^{0.6} \tag{2.22}$$

where S = longshore transport rate

p = porosity

ρ_s	=	relative density of the sediment
ρ	=	relative density of seawater
L_0	=	deep water wavelength
H_{bs}	=	significant wave height at breaking
$\tan\alpha_k$	=	beach slope to the breaker line
D_{50}	=	median particle diameter
θ_b	=	incident wave angle

Although the modified Kamphuis formula is not available in the numerical model to be used in this study, it remains a useful tool to assess the sensitivity of longshore transport to some of the parameters possibly subject to variation under the effects of climate change. A qualitative assessment of the dependence on some key parameters is done in Chapter 2.7.

A more detailed formula for the local sediment transport due to the combined effects of waves and currents is found in the van Rijn formula (van Rijn & Kroon, 1992). The total transport is calculated as the sum of the suspended and bed load transport. The suspended load transport ($q_{s,c}$) is calculated as the vertical integral of the product of the current velocity and the concentration profile, such that:

$$q_{s,c} = \int_a^h uc\, dz \tag{2.23}$$

where a is the reference level related to the ripple height or thickness of the wave boundary layer and h is the water depth. The velocity u is the local time-averaged fluid velocity at height z above the bed, while accounting for the wave effects in the near-bed layer. In this study, the fluid velocity will be the longshore current as determined in Chapter 2.3. The time-averaged concentration c at height z above the bed is dependent on the fall velocity of the sediment and the mixing coefficient for combined currents and waves. The bed load transport ($q_{b,c}$) is calculated as (van Rijn & Kroon, 1992):

$$q_{b,c} = 0.25 u'_{*,c} D_{50} T^{1.5} D_*^{-0.3} \tag{2.24}$$

where $u'_{*,c}$ is the effective current-related bed-shear velocity, taking into account a correction factor for wave-current interaction. T is a dimensionless bed-shear parameter relating the time-averaged bed-shear stress to the time-averaged critical bed-shear stress, according to the Shields parameter described above. D_* is a dimensionless particle parameter. The total transport is then computed as the sum of the bed load and suspended load transports:

$$q_{t,c} = q_{b,c} + q_{s,c} \tag{2.25}$$

Longshore currents are more or less always present. These currents therefore account for a significant portion of the annual sediment transport. Since the longshore transport is heavily dependent on wave height (see Equation 2.22), the volume of sediment transported during storm events should be considerably higher than during calmer periods. The increased wave height, however, is not the only factor which increases the rate of transport. During storms, many other effects exacerbate the erosion caused by longshore currents.

When storm events occur, the height of the still water level (SWL) may be significantly higher than predicted by astronomical tide. This phenomenon is called *storm surge* and is the sum of various components, mainly being wave set-up (discussed in Chapter 2.3), barometric tide and wind shear tide. The barometric tide occurs when the presence of a low pressure system raises the water level directly beneath it with an order of magnitude of tens of centimetres (Dean & Dalrymple, 2002). In stormy conditions, winds create a horizontal shear stress on the water surface due to the friction at the interface. When these winds are directed onshore, water is pushed toward the coast leading to a raised water level at the shore called wind shear tide.

The higher water level in combination with larger waves leads to an increase of wave energy dissipated on the shore face. Sediment is eroded from the swash zone, beach face and dunes and is deposited further offshore to form sand bars. On the south-western coast of South Africa, storm events usually occur in the winter months. Sand is eroded from the beaches and deposited in offshore banks. The wave regime in the summer months mostly consists of smaller waves with shorter periods. Low energy waves with small wave heights steadily erode the offshore banks and transport the sediment back onto the beach.

At a certain depth, the cross-shore profile is no longer affected by the seasonality in the wave climate. At this point, no significant sediment movement due to wave action takes place and the profile may be considered to be constant in the seasonal time scale. Early work by Hallermeier (1981) suggested that the annual closure depth, d_1 (m), be calculated relative to the mean low water level as:

$$d_1 = 2.28H_e - 68.5\left(\frac{H_e^2}{gT_e^2}\right) \tag{2.26}$$

where H_e is the nearshore significant wave height exceeded 12 hours per year, T_e is the associated wave period and g is the gravitational acceleration. The nearshore wave height is a statistical parameter which, when fitted with the modified exponential distribution, can be calculated as (Hallermeier, 1981):

$$H_e = \bar{H}_s + 5.6\sigma \tag{2.27}$$

where $\bar{H}_s$ and σ are the mean annual significant wave height the standard deviation, respectively. By comparing Equation 2.26 to field measurements, Birkemeier (1985) recalibrated the coefficients to obtain:

$$d_1 = 1.75H_e - 57.9\left(\frac{H_e^2}{gT_e^2}\right) \tag{2.28}$$

Erosion of beaches, however, does not only take place during storm events. Changes in the sediment budget such as the stabilisation or mobilisation of dunes may cause erosion or accretion in the long-term. In other cases, changes in the nearshore area such as the extension of a breakwater or the construction of a groyne may cut off longshore sediment transport, leading to accretion on the updrift side and erosion on the downdrift side of the obstruction.

Sediment is not only transported by currents, but also by wind. This is known as *aeolian transport*. Wind-blown sand may form a significant part of the sediment budget, moving sand from the beach into the dunes (Dean & Dalrymple, 2002). Buffer dunes on the landward side of the beach form an essential part of coastal protection and often serve as sources for the sediment eroded during storms. These dunes grow during onshore transport where the wind-blown particles settle in between the vegetation, where the wind velocity is lower. Dunes without vegetation grow by particle settlement on the lee side of the dune where the wind velocity is also lower (CEM, 2003). Dunes may remain stationary or migrate significant distances inland.

2.5 Bay shape and orientation

The shape and orientation of soft coastlines are primarily dependent on the redistribution of sediments through coastal processes. When a net loss of sediment is present, erosion occurs. Conversely, a net import of sediment leads to accretion. A state of equilibrium is said to be reached when the there is no further net movement of sediment (Dronkers, 2005; Komar, 1998). *Static equilibrium* exists where there is almost no littoral drift, such as in bays where waves break simultaneously along the entire periphery. The planform of a bay in static equilibrium is defined by the wave state and bathymetry. A state of *dynamic equilibrium* exists where a sediment source is needed to maintain the stability of the coastline in the long-term. If the sediment supply is interrupted, the planform of the bay will revert to that of the static equilibrium state. Dynamic equilibrium may also exist where the direction and magnitude of longshore transport oscillate with the seasons. A coastline may also be in the unstable state of *natural reshaping*, where changes in the

sediment supply, wave state, bathymetry or sheltering may lead to erosion or accretion of the beach (Hsu et al., 2010).

The formation of headland-bay beaches serves as an example of the tendency of coastlines to adapt in order to reach equilibrium. Consider the case where waves approach an infinitely long, straight section of a soft coastline at a constant oblique angle. As the waves break on the shore, a longshore current is generated. As there is no lateral variation in longshore transport, the net sediment transport is zero. The coast is therefore in a state of dynamic equilibrium.

Now consider the case where the section contains a segment that is less erodible than the sandy coast (such as a rocky outcrop or headland). The longshore sediment transport is interrupted leading to erosion immediately downdrift of the obstruction. Waves disperse energy through refraction and diffraction around the obstruction and break at smaller wave heights in the shadow area than at the exposed coast, leading to a longshore variation in wave set-up. The longshore current resulting from this variation erodes the downdrift coast and accretes the shadow zone until the entire planform of the coastline is normal to the incidence angle of the waves. As the waves are breaking normal to the shore, the longshore current is no longer present and the coastline is once again in a state of equilibrium.

This idealised case does not easily occur in real life, since the direction from which waves approach the coast varies with climate patterns, and is therefore also influenced by season. Stable bays are therefore much more likely to be in a state of dynamic equilibrium.

Headland-bay beaches (HBB's) are characterised by a spiral shaped beach lying in the lee of a headland. These bays are a common feature of coastlines around the world and are also especially prominent on the South African coastline. In Figure 2.9, three of these bays are highlighted – one on the western coast and two on the southern coast. Due to the presence of their characteristic long beaches, headland-bays are popular locations for holiday resorts and beach houses. These structures are present along the entire periphery – often without consideration to setback lines. Much interest has therefore been shown in gauging the possible erosion of these beaches in order to protect valuable infrastructure.

Figure 2.9: (a) Headland-bay beaches are present along the South African coast; (b) Headland-bay beach on the western coast; (c) Algoa bay in the Eastern Cape; (d) Mossel bay on the southern cape coast. Images from Google Earth™

Due to the many factors influencing the sediment dynamics in a bay, numeric modelling of sediment transport is difficult and computationally demanding. Common practise has therefore been to empirically predict the planform of the bay in static equilibrium based on the direction of the primary wave condition. This planform is then compared to the current planform of the bay to determine whether the bay is in a state of static equilibrium and, if not, the possible amount of erosion to occur should the bay become unstable (Hsu et al., 2010). Much work has also been done on the stabilisation of bays through the use of these static shapes (Silvester et al., 1972; Silvester & Ho, 1980). By predicting the stable shape of a bay, small scale bays can be designed in order to be in static equilibrium.

Many mathematical expressions have been developed to describe the static equilibrium planforms. The three primary models are (1) the logarithmic spiral model by Krumbein (1944, as cited by Yasso(1965)) and later Yasso (1965); (2) the parabolic model by Hsu and Evans (1989) and (3) the hyperbolic tangent model by Moreno and Kraus (1999).

The first model to be fitted to headland-bay beaches was that of the logarithmic spiral (henceforth log-spiral) by Krumbein (1944) and later Yasso (1965). The logarithmic equation was chosen as bays appeared to have a seaward-concave shape of which the radius increases with distance from the headland (Yasso, 1965). Bays in the U.S.A. were fitted with the logarithmic expression given by:

$$R_2 = R_1 e^{\theta cot\alpha} \tag{2.29}$$

Equation 2.29 relates the length of consecutive radii separated by an angle, θ, as can be seen in the definition sketch (Figure 2.10). The angle α is the angle between the radius and the tangent to the curve, which remains constant.

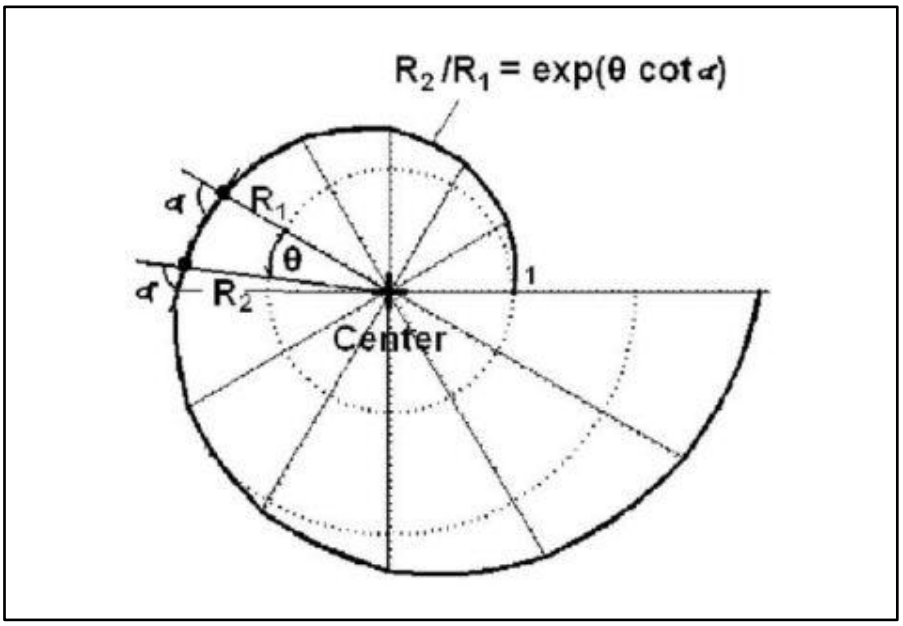

Figure 2.10: Definition sketch of the logarithmic spiral model (Hsu et al., 2010)

One of the major limitations of the log-spiral model was that the centre of the spiral often did not coincide with the wave diffraction point (Hsu et al., 2010). Although it was found that the model did approximate the updrift end of the bay reasonably well, the log-spiral failed to fit the straighter section at the downdrift end of headland-bay beaches (Hsu et al., 2010). This deficiency was aptly illustrated by Hsu and Evans (1989) and can be seen in Figure 2.11.

Because of the obvious limitations of the log-spiral model, Hsu and Evans (1989) proposed the Parabolic Bay Shape Equation (PBSE). The PBSE was derived empirically by fitting it to the planforms of 27 bays (including prototypes and models) in the static equilibrium state (Hsu et al., 2010). This model describes the static bay shape based on the obliquity of the dominant wave state, the point of diffraction and a reference point located at the downcoast limit of the beach. Further downdrift

from the reference point, the beach is assumed to be straight and parallel to the dominant wave crests. The definition sketch is shown in Figure 2.12.

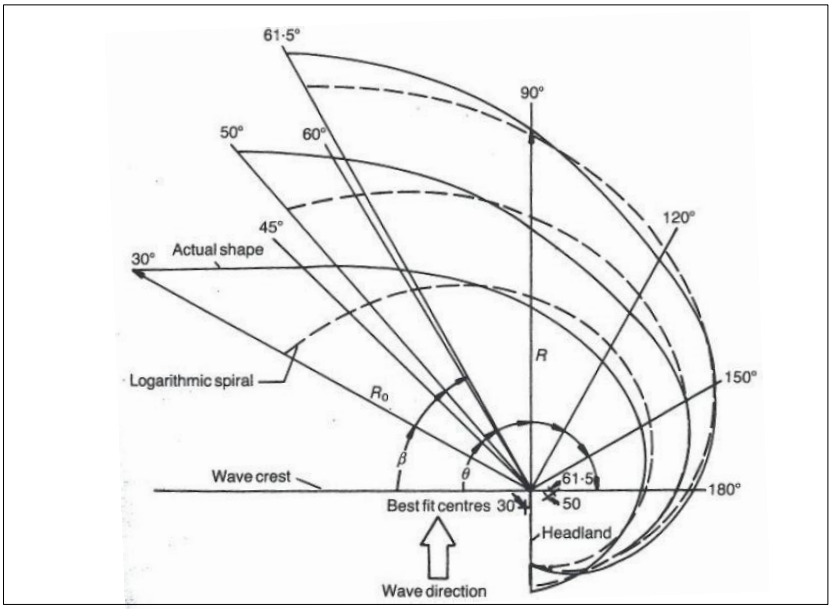

Figure 2.11: Comparison of log-spiral models to actual bays (Hsu & Evans, 1989)

Radii (R_i) are drawn from the diffraction point to points along the beach at arc angles θ_i to the wave crest line. The radius drawn to the downcoast limit of the beach is called the *control line* (R_0), which makes an angle β to the wave crest line. The ratio of each R_i to the control line is given by Equation 2.30 as:

$$R/R_0 = C_0 + C_1\left(\beta/\theta\right) + C_2\left(\beta/\theta\right)^2 \tag{2.30}$$

The constants are dependent only on the angle of obliquity, β, and can be linearly interpolated from tables and figures presented in Hsu & Evans (1989).

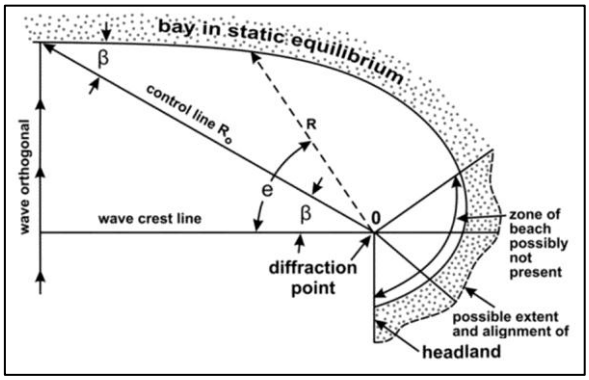

Figure 2.12: Definition sketch of the parabolic bay shape equation (Hsu & Evans (1989), adapted by Lausman et al. (2010)).

Examples of the fit of the parabolic model to two natural beaches assumed to be in static equilibrium and one model beach were also presented. A comparison of the natural bay shape and that predicted by the parabolic model is shown in Figure 2.13. Note how the model predicts the entire planform with relative accuracy, especially when comparing the downdrift end of the beach to the log-spiral model (Figure 2.10).

One of the great advantages of the PBSE is that the only information needed for its application is usually readily available. Aerial imagery or nautical charts are used to derive the positions of the three control points, being the diffraction point, the downdrift end of the beach and the start of the tangential section of the beach. These three points determine the final bay shape predicted by the model.

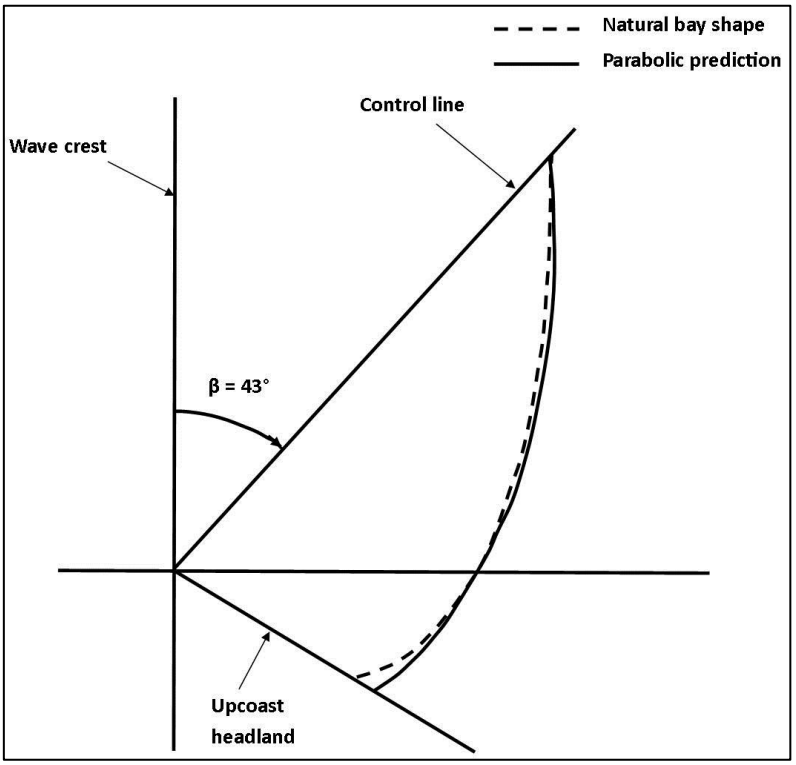

Figure 2.13: Predicted parabolic and natural planforms of Keppel Island, Queensland, Australia (adapted from Hsu & Evans, 1989)

In an effort to gauge the uncertainty caused by subjectivity in the choice of the control points, Lausman et al. (2010a; 2010b) generated a database of the chosen positions of the control points. Expert volunteers were asked to choose the control points of a stable bay. It was found that the PBSE was a robust method when the user can see the effect of the choice of the control points on the predicted planform.

González & Medina (2001) proposed a modification to the PBSE in which an angle α_{min} which determines the downdrift control point of the PBSE could be calculated. The angle is calculated as the dimensionless ratio of the distance between the diffraction point and the straight section of coast (Y) to the scaled wavelength (L_S) (calculated from the mean water depth and the mean period of wave heights exceeded 12 hours per year). The definition sketch of the modified PBSE is shown in Figure 2.14.

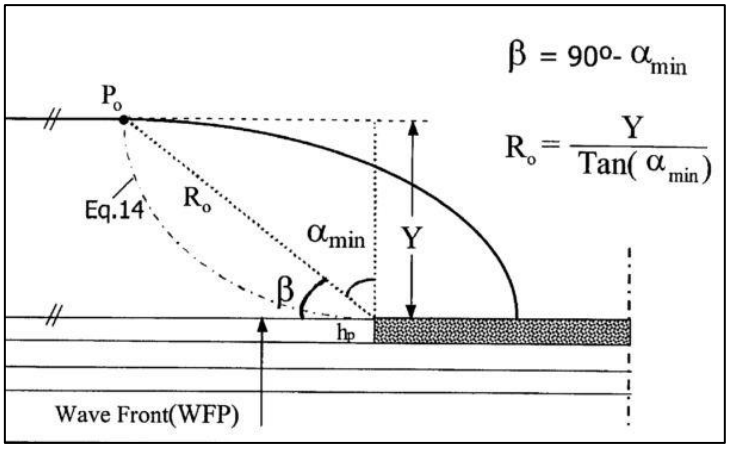

Figure 2.14: Definition sketch of the modified PBSE as proposed by González & Medina (2001)

In a study of bay shape models, Moreno and Kraus (1999) found the parabolic model to be insensitive to the parameters determining the parabolic shape. This led to the conclusion that the control point is not well defined and therefore the selection of the parameters has little influence on the final predicted planform. The authors proposed the hyperbolic tangent shape (presented in Figure 2.15) as a method that is simpler to apply and will fit bays with a single headland well. The shape is described by

$$y = \pm a \tanh^m(bx) \tag{2.31}$$

where y is the cross-shore distance, x is the alongshore distance and a, b and m are coefficients which are empirically determined. The asymptote at $y = a$ indicates the general shoreline trend. The x-axis is drawn parallel to the asymptote and the y-axis normal to that in the landward direction. The origin should be placed at a point where the tangent to the shoreline is normal to the asymptote as shown in Figure 2.15. The fitting of this model is therefore a relatively simple and well defined process. Another useful property of the hyperbolic tangent equation is the fact that the asymptote at $y = a$ defines the downdrift edge of the beach (Moreno & Kraus, 1999), thereby eliminating the confusion of the PBSE.

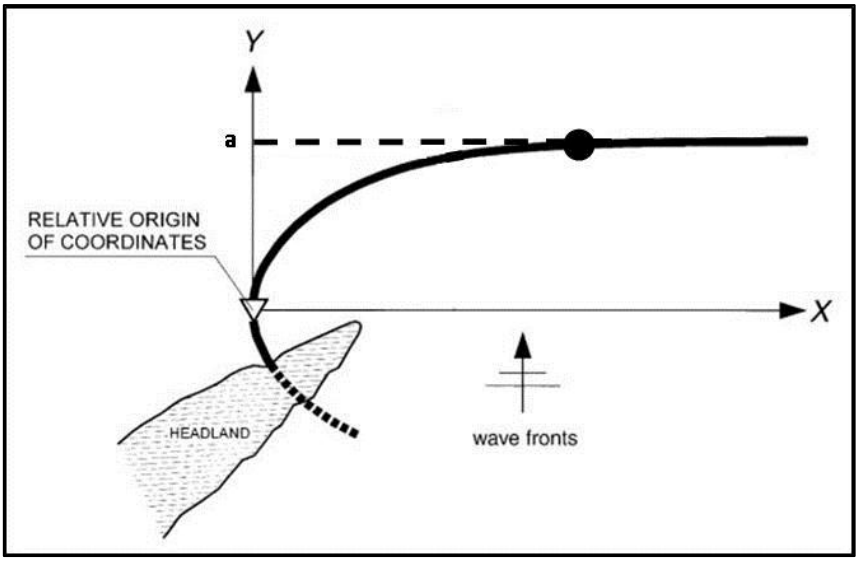

Figure 2.15: Definition sketch of the hyperbolic tangent shape model (adapted from Schwartz (2005))

Although easily applicable, the hyperbolic tangent model (like the log-spiral model) fails to place its origin at the diffraction point and to relate the bay shape to the angle of incident wave energy. It is therefore not able to test the stability of a headland-bay beach or predict the effects of changes such as varying diffraction points, e.g. the extension of a breakwater (Hsu et al., 2010).

2.6 Climate change

When considering the long-term morphology of coastlines, perhaps one of the most important factors is climate change. Climate change is caused by imbalances in the energy of the global climate which include changes in the concentration of greenhouse gases, aerosols and solar radiation (IPCC, 2007). These imbalances are driven by both natural processes and human activity.

Climate change may hold considerable impacts for the human population and environment in coastal areas. It is therefore no surprise that significant research is constantly carried out in an attempt to gauge the possible scenarios of climate change. Currently, there are two main developments on this subject, being reports by the Intergovernmental Panel on Climate Change (2007) and the Copenhagen Diagnosis (Allison et al., 2009).

The Intergovernmental Panel on Climate Change (IPCC) is a scientific body established jointly by the United Nations Environmental Programme and the World Meteorological Organisation to assess and review the scientific work on climate change. The Working Group I within the IPCC is responsible for the scientific aspects of climate change. In order to keep up with the amount of research published in this field, the IPCC publishes regular Assessment Reports (AR) to provide the world with a clear view of the current projections. The most recent report is Assessment Report 4 (IPCC, 2007), published in 2007 with AR5 due in 2013-2014.

For the future of coastal development, one of the most important consequences of climate change is sea-level rise. However, sea-level rise is not a new phenomenon. Following the last ice age approximately 21 000 years ago, the sea-level has risen by 120m and stabilised between 2000 and 3000 years ago, only to continue rising in the late 19th century. The average global rise for the 20th century is estimated at 1.7 mm yr^{-1} (Bindoff et al., 2007). Significant advances in satellite altimetry in the 1990's have allowed for a greater precision in measurements and, subsequently, the average global rise since 1993 has been estimated closer to 3 mm yr^{-1} (Bindoff et al., 2007). Furthermore, these rates are expected to accelerate in the next century.

The rise in sea-level comprises of two components; (1) the exchange of water between the sea and other sources such as ice sheets or ice caps, and (2) the thermal expansion of water. Table 2.1 contains estimates for the various contributors to sea-level rise. For the sum, the error is calculated as the square root of the sum of the squared errors (Bindoff et al., 2007).

Table 2.1: Estimates of contributors to global mean sea-level rise (adapted from Bindoff et al., 2007).

Sea-level rise (mm yr^{-1})		
Contributor	**1961-2003**	**1993-2003**
Thermal Expansion	0.42 ± 0.12	1.6 ± 0.5
Glaciers and Ice Caps	0.50 ± 0.18	0.77 ± 0.22
Greenland Ice Sheet	0.05 ± 0.12	0.21 ± 0.07
Antarctic Ice Sheet	0.14 ± 0.41	0.21 ± 0.35
Total	1.1 ± 0.5	2.8 ± 0.7
Observed	1.8 ± 0.5	3.1 ± 0.7
Difference	0.7 ± 0.7	0.3 ± 1.0

Predicting the future sea-level rise due to climate change is complex, especially when there is uncertainty in the future population, technological advances and greenhouse gas emissions. The AR4 has therefore presented a range for the possible sea-level rise for each of 6 possible emission scenarios. The 6 scenarios are briefly summarised below (IPCC, 2007):

A1: Rapid economic growth and technological advances with the world population peaking in the mid-21st century declining thereafter. Scenario A1 is divided into three groups:
- A1F1 (fossil-fuel intensive)
- A1T (non-fossil energy sources)
- A1B (balanced across energy sources)

A2: Heterogeneous world with continuously growing population, regionally orientated economic growth and slow technological advancement.

B1: The same population as in A1, but with significant advances in clean technology and emphasis on economic, social and environmental sustainability.

B2: Continuously increasing population (but slower than A2) with slower and more diverse technological development than A1 and B1.

Table 2.2 and Figure 2.16 summarise the estimates presented in AR4. These estimates are based on the results of various models and observations and do not include the effects of changes in ice sheet flow. Because of these uncertainties, a definite upper limit to sea-level rise was not presented.

Table 2.2: Estimates for sea-level rise (IPCC, 2007)

Scenario	Sea-level rise (m at 2090-2099 relative to 1980-1999)
B1	0.18 – 0.38
A1T	0.20 – 0.45
B2	0.20 – 0.43
A1B	0.21 – 0.48
A2	0.23 – 0.51
A1F1	0.26 – 0.59

Figure 2.16: Estimates for sea-level rise (Bindoff et al., 2007)

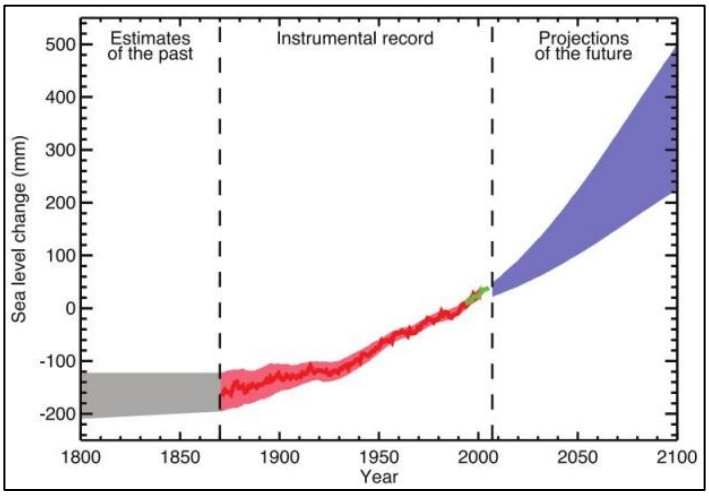

The Copenhagen Diagnosis (Allison et al., 2009) is a report which was published to synthesise the research on climate change since the IPCC's AR4. Its goal was to produce an intermediate report between the AR's and to provide science updates before the UN Climate Change Conference in

2009. Some key findings of this report regarding sea-level rise include the following (Allison et al., 2009):

- The contribution of glaciers and ice caps has increased significantly since the 1990's and may cause a rise between 18cm and 55cm by 2100
- Melting of Arctic ice and ice sheets on Greenland and Antarctica are accelerating faster than predicted by AR4 due to dynamic processes
- Satellite altimetry indicates that the sea-level has been rising at 3.4 mm yr^{-1} between 1993 and 2009

As the AR4 models did not include dynamic processes in the Greenland and Antarctic ice sheets, the Copenhagen Diagnosis concludes that projections might be almost double those suggested by AR4, leading to a range of 0.4m to 1.2m, with an upper limit of 2.0m (Allison et al., 2009). The projections for sea-level rise in the Copenhagen Diagnosis are presented in Figure 2.17.

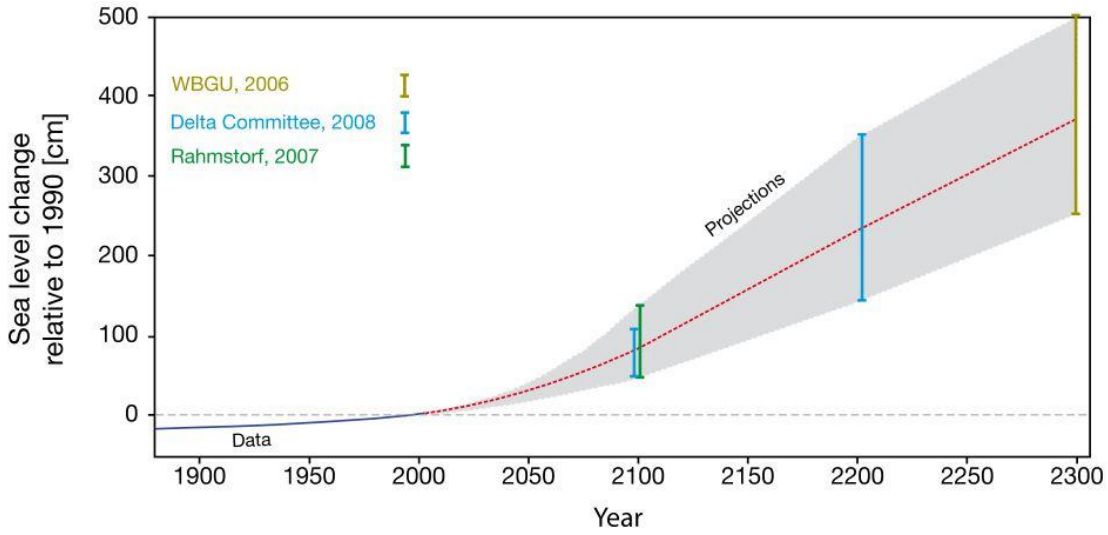

Figure 2.17: Estimates for sea-level rise projections (sources as cited in The Copenhagen Diagnosis (Allison et al., 2009))

In an analysis of 33 years of tidal data from the port of Durban, Mather et al. (2009) have given the rate of sea-level rise for the southern coast of South Africa 1.48mm/year and eastern coast of South Africa between 2.4 ± 0.29 and 2.7 ± 0.05mm. These values compare well with analyses of global sea-level rise trends from records with the same length (Mather, 2008).

Although very important, sea-level rise is not the only consequence of climate change expected to impact the coastal zone. The changes in climate patterns are affecting winds and consequently also the generation of waves.

Based on a review of multiple studies, the UK Department for Environment, Food and Rural Affairs (DEFRA) have suggested that a 10% increase in offshore wind speeds by 2115 be considered (DEFRA, 2006). Following the equations for wave generation by winds presented in the Coastal Engineering Manual (CEM, 2003), a 10% increase in wind speed results in a 17% increase in wave height under duration-limited conditions (PRDW, 2010).

Through the combination of a global circulation model and global wave model, Mori *et al.* (2010) have predicted an increase of 6-9% in the average significant wave height in the Antarctic Ocean, with a small decrease in extreme wave heights. Conversely, the waves originating from tropical cyclones are expected to experience a decrease in mean significant wave height, but an increase in maximum significant wave height. Consequently, Theron et al. (2012) have adapted an increase in extreme wave height of 6-10% by 2100 for the coast of Mozambique. A study of a dataset of tropical cyclone activity in the South-West Indian Ocean by Mavume et al. (2009) has indicated an overall increased activity in the frequency and intensity of cyclones. Furthermore, an analysis of wave data from Durban and Richards Bay by Corbella and Stretch (2012) has indicated weak increasing trends for the extreme significant wave height and storm frequency, but without statistical relevance.

Not only the wave heights, but also the wave directions are affected by climate change. In AR4, the IPCC predicts that the storm-tracks of extra-tropical storms will experience a poleward shift (IPCC, 2007). For the South-African wave climate, this results in a southerly rotation of the south-westerly waves originating from the frontal systems. Furthermore, the above-mentioned analysis by Corbella and Stretch (2012) has indicated a 0.91° increase in nearshore wave angles at Durban, suggesting an opposite rotation on the eastern coast of South Africa.

Unfortunately, the extent to which rotations in the offshore wave climate are expected to occur is not well quantified in the literature. In order to investigate the impact of changing offshore wave angles on the stability of headland-bay beaches, a hypothetical scenario was therefore derived. The rotations observed on the east coast and the poleward shift of frontal systems were combined to produce a hypothetical scenario whereby all wave conditions experience a southerly rotation in offshore wave angle. This scenario was then used to test the sensitivity of headland-bay beaches to rotations in offshore wave angles.

From the above literature, the main consequences of climate change expected to have a significant impact on the coastal zone are summarised in Table 2.3. Although trends in the intensity and frequency of storms are also expected, the effects of these changes are not considered further in this study. The extent of sea-level rise was chosen from the predictions laid out in the Copenhagen

Diagnosis. The increase in wave height was chosen as 10% by 2100, which agrees well with predictions presented above. The change in wave directions is highly uncertain and not well quantified. The scenario of a southward rotation of offshore wave directions was therefore approximated by rotating all wave conditions towards the south. This approach is not quantified by any literature, but serves as a qualitative assessment of the changes in the shoreline resulting from such a scenario. The range of rotations were kept between 1° and 2°, which are in the order of the rotations observed for the Durban wave climate (Corbella & Stretch, 2012).

Table 2.3: Summary of considered climate change effects

Climate change effect	Extent
Sea-level rise	0.8m to 1.2m, with an upper limit of 2.0m
Increased wave height	10% increase in average wave height
Changed wave direction	1°-2° southward rotation of wave directions

It is clear that climate change may hold significant implications for coastal areas. Not only sea-level rise, but also increasing wave heights and changing wave directions are causes for concern. Knowledge of the extent of the changes only becomes useful once the impact of the changes can be understood.

2.7 The impact of climate change on soft coastlines

From Chapter 2.6 insight was gained from the literature on the possible climate change scenarios affecting the coastal zone. In this chapter, possible responses caused by these scenarios will be investigated.

Sea-level rise poses a great threat to the more than 160 million people living within 1m above mean sea level. Not only loss of infrastructure, but also damage and destruction of sensitive environments such as mangrove forests and saltwater intrusion into inland freshwater water reservoirs are causes for concern. Theron (1994) summarises the probable impacts of sea-level rise into 5 main groups:

- Greater exposure to storm events
- Saltwater intrusion into freshwater systems
- Greater tidal influence
- Flooding
- Coastal Erosion

The effect of a rise in sea level on a hard, rocky coast is purely related to the slope of the shore through inundation. When soft coastlines are considered, however, other factors come into play. The impact of sea-level rise on soft, sandy coastlines can be divided into two mechanisms, being (1) inundation, and (2) erosion of the coastline (Zhang et al., 2004). The former occurs as the rising sea causes parts of the land to become flooded as the shoreline moves landward proportional to its slope. In areas where the slope of the shore is very gradual, significant areas of land may become inundated. The latter occurs by means of redistribution of sand, usually during storms (as described in Chapter 2.3). Much discussion and research has been focused on the erosion as a result of sea-level rise, some of which will be discussed in this section.

The first and most widely implemented theory on beach erosion due to sea-level rise was presented by Bruun (1954, 1962, as cited by Schwartz (1967)) and is known as the Bruun Model. The theory proposes that the rise in sea level causes sediment to be eroded from the beach face and deposited on the nearshore bottom in equal amounts. The raise in the elevation of the bottom is equal to the rise in sea level and therefore maintains a constant water depth. The consequence is thus a landward migrating shoreline (Schwartz, 1967).

The model proposed by Bruun is based on the following assumptions (Davidson-Arnott, 2005):

- A two-dimensional normal section through the shoreline is considered such that the net sediment transport is onshore-offshore and longshore transport is not included
- The profile is in the equilibrium state related to the wave climate and sediment characteristics
- The material landward of the beach is of similar characteristics and is easily erodible

A schematic diagram illustrating the Bruun Model is shown in Figure 2.18.

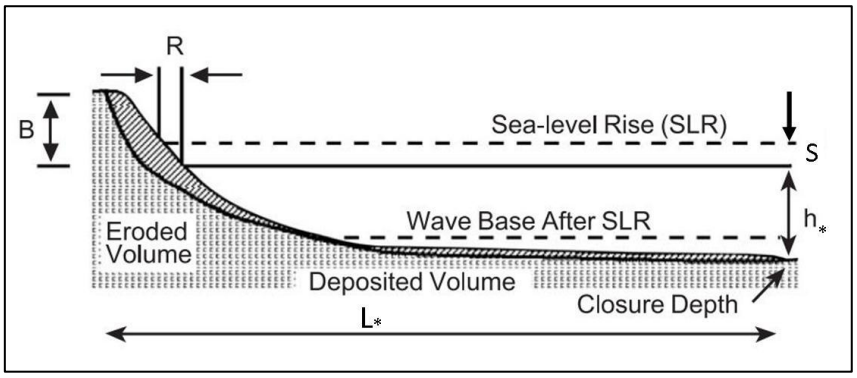

Figure 2.18: Bruun's Model for beach erosion due to sea-level rise (Cooper & Pilkey, 2004)

After some testing regarding its validity, Schwartz (1967) named the equation resulting from the theory, the Bruun Rule for beach erosion. The Bruun Rule gives the shoreline retreat (R) resulting from the sea-level rise (S) as

$$R = \frac{L_*}{B+h_*}S \tag{2.32}$$

where h_* is the threshold depth after which no significant sediment movement takes place – the depth of closure (Chapter 2.4), L_* is the cross-shore distance to h_* and B is the height of the sand source being eroded (Davidson-Arnott, 2005).

The Bruun Rule has been widely implemented since its conception, primarily due to its simplicity and ease of application. Many scientists (as cited by Cooper & Pilkey (2004) and Davidson-Arnott (2005)) have attempted to prove the model. These attempts, however, have since been challenged as proving the Bruun model is difficult due to its restrictive assumptions.

Cooper and Pilkey (2004) find many fundamental faults in the Bruun Rule which can mainly be summarised in three groups. Firstly, its assumptions are too restrictive to be found in nature. For the Bruun Rule to be applicable, no net sediment transport into the profile is allowed – whether by means of longshore, cross-shore or aeolian sediment transport. Secondly, some important variables are not considered. The concept of the depth of closure considers sediment movement only by means of the orbital motion of waves even though there are various non-wave related currents moving sediment within the nearshore area. Finally, the Bruun Rule uses out-dated relationships. The equilibrium profile is based solely on the sediment grain size when many other factors such as wave energy and sand supply also affect the equilibrium profile (Cooper & Pilkey, 2004).

Davidson-Arnott (2005) also found the Bruun Model to contain limitations, the most pronounced of which – the failure to include the dune sediment budget. Exchanges of sediment between the dune system and the nearshore occur regularly during storms or onshore aeolian transport. This limitation resulted in the proposal of a new conceptual model of coastal response to sea-level rise.

The exclusion of the dune sediment budget causes some uncertainty regarding the basic hypothesis that the eroded sediment would be deposited in the nearshore. Using the same initial assumptions as the Bruun Model (with the added assumption of a foredune system landward of the beach), Davidson-Arnott (2005) proposed the Robert Davidson-Arnott (RD-A) model with the following hypotheses:

- Sea-level rise causes both the beach and foredune to be eroded and the junction between the two to move landward and upward with the rise in sea level.

- The outer part of the nearshore is eroded and the sediment is moved landward. The depth of closure therefore also moves landward and upward with the rise in sea level.
- Sediment is eroded from the foredune and is deposited landward in equal amounts, thereby resulting in a net landward migration of the foredune of which the volume remains constant.

A schematic diagram of the RD-A Model is presented in Figure 2.19.

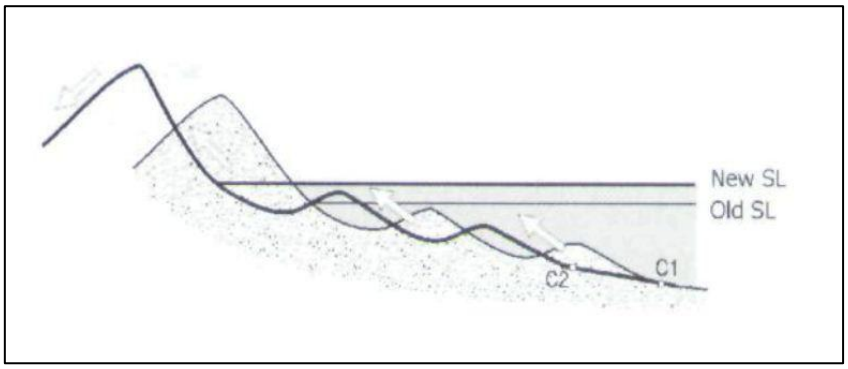

Figure 2.19: The RD-A Model for coastal response to sea-level rise (Davidson-Arnott, 2005)

Although the Bruun Model has received much criticism, a recent study by Mather (in submit, as cited by Mather and Stretch (2012)) has provided some confidence in the applicability of the Bruun Rule for the South African coast. In this study, the Bruun Rule was used to predict the coastal retreat caused by historical sea-level rise. The predictions were then compared to retreat observed by measuring the difference between 14 successive historical shoreline positions (paleoshorelines). The study indicated that the Bruun Rule could predict the setback caused by sea-level rise within 10% accuracy.

A study regarding the relative impact of sea-level rise on pocket beaches as opposed to exposed coasts has also been done. By means of comparing the expected retreat due to sea-level rise with historical retreat on 25 pocket beaches and 90km of exposed coastline in southern France, Brunel and Sabatier (2009) found that sea-level rise has a more pronounced effect on pocket beaches than on exposed coasts. Even though the retreat on the exposed coasts is significantly larger, it was found that only roughly 8% is directly due to sea-level rise while the rest this is said to be due to other processes such as longshore and cross-shore currents. In pocket beaches which are relatively protected from wave action and other erosive processes, the direct effect of sea-level rise constituted 40% of the shoreline retreat.

It should be noted, however, that the retreat due to sea-level rise was calculated by the concept of active flooding – an estimation which considers only inundation and the landward migration of the dune defence structure. The impact of sea-level rise goes far beyond the limits of inundation, as a

rise in sea level also exacerbates the erosive processes (Brunel & Sabatier, 2009). In order to gauge the full effect of sea-level rise on sandy coasts, Brunel and Sabatier (2009) therefore suggest that the future position of shorelines be calculated by integrating the rise in sea level with the processes eroding the shore.

The effects of the changes to wave climate due to the rotations and increased wave heights are very site-specific. As opposed to sea-level rise, local sheltering from breakwaters and headlands causes the effect of a changed wave climate to vary along the coastline. The local effect of changes in wave height and incidence angle will therefore be assessed in terms of their effect on sediment transport. The effects are qualitatively assessed according to the modified Kamphuis equation presented in Chapter 2.4. For convenience, the equation is reproduced here:

$$S = 63\,433\, X_{Kamphuis}\ (m^3/year) \tag{2.21}$$

where

$$X_{Kamphuis} = \frac{1}{(1-p)\rho_S} . \frac{\rho}{T_p} L_0^{1.25} H_{bs}^2 (\tan \alpha_k)^{0.75} . \left(\frac{1}{D_{50}}\right)^{0.25} (\sin 2\theta_b)^{0.6} \tag{2.22}$$

The Kamphuis factor ($X_{Kamphuis}$) is indicated to have a second-order dependence on the wave height. The sediment transport is therefore very sensitive to the nearshore wave height. A local increase of 10% should result in a 21% increase in sediment transport magnitude.

Equation 2.22 also indicates a dependence on the incident wave angle (θ_b). If a normal incidence angle of 2° is assumed, a 1° rotation in the nearshore angle could cause a 27% increase in transport magnitude. However, the rotation of offshore wave conditions does not translate linearly to the nearshore. Rotational processes such as refraction and diffraction may significantly reduce the rotational effect experienced in the nearshore.

The wave climate change effects are therefore extremely site specific. The only method to assess the impact of such changes is through a detailed investigation at the site under consideration. This can be achieved by means of a physical or numerical model. The modelling of shoreline morphology is therefore discussed in the following chapter.

2.8 Modelling of shoreline morphology

In coastal applications, mathematical models are used to describe coastal processes and predict shoreline change. These mathematical models are incorporated into numerical models thereby enabling fast and accurate calculation. However, numerical models are merely computerised versions of our knowledge of coastal processes. Any uncertainty involved in the fundamental

equations or empirical relations used to describe the processes, is therefore reflected in the model results.

The complexity arising from the interaction of various coastal processes is far too great to be mathematically described with absolute accuracy. Physical models which fundamentally include all processes are therefore often used. However, when long-term large-scale scenarios are investigated, physical models are not feasible due to the scale effects caused by the use of large spacial and time scales. Long-term morphological behaviour in the coastal zone is therefore mainly modelled numerically.

Coastal mathematical models can be divided into two main categories, being: (1) process-related models; and (2) behaviour-related models. Process-related models aim to model the morphology by describing the relevant coastal processes in detail. These processes are presented in sub-models which are fed back into the main model in order to include the interaction between processes (van Rijn, 1998). The process-related approach is mainly used in cross-shore models (such as 2D profile models) and area models (both 2D and 3D). Although this approach allows for relatively accurate modelling, significant computing time is required for these simulations when the model includes complex processes or covers a large spatial or time scale.

As described in Chapter 2.7, shoreline morphology is caused by the complex interaction between hydrodynamic and sediment transport processes. This does not, however, necessitate the use of a process-related model to obtain accurate results. Behaviour-related models exclude computationally demanding details and describe the behaviour of the coastal system based on simple relationships which reflect the phenomena on a larger scale (van Rijn, 1998). Processes are mainly described by parameterised functional relationships and coefficients. It is therefore essential that long-term data are available for the calibration of these parameters (van Rijn, 1998). Behaviour-related models may include statistical models, empirical models (such as the bay shape models presented in Chapter 2.5) and equilibrium models.

Shoreline models are one-dimensional behaviour-related models used for the modelling of long-term coastal morphology, also commonly referred to as *one-line models*. The one-line theory is based on the fundamental assumption that the equilibrium cross-shore profile remains constant in the long term, apart from short-term changes caused by storms or seasonality in the wave climate (Hanson, 1989). This assumption implies that no cross-shore sediment transport is accounted for and only longshore transport is considered (WL|Delft-Hydraulics, 2005).

The second important assumption is that the longshore transport is limited to the profile bounded by the active height at the top and the closure depth at the bottom. Erosion or accretion of the coastline is therefore caused by gradients in the longshore sediment transport, resulting in a landward or seaward migration of the equilibrium profile. The one-line theory is summarised in Figure 2.20.

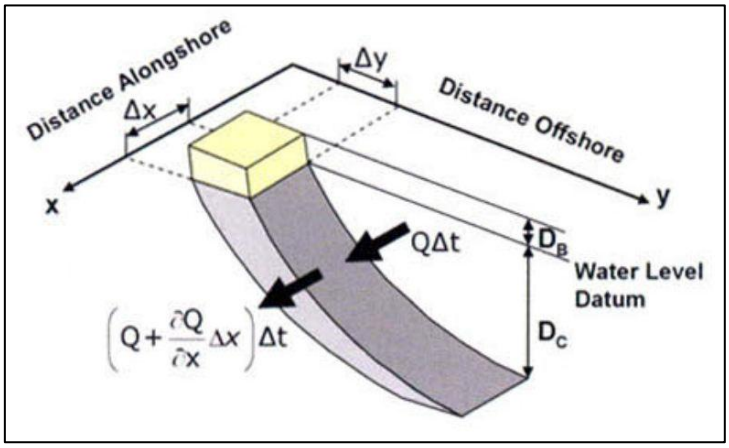

Figure 2.20: Definition sketch for one-line theory (Hanson & Kraus, 2011)

In Figure 2.20, D_B refers to the height of the active profile above the water level datum and D_C is the closure depth. Q is the rate of longshore sediment transport. For the simplified case of a straight profile, a seaward movement of the coastline of ΔY would require a net imported volume of:

$$\Delta x \Delta Y d$$

where $d = D_B + D_C$, the total active profile height. The local balance at the section of coast defined by Δx is found by equating the accumulated sediment and the net imported sediment, yielding the continuity equation (Bosboom & Stive, 2012):

$$\frac{\partial y}{\partial t} + \frac{1}{d}\frac{\partial Q}{\partial x} = 0 \tag{2.33}$$

Since the sediment transport (Q) is largely influenced by the angle of wave attack relative to the coastline, φ, Equation 2.33 can be rewritten as (Bosboom & Stive, 2012):

$$\frac{\partial y}{\partial t} + \frac{1}{d}\frac{\partial Q}{\partial \varphi}\frac{\partial \varphi}{\partial x} = 0 \tag{2.34}$$

where $\partial Q/\partial \varphi$ represents the effect of the angle of wave attack on the magnitude of sediment transport and can be calculated from any longshore sediment transport formulation. After some time, the local coastline may have deviated from its original position and rotated an angle of dY/dx.

This rotation changes the angle of wave attack (φ) and introduces a nonlinear term into Equation 2.34:

$$\frac{\partial y}{\partial t} + \frac{1}{d}\frac{\partial Q}{\partial \varphi}\frac{\partial^2 Y}{\partial x^2} = 0 \tag{2.35}$$

The instantaneous position of the coastline is thus described in Equation 2.35 as a function of the active profile height, the angle of wave attack and the rotation of the shoreline.

2.9 Conclusions from the literature

From Chapters 2.1 and 2.2 it was learnt that significant changes to the offshore wave climate occur due to a number of deep sea and nearshore processes. These processes affect the waves such that the nearshore wave climate is very different from the offshore climate.

In Chapters 2.3 and 2.4, the nearshore wave climates were shown to drive coastal processes, such as currents, which are responsible for the movement of sediment and the stability of the beach. Changes to the nearshore wave climate are therefore expected to alter the coastal processes and, consequently, the sediment transport regime.

Chapter 2.5 provided a description of headland-bay beaches (HBB's) which are prominent along the South African coast. These bays are often areas of high economic value. From the literature, it was learnt that the planforms of HBB's are equilibrium shapes based on the local nearshore wave climates and consequent sediment transport regimes.

In Chapter 2.6, a review of literature regarding climate change was presented. From this review, a number of consequences of climate change which could affect the transformation of offshore waves into the nearshore were identified. These climate-change effects were identified as:

- Sea-level rise
- Increased average wave heights
- Changing offshore wave directions

Chapter 2.7 presented an investigation into the possible impacts of the above effects on a soft coastline. It was found that not only direct inundation and erosion from sea-level rise, but also the secondary effects on the wave climate and sediment transport need to be considered. Furthermore, from a sensitivity analysis of a sediment transport formula, it was shown that the sediment transport is sensitive to changes to the wave direction and wave height. Changes to the nearshore wave climate are therefore expected to destabilise the planforms of HBB's, possibly leading to erosion.

These changes are, however, site specific and modelling is needed to gauge the impacts resulting from these effects.

In Chapter 2.8, the modelling of shoreline morphology was discussed. It was found that the large time and spatial scales did not allow for physical modelling and that numerical modelling was needed. Empirical models were found to be applicable and cost-effective when modelling scenarios of large spatial and time scales involved with the investigation of long-term climate-change effects on a large-scale bay.

In this study the impacts of the climate-change effects on a headland-bay beach are investigated. A study site for this investigation is chosen and presented in Chapter 3. Based on the specific characteristics of the chosen site, a hypothesis is formulated. Taking into account that which has been learnt from the review of literature, the modelling approach to test the hypothesis is presented in Chapter 4. A summary of the available data for the modelling is also included.

3 Description of the selected site

3.1 Site characteristics

Mossel Bay[4] is located in the Eden District Municipality on the southern coast of South Africa. It is a headland-bay beach located in the lee of Cape St. Blaize. The position of the study area on the South African coast is shown in Figure 3.1a.

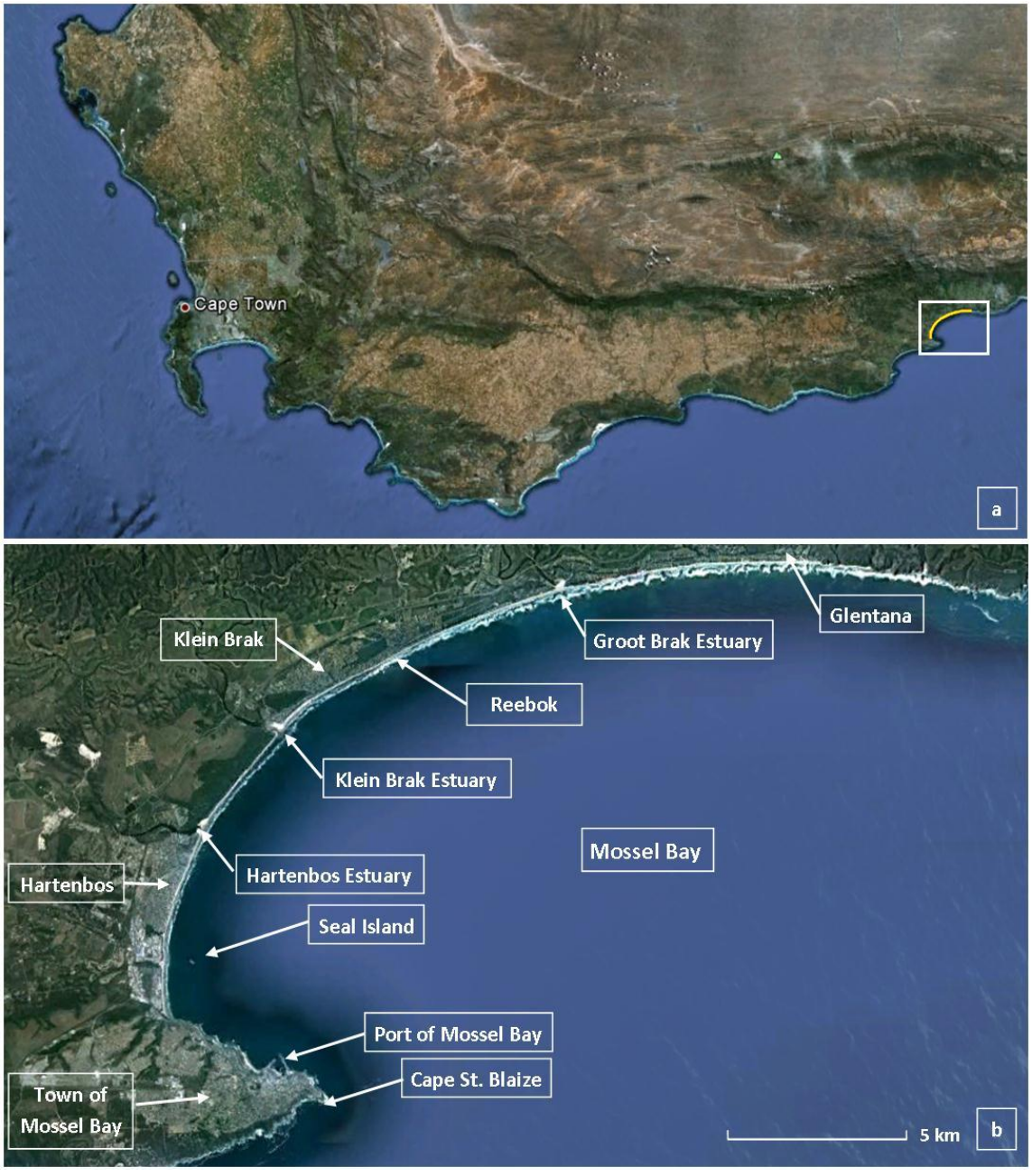

Figure 3.1: Mossel Bay locality map (Google Earth)

[4] Mossel Bay is the name of both the bay located in the lee of Cape St. Blaize and the town situated on the headland. In order to avoid confusion, this thesis will refer to the town as "the town of Mossel Bay". The name "Mossel Bay" therefore always refers to the headland-bay beach.

In Figure 3.1b, a detailed map of the bay indicates the positions of towns, river mouths and the Port of Mossel Bay. In the west, Cape St. Blaize separates Mossel Bay from Vlees Bay, another headland-bay beach. In the east, the bay is bounded by a rocky outcrop east of Glentana. Seal Island is a small island (roughly 160x60m) located in the far western corner of the bay.

The characteristic headland and plan shape of a headland-bay beach are clearly visible. In Figure 3.2, the planform of the bay is shown together with the planforms of 5 other bays on the south-western coast of South Africa. Note that only St. Helena Bay has been rotated and mirrored, since it is located on the western coast and therefore has a completely different orientation. To indicate the similarity in the shapes, the bays are scaled to match the size of Algoa bay. The scales are indicated in the figure.

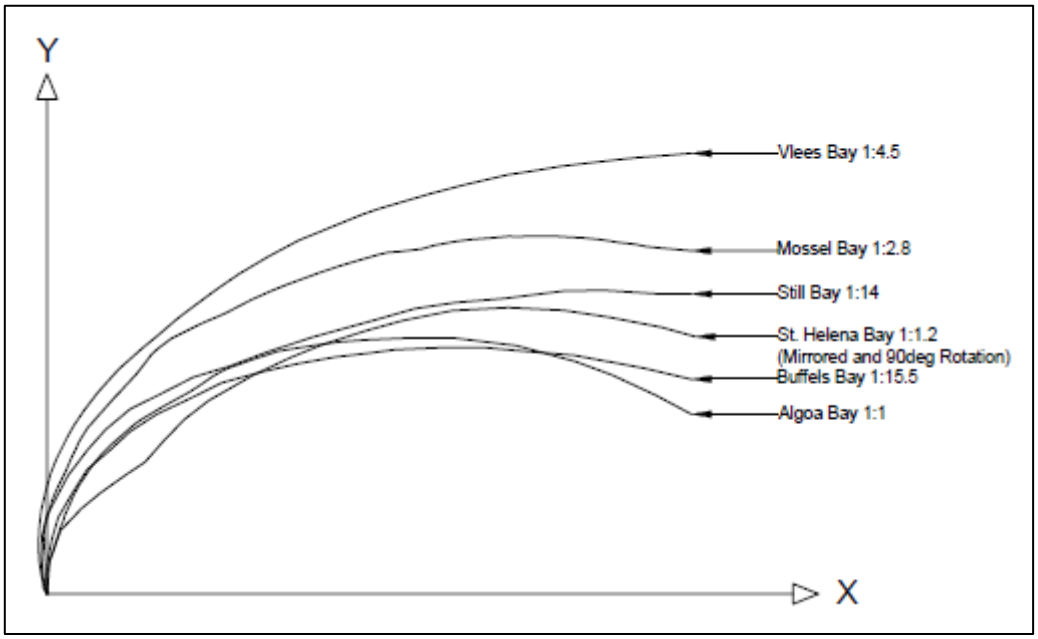

Figure 3.2: Planforms of headland-bay beaches on the south-western coast of South Africa

In Figure 3.3, a map depicting the geology of the greater Mossel Bay region is shown. The rocky headland of Cape St. Blaize is formed by east-west stretching sandstone and shale of the Table Mountain and Bokkeveld Groups. North of this formation, an east-west rock formation stretches offshore below the sediments and consolidated deposits (Melis & Du Plessis, 1990). An outcrop of this formation is found in the form of Seal Island.

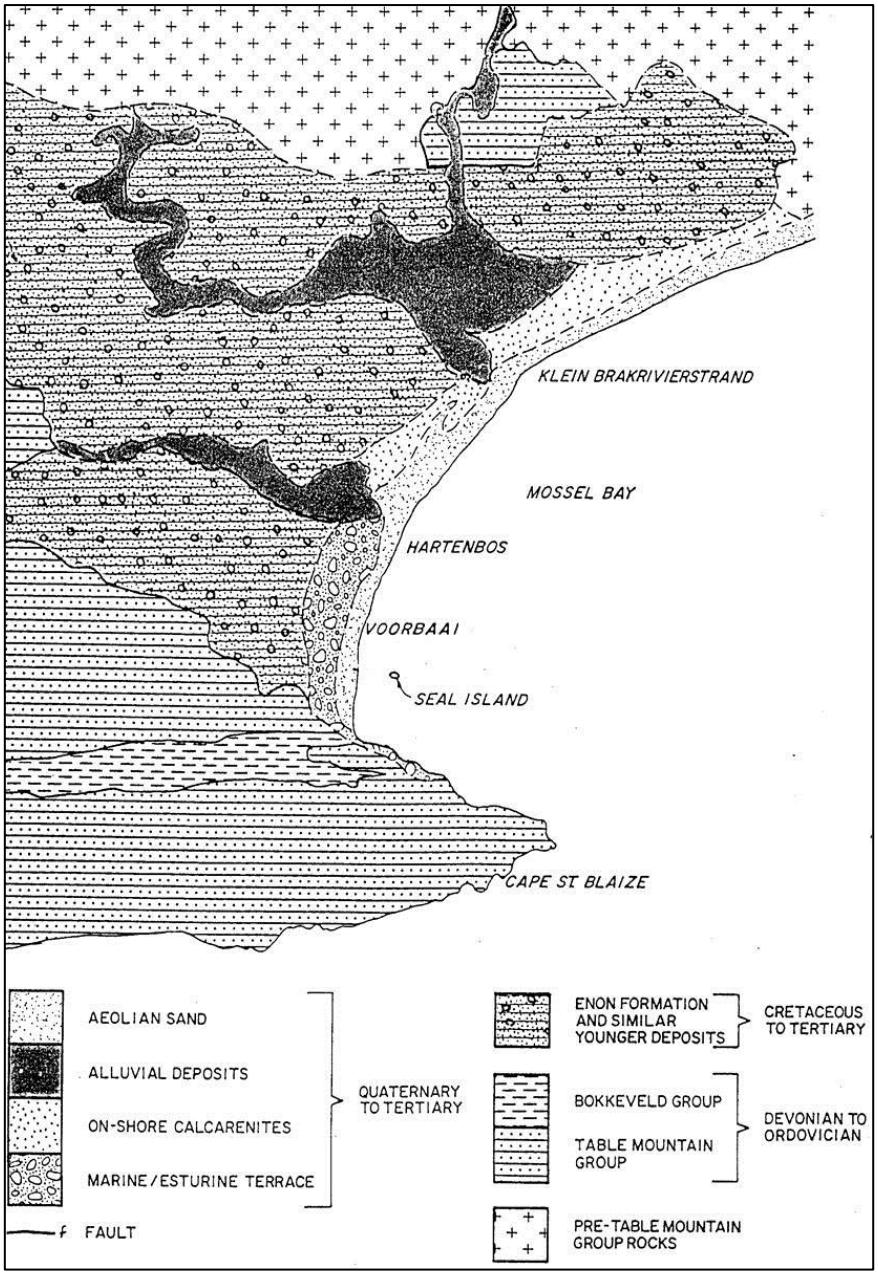

Figure 3.3: Regional geology of Mossel Bay (Melis & Du Plessis, 1990)

A relatively thin, sandy layer of unconsolidated sediment stretches between 20km and 30km offshore of the Mossel Bay coast. Beneath this layer, calcareous cemented sandstone extends to the shore to form reefs which are mostly exposed in the intertidal range. This layer may extend further landward beneath the stable, vegetated dune ridge found along the most of the Mossel Bay periphery (Melis & Du Plessis, 1990). Figures 3.4 and 3.5 are photographs taken at the stretch of coast between Hartenbos and Klein Brak and at Reebok, respectively. In these photographs (taken at low water during spring tide) the sandstone reefs are clearly visible.

Figure 3.4: Intertidal sandstone reefs visible between Hartenbos and Klein Brak

Figure 3.5: Intertidal sandstone reefs visible at Reebok

The presence of the reefs in the intertidal zone is significant due to a number of factors. Since the reefs take up a significant part of the profile, less sediment is available for cross-shore and longshore transport. Furthermore, the location of the reefs is such that during low tide, waves do not reach the sediment landward of the reefs. Moreover, at high tide, the reefs are submerged and a significant amount of wave energy is dissipated on the reefs through wave breaking. The presence of coastal protection works along the coast at Hartenbos suggest that, even with the presence of the reefs, storm waves are nevertheless able to reach the dunes at extreme water levels and do cause short term erosion. The overall effect is thus a partial protection of the beach face located directly behind the reefs, but not a protection against erosion during storm conditions.

When inspecting the plan shape of Mossel Bay, it becomes apparent that the periphery is not smooth, but contains kinks at a few locations. Figure 3.6 indicates the locations of the reefs and the kinks. The kinks are clearly visible at the locations where reefs are not present. Instead of allowing the bay to reach the smooth HBB shape, the reefs are causing local interference with the erosive processes which form headland-bay beaches. The effect is therefore that the coast angle deviates slightly from the equilibrium shape expected for HBB's where the reefs are present.

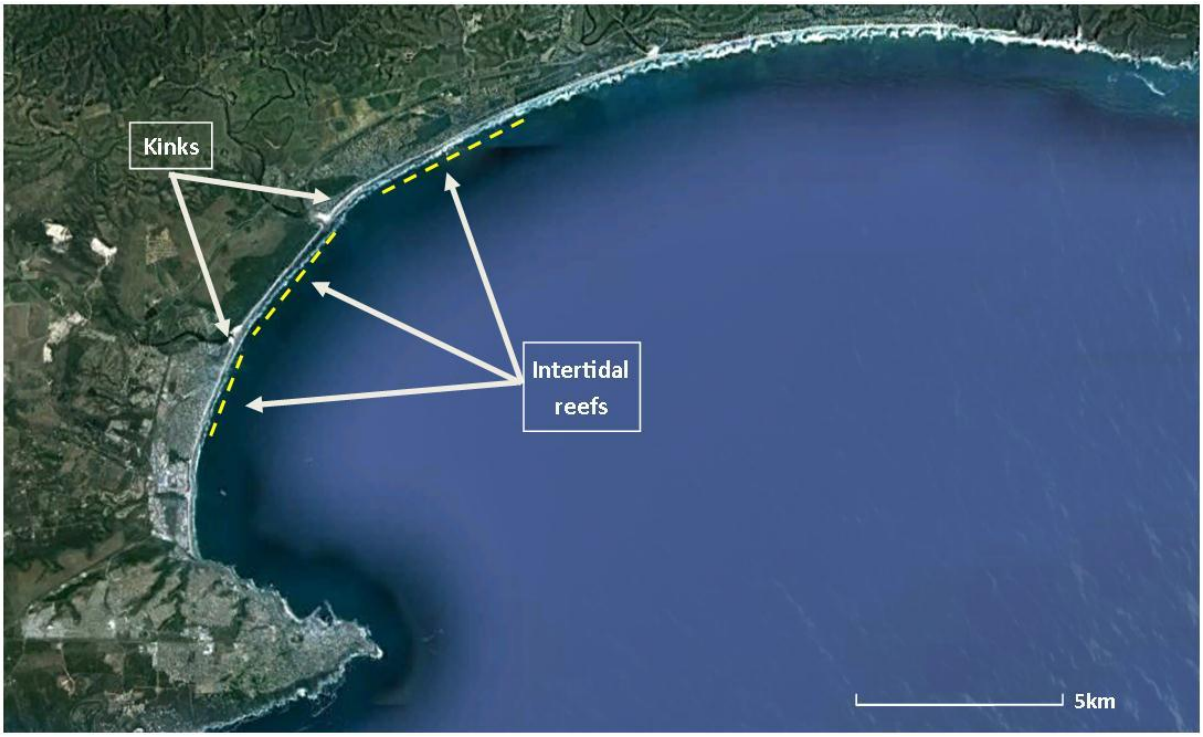

Figure 3.6: Locations of reefs and kinks in Mossel Bay (GoogleEarth)

3.2 Hypothesis

From the literature review, headland-bay beaches such as Mossel Bay are expected to be sensitive to the nearshore wave climate, from which they obtain their planforms. Changes to the nearshore

wave climate could alter the local sediment transport regime and destabilise the planform of Mossel Bay.

Since the refraction of waves from offshore is a function of the water depth, changes in the water level are expected to affect the refraction of waves into Mossel Bay. The effect on wave refraction is expected to be such that the angles of waves in the nearshore are altered, thereby changing the nearshore wave climate. Direct changes to the nearshore wave climate are also expected to occur due to changes in offshore significant wave height and offshore wave direction.

It is therefore hypothesised that the nearshore wave climate will be affected by (1) sea-level rise; (2) increasing wave heights; and (3) changing offshore wave angles, such that the sediment transport regime in the bay is altered. The altered sediment transport regime is expected to cause instability in the planform of Mossel Bay. A further site-specific hypothesis is that the presence of the intertidal reefs is important to the current shape of Mossel Bay.

In the following chapter, the modelling approach adapted in this study to test these hypotheses is discussed.

4 Methodology

4.1 Modelling Approach

Following from the review of literature in Chapter 2 and the hypothesis in Chapter 3.2, the following effects of climate change were identified to be investigated in this study:

- Sea-level rise,
- Increased wave height
- Southward rotation of offshore wave directions

The impact of each of the above effects on the stability of the planform of Mossel Bay was investigated. Since the predictions for sea-level rise (SLR) vary significantly, a range of possible scenarios were tested. These were a total rise of 0.5m, 1.0m and 2.0m in the next 100 years. For the increased wave heights, a universal increase of 10% was assumed. This value falls well within the limits proposed by other authors. The southward rotation of offshore wave directions is not well quantified in the review of literature. The two scenarios of a 1 degree and 2 degree angular rotation of all wave directions were therefore considered. The total set of scenarios is presented in Table 4.1.

Table 4.1: Set of climate change scenarios

Scenario	Description
SCN1	Linearly increasing sea-level from +0m MSL to +0.5m MSL
SCN2	Linearly increasing sea-level from +0m MSL to +1.0m MSL
SCN3	Linearly increasing sea-level from +0m MSL to +2.0m MSL
SCN4	Wave height increase of 10% from 2010 onwards
SCN5	1° southward rotation of offshore wave directions
SCN6	2° southward rotation of offshore wave directions

Due to the advantages in computational runtime, a one-dimensional coastline model was chosen to simulate the stability of the bay under a changing climate. Relatively quick model runs allowed for 100 year simulations, which correspond well to the time scales of climate change predictions. Although cross-shore processes are not included in the model, the changes to the sediment transport regime (as hypothesised) causing long-term changes in the bay shape are primarily confined to longshore sediment transport. The one-line model was therefore assumed to be sufficient for this study.

The chosen model is UNIBEST, which is based on the one-line theory described in Chapter 2.8. A detailed description of UNIBEST follows in Chapter 6. The UNIBEST modelling software is not open-source. The author was granted access to use the model under the licence of the Council for Scientific and Industrial Research (CSIR).

The coastline model requires a nearshore wave climate as input. This climate is expected to show significant variation along the bay periphery due to the sheltering effect of the headland. A detailed wave transformation model was therefore used to calculate the nearshore climates at positions along the 10m depth contour inside Mossel Bay. The chosen wave model is the widely-used open-source model, SWAN, developed at the Delft University of Technology, in Delft, the Netherlands. A detailed description of SWAN is presented in Chapter 5 and Appendix A. SWAN was operated within the open-source shell of Delft3D, a suite of modelling software developed by Deltares in Delft, the Netherlands.

The two numerical models were chosen primarily due to the fact that they were both developed by the same institution. The software has been developed such that the coupling between the two models is achieved with relative ease. Moreover, the author visited the Technical University in Delft on a three month exchange where a practical modelling experience with UNIBEST and Delft3D was gained as part of a Master's course in coastal dynamics.

For the investigation of the SLR effects, a series of wave computations were made at different water levels. For each water level, the wave model would produce nearshore wave climates along the bay periphery. For each SLR scenario, the ultimate water level after 100 years was reached in 5 increments, spaced 20 years apart. The increments were chosen such that – to a certain extent – the rise in sea-level was gradual, while keeping the number of runs realistic. The effect of an accelerating rate of SLR was not considered. The water levels for each scenario and year range are presented in Table 4.2.

Table 4.2: Scenarios for sea-level rise

Year	1980-2010	2010-2030	2030-2050	2050-2070	2070-2090	2090-2110
SCN1	0.0m	0.1m	0.2m	0.3m	0.4m	0.5m
SCN2	0.0m	0.2m	0.4m	0.6m	0.8m	1.0m
SCN3	0.0m	0.4m	0.8m	1.2m	1.6m	2.0m

For the scenario of an increased wave height, a SWAN computation was done in which the offshore wave heights were increased by 10%. The wave periods and directions were kept constant. For the

southward rotation of offshore wave directions, all wave angles were rotated towards the south (180° according to the nautical convention). South-westerly waves therefore experienced a decrease in offshore wave angle while easterly wave angles were increased.

When two numerical models are coupled to achieve a final result, consideration needs to be given to the uncertainty produced by such a coupling. Any uncertainties in the input parameters of a model are also reflected in the output thereof. For the wave transformation model, uncertainties may be found in input parameters such as the offshore wave data, wind data or bathymetrical data. The output of the wave model is then used to represent the nearshore wave climate used as input for the coastline model. Any uncertainty from the wave model is therefore carried forward into the coastline model.

The coastline model is a one-dimensional model which only considers the longshore transport in the midst of a very complex hydrodynamic zone. From the literature review, it is also evident that further uncertainty is found in the calculation of longshore sediment transport. Considering the above, it should be expected that the model results contain significant uncertainty.

Especially in sediment transport modelling where accurate calibration data is very rare, the model results should be interpreted qualitatively. Although quantitative results are not necessarily obtained, valuable insight is gained into coastline trends caused by the climate change effects considered.

In Chapter 4.2, a summary of available data is given. Subsequently, Chapters 5 and 6 present the model descriptions, setup, calibration and results of the wave transformation model and coastline model, respectively. The final results are presented in Chapter 7. The conclusions of this study are presented in Chapter 8 where some recommendations are also made.

4.2 Available data

4.2.1 Tides

The South African coast experiences semi-diurnal tides with a range of approximately 2.4m. The tide at Mossel Bay is described in Table 4.3 (SANHO, 2012). The reader is referred to the Nomenclature section for a description of the acronyms used.

Table 4.3: Tide table for Mossel Bay (SANHO, 2012). Values are in metres above chart datum (CD=LAT).

LAT	MLWS	MLWN	ML	MHWN	MHWS	HAT
0	0.26	0.88	1.17	1.46	2.10	2.44

4.2.2 Waves

The most severe wave conditions along the southern African coast occur along the south-western and southern coasts of South Africa. It is along this section of coast where the study site is located, with Mossel Bay situated in the lee of Cape St. Blaize.

The southern African wave climate is mainly generated by three synoptic patterns. Cold frontal systems originating from the Atlantic generate the most of the waves along the South African coast, with high waves occurring along the western and south-western coasts. Cut-off low systems primarily cause high waves along the southern and eastern coasts while waves originating from occasional tropical cyclones generate high waves on the east coast (Rossouw & Theron, 2009).

Significant seasonality is found in the South African wave climate. The winter months are characterised by swell from the south-westerly quadrant with large wave heights and long periods. These waves are generated by the cold frontal systems migrating north-eastward along the coastline. In the summer months, the cold frontal storm tracks shift southward. The wave climate is still dominated by south-westerly waves, but wave heights are generally smaller with shorter wave periods. Cut-off lows can generate high southerly to easterly waves and occur mostly in the spring and autumn with some in the winter months (Singleton & Reason, 2007). A wave rose for the location roughly 85km south of Cape St. Blaize is presented in Figure 4.1.

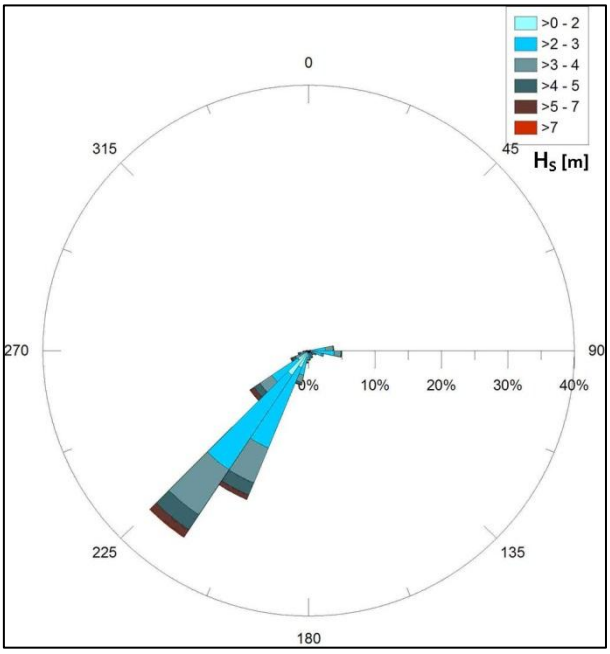

Figure 4.1: Wave rose from offshore data (compiled from full dataset)

The rose was constructed from a 10 year wave dataset obtained from the United States National Centres for Environmental Prediction (NCEP). The dataset covers the period from January 1997 to

June 2008. The wave parameters do not reflect real measurements, but rather wave conditions calculated from the results of a global scale numerical climate model, WAVEWATCH III. This data is referred to as *hindcast* data. To indicate the seasonality found in the wave climate, seasonal wave roses are shown in Figure 4.2. Note that the scales of these figures differ.

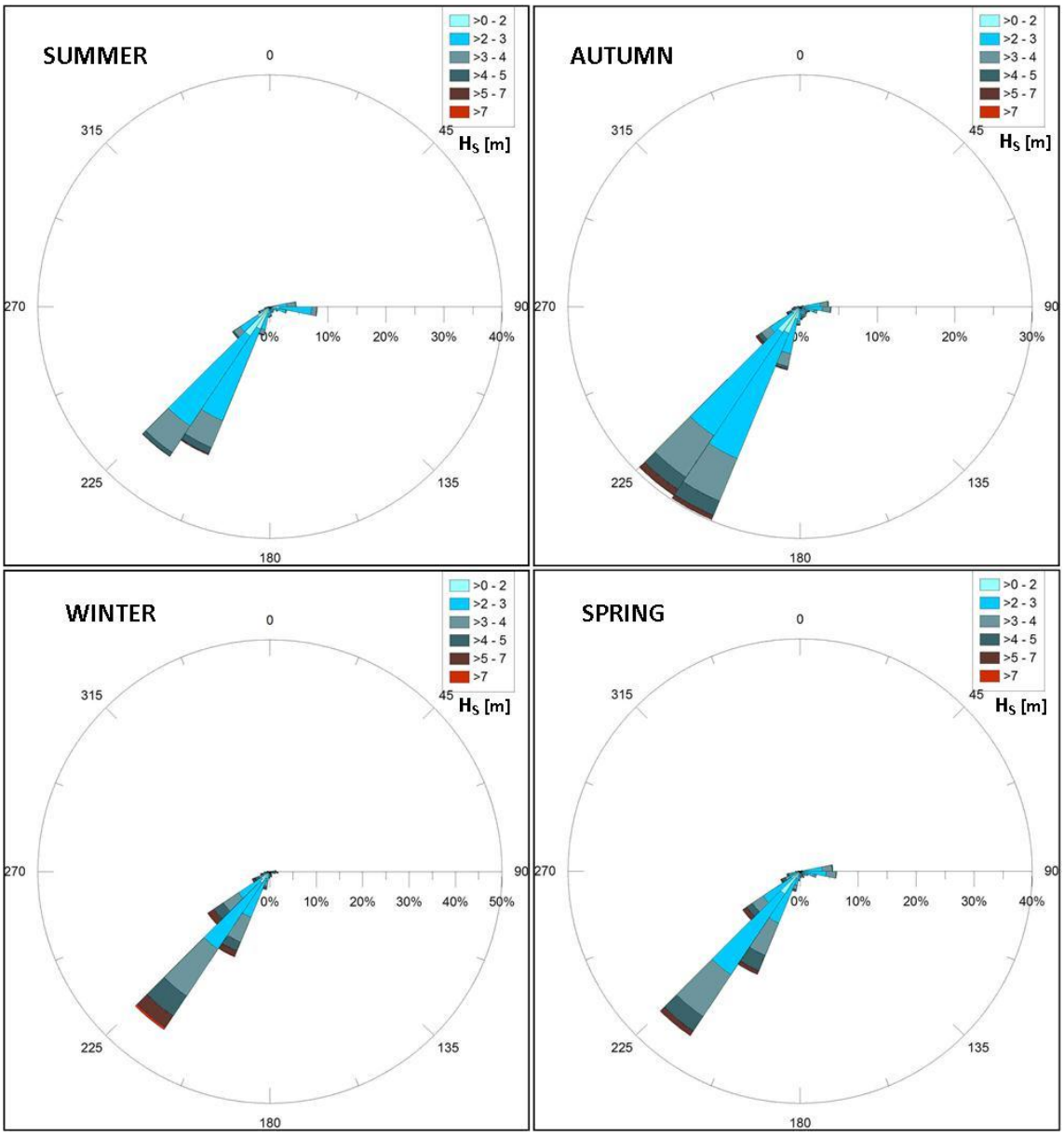

Figure 4.2: Seasonal wave roses from offshore data

The wave conditions inside the bay are constantly measured by a non-directional WAVERIDER buoy which is operated by the CSIR. A set of directional wave data from a S4DW wave buoy was also available for the period from April 1997 to February 2000 (PRDW, 2001). Unfortunately, due to magnetic disturbances and difficulties associated with underwater construction, the accuracy of the directional measurements is questionable. The locations of the two measurements are indicated in Figure 4.3.

Figure 4.3: Location of nearshore wave measurements (Google Earth)

4.2.3 Wind

Together with the set of offshore wave data, hindcast wind data was also available from NCEP for the same period. Figure 4.4 presents the wind rose constructed from the 10 years of hindcast wind data.

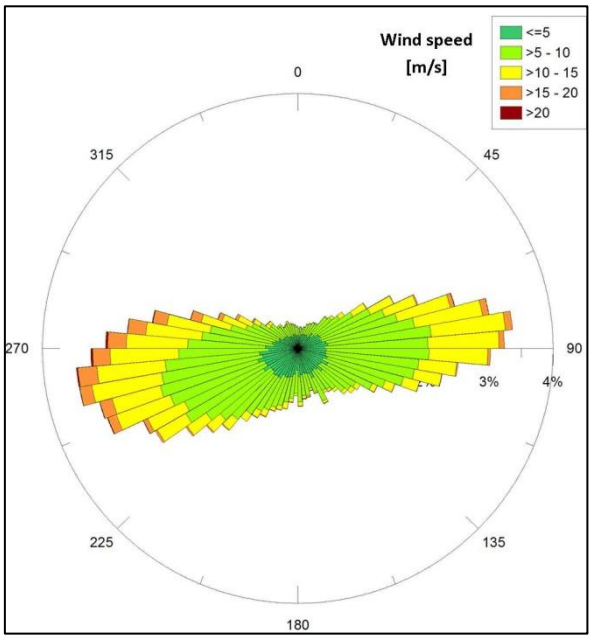

Figure 4.4: Wind rose from offshore data (compiled from entire dataset)

The following local wind datasets were also available:

- Daily average wind speed and direction measured at Mossel Bay by the South African Weather Service
- Hourly average wind speed and direction measured at Seal Island for the period of March 1998 to August 2000 (PRDW, 2001)

The locally measured wind speeds are generally lower than the offshore hindcast wind data. The directions do not correlate well, probably due to the local effects of the land and the presence of Cape St. Blaize.

4.2.4 Sediment characteristics

Sediment datasets from beach sampling in the late 1980's and early 1990's are available for Mossel Bay. The median and 90th percentile particle diameters are summarised in Table 4.4. The 1988 and 1990 sieve analyses were carried out by the CSIR and were obtained from Laurie Barwell (Barwell, Pers. Comm., 2012). The 1996 sieve analyses were obtained from published reports (CSIR, 2000).

Table 4.4: Summary of the existing particle size data for Mossel Bay

	Hartenbos		Klein Brak		Groot Brak	
	D_{50}	D_{90}	D_{50}	D_{90}	D_{50}	D_{90}
1988	238	365	350	504	-	-
	-	-	300	453	-	-
	-	-	281	432	-	-
1988 Average	238	365	310	463	-	-
1990	257	367	363	564	313	403
	228	309	388	660	278	367
	265	361	370	506	301	368
	275	403	333	456	340	424
1990 Average	256	358	364	541	306	386
1996 (Average)	341	435	462	608	398	543
Overall Average	278	386	378	537	352	465

The median particle sizes indicate medium-sized sediment grains. The particle size distribution indicates a slight prevalence of smaller particle sizes in the area more sheltered from the prevailing south-westerly swell (Hartenbos). Larger particle sizes are found in the more exposed sections of the bay (Klein Brak and Groot Brak).

4.2.5 Sediment budget

A very important aspect of shoreline modelling is that of the local sediment budget. Since beaches are in often in a state of *dynamic* equilibrium, the overall stability is determined by the volume of sediment entering and leaving the system. Small changes in sediment supply or demand can therefore significantly affect the long-term stability of a coastline.

The primary supply of sediment to the southern coast of South Africa is by means of fluvial deposits. The greatest contributions are deposited through the estuaries of the Gouritz, Gamtoos and Sundays

rivers during floods (Kapp, Prestedge & Retief, 1988). Figure 4.5 indicates the position of the Gouritz river mouth in relation to Mossel Bay.

Due to the south-westerly dominance in the southern African wave climate, sediment is generally shifted east- and northwards along the South African coast. The deposits from the Gouritz River are transported towards Visbaai, Vleesbaai and ultimately, Mossel Bay. Since the plan shapes of these bays are generally in equilibrium, significant net sediment transport mostly occurs only during abnormal wave conditions or when there is an oversupply of sediment in the bay. Any possible sediment transported from Vleesbaai toward Mossel Bay would be further suppressed by a rocky stretch of roughly 8km between the bays (Kapp, Prestedge & Retief, 1988).

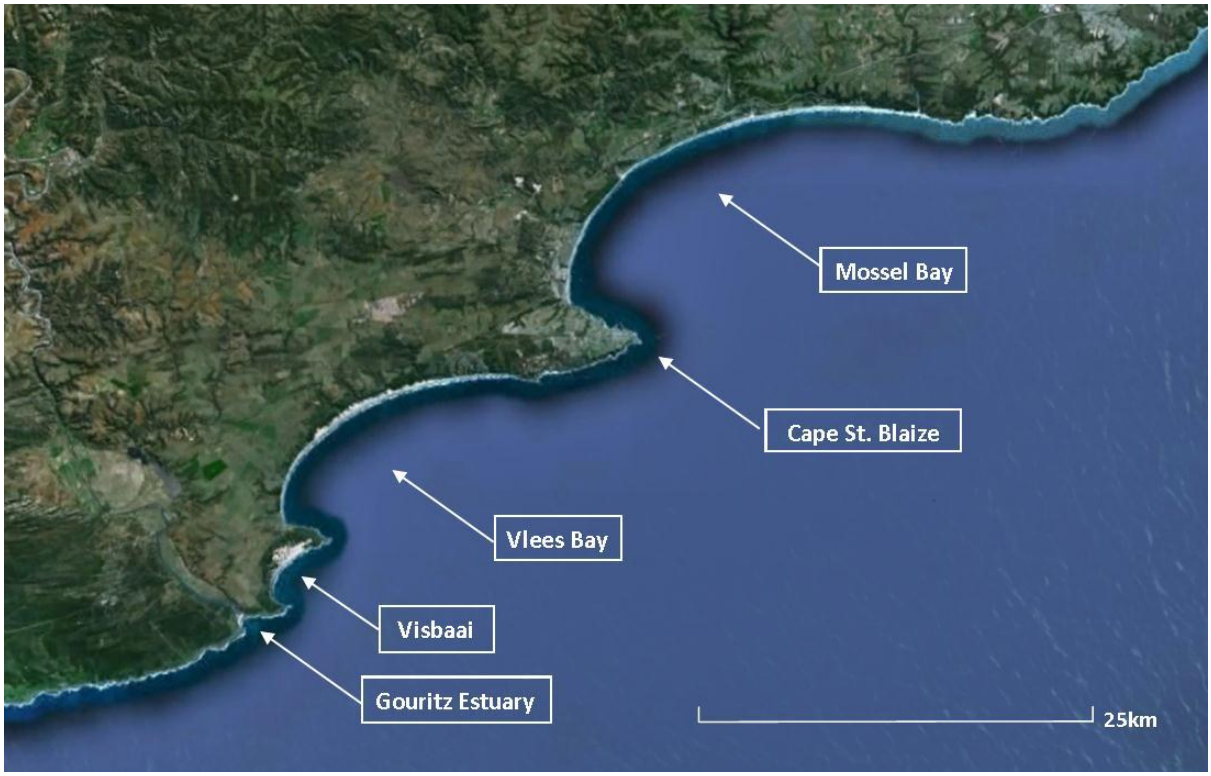

Figure 4.5: Locality map for regional sediment transport regime (Google Earth)

Very little of the sediment deposited by the Gouritz River is therefore transported past Cape St. Blaize. Moreover, any sediment which does reach the bay is intercepted by the entrance channel to the Port of Mossel Bay located in the lee of Cape St. Blaize (as indicated in Figure 3.1b). A study of the dredging records between 1981 and 2001 indicated an average of 43 000 m^3 dredged from the entrance channel and the area adjacent to the breakwater head every year (CSIR, 2003). This

sediment is subsequently dredged and deposited offshore, thereby effectively cutting off the littoral drift into Mossel Bay[5] (Kapp, Prestedge & Retief, 1988).

In addition to sediment from the Gouritz River, some sediment is deposited through the estuaries of the Hartenbos, Klein Brak and Groot Brak Rivers directly into Mossel Bay (indicated in Figure 3.1b). A study by Rooseboom (1975), estimates the maximum relative annual sediment discharges in the order of 14 000m^3 per annum for the Hartenbos and Groot Brak Rivers, and 40 000m^3 per annum for the Klein Brak River. Considering the construction of dams in the Klein Brak and Great Brak rivers and the fact that only a small percentage of the above volumes are course enough to contribute to the beach profile, the amount of sediment entering Mossel Bay is very small.

Due to the difficulty involved in the measurement of sediment transport, not much can be said regarding the amount of sediment being transported out of Mossel Bay past Glentana. This stretch of coast is characterised by rocky cliffs and is not easily erodible. Due to the dominance of south westerly waves in the offshore climate, it is expected that the net transport at Glentana will be directed eastward. However, the magnitude of the transport is unknown.

In some headland-bay beach systems, dune fields supply a significant amount of sediment across the headland into the bay. However, in Mossel Bay, Cape St. Blaize reaches a height of roughly 150m above sea level and no migrating dune fields are present. An analysis of historical imagery has indicated the systematic vegetation and development of three dunes in the bay periphery. These dunes were roughly 150m wide and were located at (a) Diaz beach (in the westernmost corner of the bay); (b) northeast of the Klein Brak estuary; and (c) west and east of the Groot Brak estuary. These dunes are indicated in Figure 4.6 a1, b1 and c1, respectively, from aerial photographs taken in 1957. In Figure 4.6 a2, b2 and c2, the development of these dunes by 2010 is shown.

Along the coastline, currently almost all dunes are shown to be vegetated or developed, thereby protecting the sediment from being transported out of the system by wind. However, some sediment may be blown from the beach face and settle in the vegetated dunes. During storms, unprotected dunes may be eroded, introducing some of the wind-blown sediment back into the sediment budget. Some of the eroded sediment may also be lost offshore due to high waves with long periods.

[5] Despite the interception of the littoral drift, the beaches directly downdrift from the harbour remain stable, thereby suggesting that this section of the coastline is in a state of equilibrium (Kapp, Prestedge & Retief, 1988) or that sediment is transported to that section of the coast from another source.

Figure 4.6: Vegetation and development of dunes from 1957 to 2010 at (a) Diaz beach (in the westernmost corner of Mossel Bay); (b) northeast of Klein Brak estuary; and (c) west and east of Groot Brak estuary (Google Earth).

5 Wave transformation

In this chapter, the approach of the wave transformation modelling is discussed. A description of the chosen model is provided, followed by a description of the model set-up. The calibration of the model is presented, as well as the sensitivity of the model to some key parameters. The results of the wave model are also presented in this chapter.

5.1 Model description

The wave model used in this study is SWAN (Booij et al., 1999). SWAN (Simulating Waves Nearshore) is an open-source numerical wave transformation model which, for this study, was operated within the Delft3D graphical user interface.

SWAN uses implicit numerical schemes which are fundamentally stable. Nevertheless, grid dimensions need to be chosen such that the dominant physical processes are well resolved. Wave energy is propagated through geographical space by solving a wave energy balance equation (or wave action balance equation – see Appendix A) at every grid point for every time step. Waves are not resolved individually, rather a wave spectrum is assumed at the boundaries. This spectrum represents the wave energy found across a range of frequencies and directions.

Table 5.1 summarises the processes for generation and dissipation and transformation included in SWAN. A more detailed description of how these processes are included is found in Appendix A.

Table 5.1: Processes included in SWAN

Wave generation and dissipation	Wave transformation
• Generation by wind	• Propagation
• Nonlinear wave-wave interactions	• Refraction and shoaling
• White-capping	• Reflection and transmission
• Bottom friction	• Diffraction
• Depth-induced wave breaking	• Wave-current interactions

The SWAN model provides spectral output at user-specified locations. The spectral energy is described by H_{m0} and T_P as discussed in Chapter 2.1. The direction of the wave energy is presented as a weighted mean of all wave components in the spectrum.

5.2 Model set-up

The required model output is a set of wave climates on the 10m depth contour inside the bay. Wave climates are constructed statistically from a long-term dataset. Since the wave model runs are

computationally intensive, transforming the full 10 year wave dataset into the bay is not possible. Instead, a wave climate representative of an average year is constructed offshore. The wave climate contains significantly fewer wave conditions and can therefore be transformed into the bay with relative ease. Every wave condition, together with its probability of occurrence, forms part of the climates inside the bay.

The offshore wave climate was constructed by grouping the 10-year time series into bins of wave height, period and direction. For each of these bins, the average wave condition and percentage occurrence were calculated. The result is a set of 150 wave conditions, each with a probability of occurrence. Figures 5.1 and 5.2 indicate the wave bins in the three dimensions.

Although the size of each bin is chosen subjectively, the overall effect is small since a higher resolution is given to ranges with high occurrences and no conditions are left out of the final wave climate.

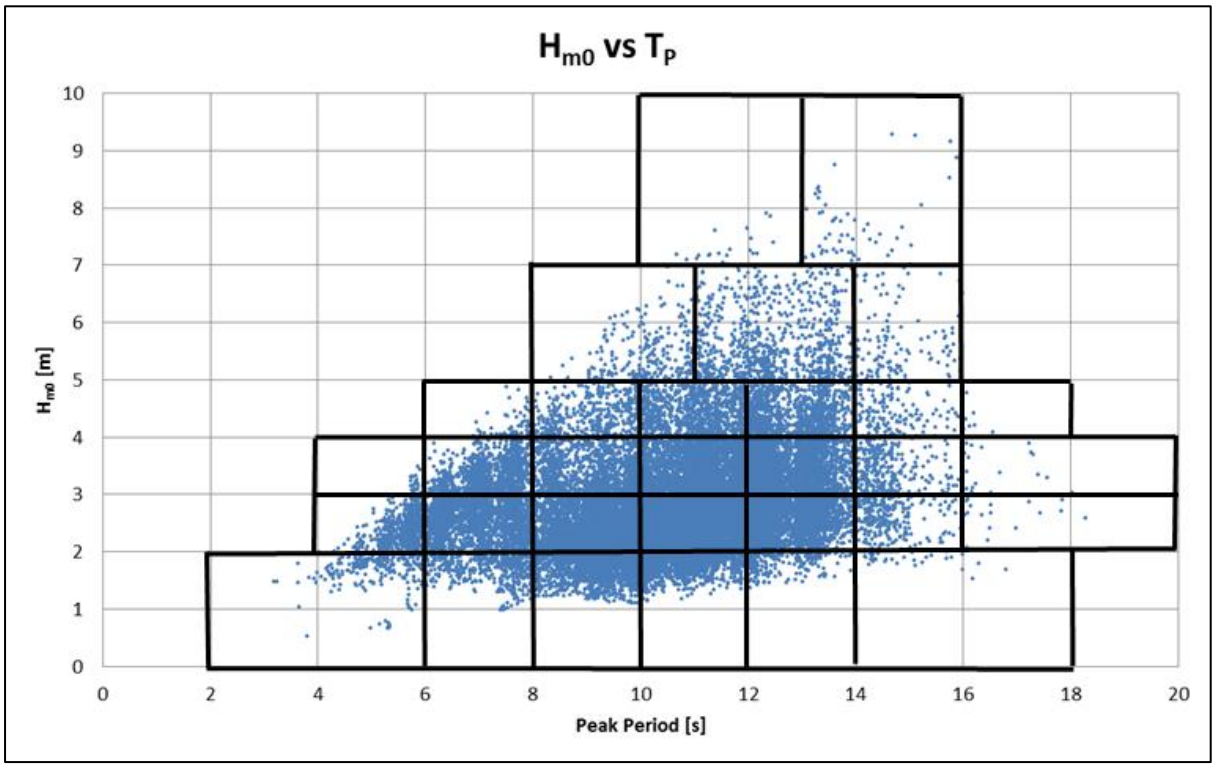

Figure 5.1: Schematisation of wave bins (wave height vs. period)

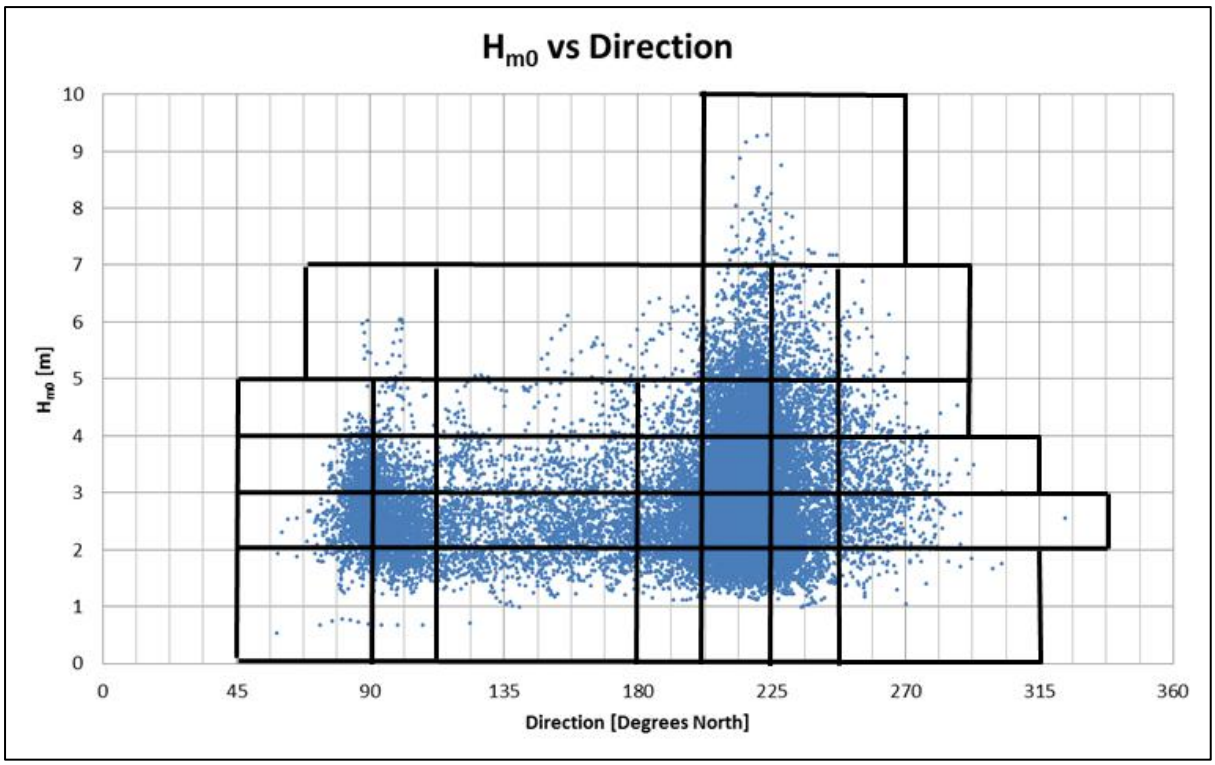

Figure 5.2: Schematisation of wave bins (wave height vs. direction)

The wave conditions are specified at all offshore boundaries, with the JONSWAP spectral shape. The peak enhancement parameter is chosen to be 2.2, as proposed by Rossouw (1989). The parameter for the directional spreading is chosen according to directional data collected at Slangkop, near Cape Point, since no directional measurements are available offshore of Mossel Bay.

An important consequence of the JONSWAP shape is that without wind generation in the model, there is only one peak in the spectrum. The wave state is thus described as an evolving unidirectional sea state, which is subjected to a directional spreading. If a secondary set of components is present, it is not represented in the NCEP data and will not be included in the model. The effect of wind therefore needs to be included to allow for the generation of local wind waves. The statistical inclusion of wind was achieved with some difficulty. The schematisation is discussed together with the calibration of the model in Chapter 5.3.

A set of bathymetric data was obtained from the General Bathymetric Chart of the Oceans (GEBCO). Although very coarse (resolution of 30 seconds latitude/longitude), this data is sufficient to resolve wave transformation processes in relatively deep water. For the area within and immediately offshore of Mossel Bay, data of a much higher resolution was obtained from the South African Navy Hydrographic Office (SANHO). A contour plot of the nearshore bathymetry is shown in Figure 5.3.

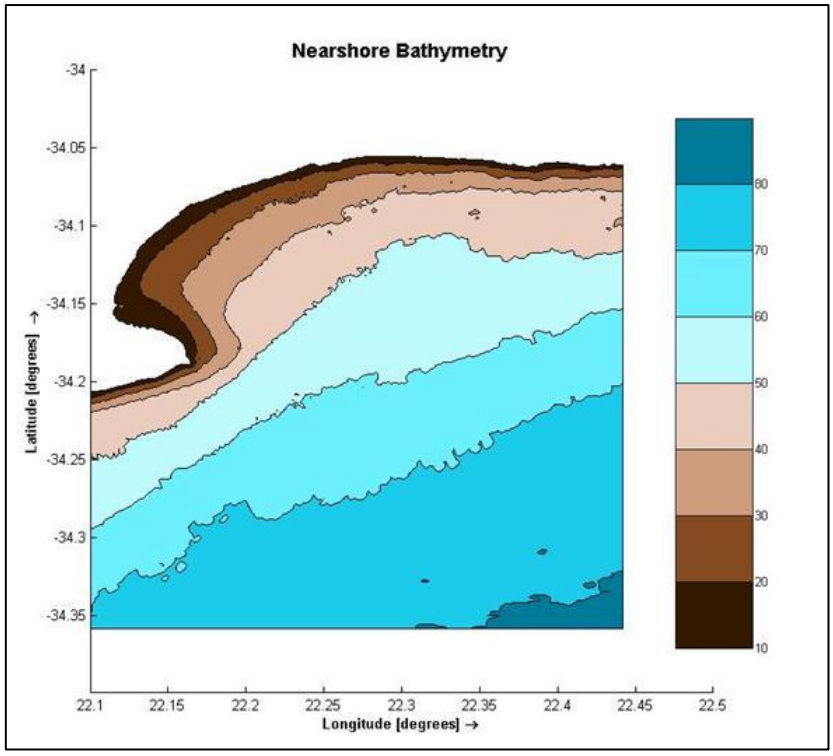

Figure 5.3: Nearshore bathymetry

In order to save computational time and avoid losing the high resolution of the SANHO bathymetric data into a coarse grid, the two datasets were each coupled to a separate computational grid. The fine grid is nested within the coarse grid and uses the output of the coarse wave transformation as its boundary condition. Figure 5.4 indicates the position of the two computational grids.

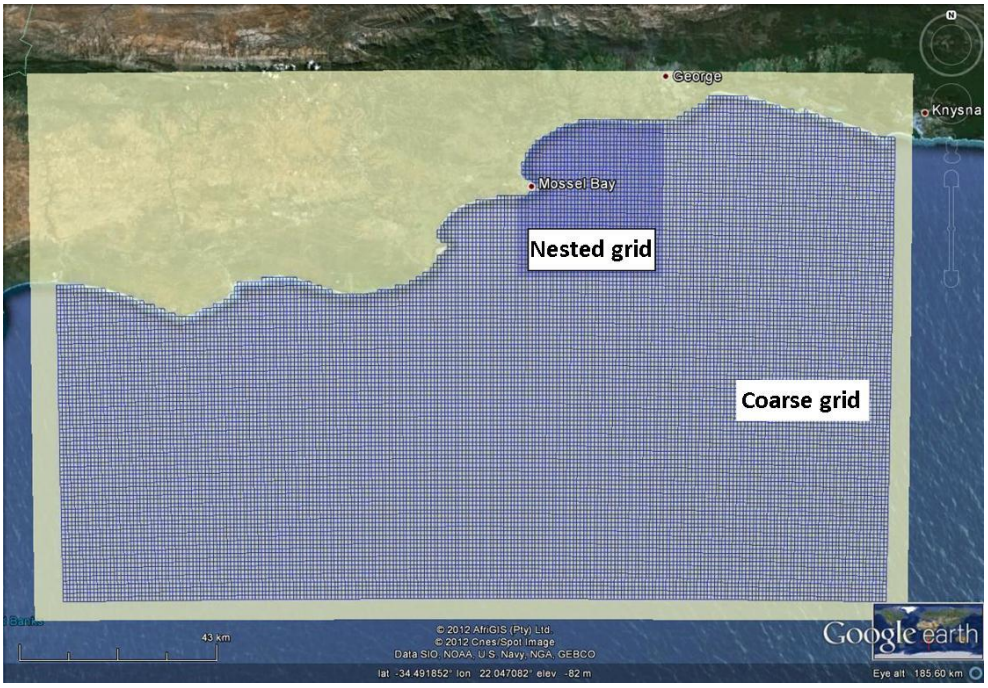

Figure 5.4: Layout of computational grids (Google Earth)

5.3 Model calibration

Very often the output of a numerical model seems realistic, but it is difficult to gauge whether the output is, in fact, accurate. It is therefore important to calibrate the model by having a set of prototype data with which to compare the model output and make changes to improve the degree to which the model reproduces the natural process. In this study, the model was assessed by considering storm events and long-term wave climates.

5.3.1 Storms

In order to gauge the accuracy of the wave transformation model, a south-south-westerly storm was modelled and compared with prototype wave heights measured by the WAVERIDER buoy. In addition to the offshore wave time series, a wind time series was applied over the duration of the storm. This allowed the model to include not only the swell originating from distant storms, but also locally generated wind waves, thereby representing the event as accurately as possible. The wind data was taken from the NCEP climate model. The comparison of measured to calculated wave height during a south-south-westerly storm in February 2008 is presented in Figure 5.5.

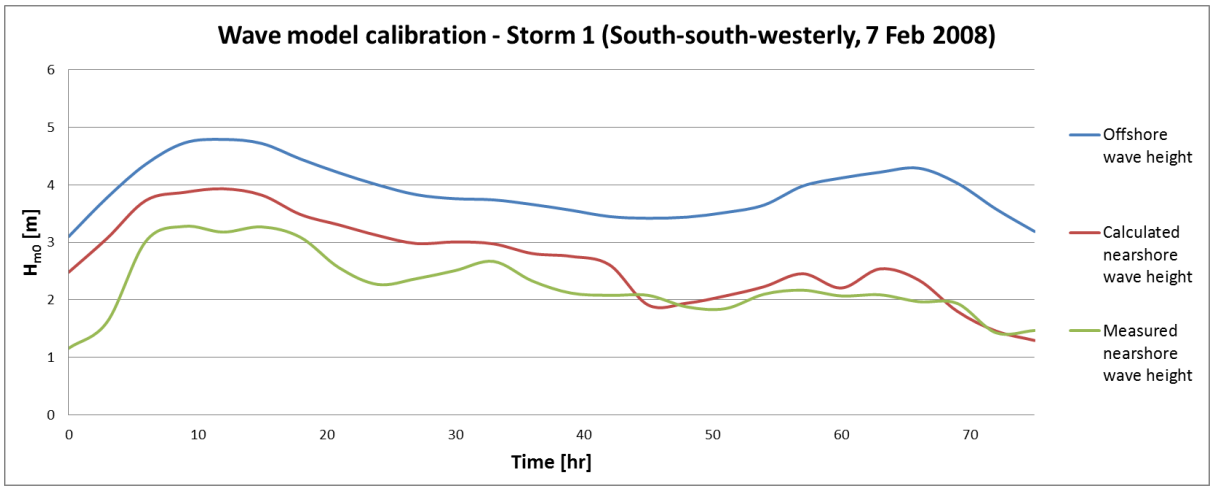

Figure 5.5: Wave model calibration: Storm 1 (SSW)

From the comparison, it is apparent that the model is slightly overestimating the wave height at the location of the wave buoy during the first 40 hours, but within reasonable limits. A possible cause for this overestimation is a change in wind direction around the 40 hour mark. During the first 40 hours wind energy is propagating into the model domain from the east-south-east. However, from the 40 hour mark onwards, the wind direction has shifted to east-north-east and some of the wind energy is propagating away from the buoy location.

Although the most severe offshore conditions originate from the south-western sector, much of the energy is dispersed through wave refraction around Cape St. Blaize. However, easterly storm waves

do not encounter the headland and maintain much of their original energy. It is therefore also important to validate the model for easterly storm events. In Figure 5.6, the comparison for an easterly storm in June 2008 is shown.

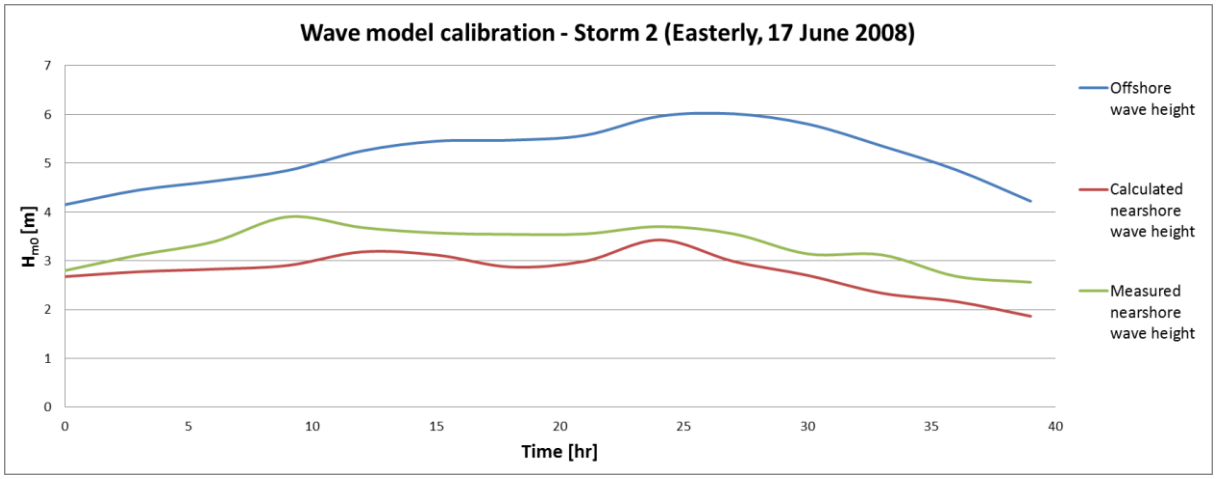

Figure 5.6: Wave model calibration: Storm 2 (E)

In this case, the model is slightly under predicting the wave height, but again within reasonable limits.

5.3.2 Wave climate

For this study, the main focus of the wave modelling is to provide an accurate year-averaged wave climate, rather than one wave condition. This allows the shoreline model to calculate the annual longshore transport based on a set of up to 1000 wave conditions – each with a probability of occurrence. It is therefore important that the model is not only able to reproduce storm events, but also the long-term wave climates in the nearshore.

From the calibration of storms presented above, it is apparent that the inclusion of wind is important to the accuracy of the model. The limit of 1000 wave conditions in UNIBEST excludes the possibility of choosing a representative year and transforming the complete year of wave and wind conditions into the bay, even when a six-hourly interval between data points is used.

A different approach towards the inclusion of wind therefore needed to be employed. In this model, wind was included based on a statistical relationship to couple one of two wind conditions to each wave condition determined in Chapter 5.2. Figure 5.7 is a plot presenting the relationship between the offshore wave direction and the local wind direction. The wind data is from the dataset measured at Seal Island (PRDW, 2001) for the full year of 1999.

The distribution of data points clearly indicates the predominance of two offshore wave directions – those clustered around the 90° and 215° ranges. Furthermore, for each of these wave directions, the corresponding wind directions seem to be roughly grouped around the easterly and westerly sectors. This trend can also be observed in the wind rose for the offshore conditions presented in Figure 4.4. The data was binned as indicated by the black lines in Figure 5.7. For each bin, the averages of wind speed, direction and occurrence were calculated (see Tables 5.2 and 5.3). Finally, each of the 150 wave conditions was coupled to two wind conditions. The occurrence of the wave condition was divided according to the distribution presented in Table 5.2. The result is a set of 300 wave and wind conditions, which are presented in Appendix B.

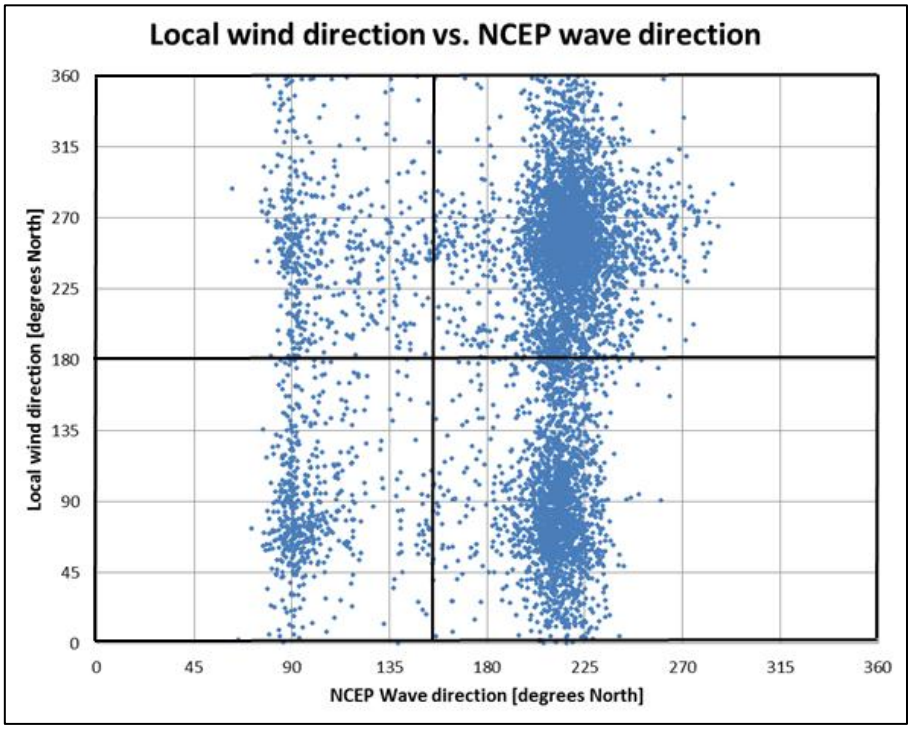

Figure 5.7: Schematisation of wave and wind bins

Table 5.2: Occurrence of wind and wave conditions

Percentage Occurrence		Wave direction	
		<157.5	>157.5
Wind direction	<180	56.3	40.52
	>180	43.7	59.48
Total		100	100

Table 5.3: Average direction and speed of wind conditions

Average direction [deg]		Wave direction	
		<157.5	>157.5
Wind direction	<180	91	90
	>180	250	254

Average speed [m/s]		Wave direction	
		<157.5	>157.5
Wind direction	<180	4.2	4.22
	>180	3.77	4.24

In order to test the ability of this approach to reproduce the actual nearshore wave climate, the full climate was investigated. In Tables 5.4 and 5.5, the wave heights and periods predicted by the model at the Waverider buoy location are compared to those measured by the buoy.

Table 5.4: Occurrence table of nearshore wave measurements (Waverider buoy)

Waverider		T_P											
		0	2	4	6	8	10	12	14	16	18	20	
H_{m0}		2	4	6	8	10	12	14	16	18	20	MAX	Total
0	0.5						0.14						0.14
0.5	1			0.76	1.15	1.70	20.06	11.11	4.73	0.25	0.11	0.04	39.90
1	1.5		0.07	0.65	3.43	1.91	13.35	10.43	5.99	0.58	0.11		36.51
1.5	2			0.54	2.09	1.91	4.18	3.64	2.42	0.32		0.04	15.15
2	2.5			0.07	1.05	1.26	0.94	0.29	0.79	0.51	0.25	0.04	5.19
2.5	3				0.69	0.51	0.14	0.07	0.14	0.18	0.18	0.04	1.95
3	3.5				0.07	0.29	0.07		0.07	0.11	0.14		0.76
3.5	4					0.07	0.18					0.14	0.40
4	4.5												0.00
4.5	5												0.00
5	5.5												0.00
	Total	0.00	0.07	2.02	8.48	7.65	39.07	25.54	14.14	1.95	0.79	0.29	100.00

Table 5.5: Occurrence table of calculated nearshore wave conditions

SWAN Output		T_P											
		0	2	4	6	8	10	12	14	16	18	20	
H_{m0}		2	4	6	8	10	12	14	16	18	20	MAX	Total
0	0.5		0.34	0.14	1.26	0.83	0.62	0.05					3.24
0.5	1		0.46	2.16	0.57	7.51	16.86	5.88	0.56	0.03			34.02
1	1.5			0.24	2.85	5.51	20.08	13.09	1.31	0.08			43.16
1.5	2				4.21	5.23	2.48	3.26	0.51				15.70
2	2.5				0.48	1.79	0.47	0.17	0.02				2.93
2.5	3					0.20	0.34	0.20					0.73
3	3.5					0.04	0.02	0.02					0.08
3.5	4				0.04	0.01	0.00	0.02					0.07
4	4.5					0.01	0.01	0.03					0.06
4.5	5					0.01							0.01
5	5.5					0.01							0.01
	Total	0.00	0.80	2.54	9.40	21.15	40.88	22.72	2.40	0.11	0.00	0.00	100.00

The occurrence tables suggest a good overall comparison between the model output and the measured data. For both the simulated and measured data, about 55% of all waves occur within the

0.5-1.5m wave height and 10-14s period ranges. However, the wave model does have a higher occurrence in the slightly lower periods (8-10s) and a lower occurrence in the slightly higher periods (14-16s). It should be kept in mind that the simulated data was constructed from a 10-year wave climate while the measured data is only based on one year.

Although the wave height and period have significant effects on longshore sediment transport, the rate of transport is also very sensitive to wave angle. It is therefore important to consider the accuracy of wave angles calculated by the model. Furthermore, the method of wind schematisation may have a significant effect on the balance between the easterly and westerly wave sectors. The directional occurrence of waves can be used to test this approach.

Due to the absence of accurate directional wave data, not much can be said regarding the accuracy of the wave directions predicted by the model. Moreover, it is not possible to judge the method of wind schematisation. The only remaining method of calibration for the wave model is by means of a backwards calibration of the coastline model. The stability of the coastline model will be used as an indication of the accuracy of the wind schematisation used in the wave model.

Based on the above calibration studies, it is assumed that the wave heights and periods predicted by the model are sufficiently accurate for the scope of this study. The effect of the wind schematisation on the overall wave climate will only become known through the results of the coastline model.

5.4 Model sensitivity

In order to test the impact of assumptions made regarding certain parameters and processes involved in the wave transformation calculation, the sensitivity of the model to these parameters was investigated. Sensitivity of the output wave height at various points on the 10m depth contour was tested by comparing the results of a set of wave conditions with periods and directions ranging from 8s to 14s and from south-west to east, respectively. The sensitivity of the model to bottom roughness, directional spreading, JONSWAP spectral peak enhancement factor (gamma), diffraction and the length of the side boundaries was tested. The output was inspected at 5 locations along the 10m depth contour inside the bay. The positions of these locations are indicated in Figure 5.8.

Figure 5.8: Location of points for sensitivity analysis

The sensitivity analysis delivered the following results:

- The wave height is insensitive to the bottom roughness coefficient. Major changes in its value (±50%) resulted in small mean changes (±7%) in H_S at Point 1. The bottom friction is expected to have a more pronounced effect on Point 1, since the bottom has a more gradual slope in the lee of Cape St. Blaize. The effect of bottom friction is therefore felt over a longer distance than the other points in the bay.
- The wave height is insensitive to the cosine power of the directional spreading function. Major changes in its value (±50%) resulted in small mean changes (±4%) in H_S at Point 3.
- The wave height is very insensitive to the peak enhancement factor of the JONSWAP spectrum. Major changes in its value (±50%) resulted in negligible mean changes (±0.5%) in H_S. The factor of 2.2 as proposed by Rossouw (1989) for the southern African coast will thus be used.
- The wave height is very insensitive to the inclusion of diffraction and the value of the diffraction coefficient. Its inclusion results in negligible mean changes (±0.8%) in H_S. This is to be expected since the penetration of waves behind Cape St. Blaize is mainly due to the processes of refraction and directional spreading, rather than diffraction. The water depth immediately around the headland causes the waves to refract around the headland. See Figure 5.3 for the nearshore bathymetry. Moreover, SWAN requires a grid resolution of about one tenth of the wavelength to resolve the diffraction process accurately (Deltares, 2010). The fine grid of the model is equal to the wave length at best, which is therefore insufficient. Diffraction will therefore not be included in the model.

- The length of the western boundary has no significant effect on the model for any of the wave conditions tested. The offshore boundary stretches sufficiently far to the west in order to include waves coming from the south western sector. The length of the eastern boundary has a significant effect on the model. If the boundary only stretches from the offshore boundary halfway to the coast, the model significantly underestimates the wave height from easterly waves. The full eastern boundary will be included in the model, since spatially varying boundary conditions cannot be specified in SWAN when the coupling with UNIBEST is desired.

The model is therefore found to be insensitive to the parameters tested above. The most important parameters are the bathymetry and the boundary conditions. As seen in the calibration exercise, the model is very sensitive to the inclusion of wind and the schematisation thereof.

5.5 Model results

To illustrate the model results under current conditions, the results for four wave conditions at the current water level (MSL) are shown in Figures 5.9 and 5.10 as contour plots of significant wave height. Figure 5.9 contains the output of the highest occurring south-westerly wave condition with two wind conditions. Similarly, Figure 5.10 presents the easterly wave conditions with wind. The conditions are summarised in Table 5.6:

Table 5.6: Wave conditions for presentation of results

Condition	H_{m0} [m]	T_P [s]	Wave Direction [deg's North]	Wind Speed [m/s]	Wind Direction [deg's North]
1	2.45	11.0	215°	7.0	90
2	2.45	11.0	215°	4.2	254
3	2.50	7.0	95°	6.9	91
4	2.50	7.0	95°	3.8	250

The two south-westerly wave conditions in Figure 5.9 indicate the important effect of the easterly wind. The inclusion of the easterly wind (left-hand figure) results in a much higher wave energy in the lee of Cape St. Blaize than the westerly wind (right-hand figure). This is primarily since the easterly generated wind waves do not need to refract as much. From Figure 5.10, it can be seen that the different wind conditions added to easterly waves have a much less pronounced effect on the penetration of waves behind the headland.

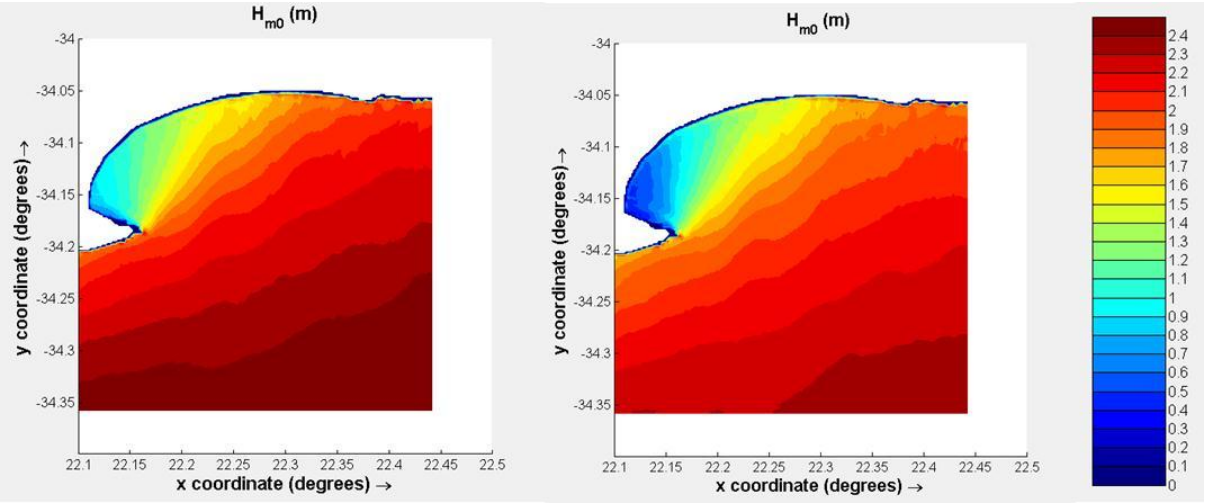

Figure 5.9: Model results for Condition 1 (left) and 2 (right)

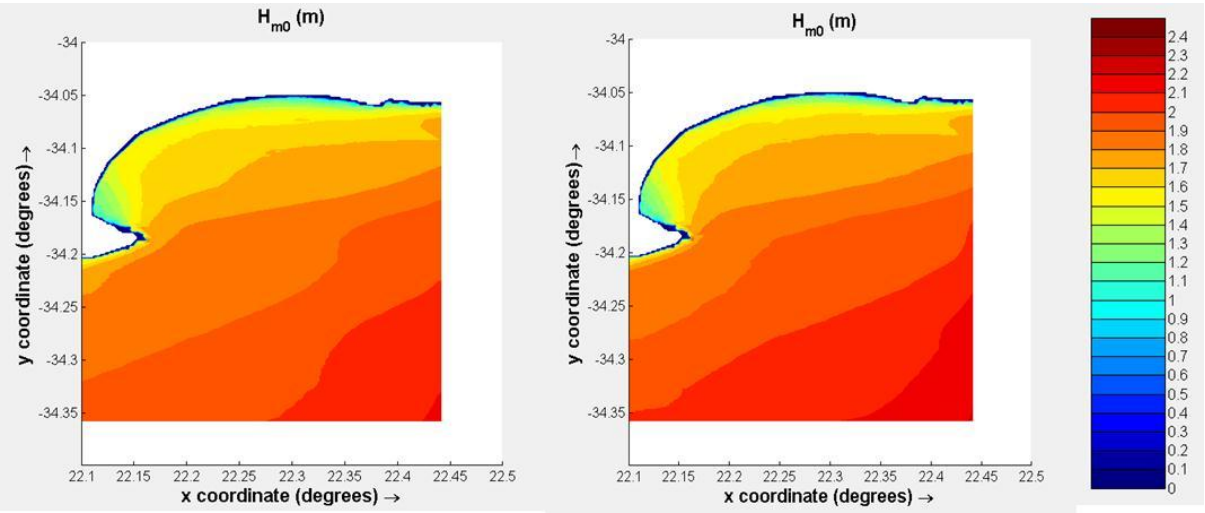

Figure 5.10: Model results for Condition 3 (left) and 4 (right)

It is useful to compare the model results with a similar model used for the development of a buffer dune integrity assessment by Barwell (2011). In this study, it was proposed that headland-bay beaches could be divided into sectors of similar wave transformation coefficients, thereby identifying the level of erosion risk for each sector. The proposed distribution is indicated in Figure 5.11, with sectors A to D ranging from low to high wave transformation coefficients.

When this distribution is superimposed on the model results presented in Figure 5.9, a similar distribution is observed. From the lee of the Cape St. Blaize, the wave height is increasing toward the more exposed coast at the eastern end of the bay. However, the model results from this study do not support the proposed higher wave height in the section immediately in the lee of the headland.

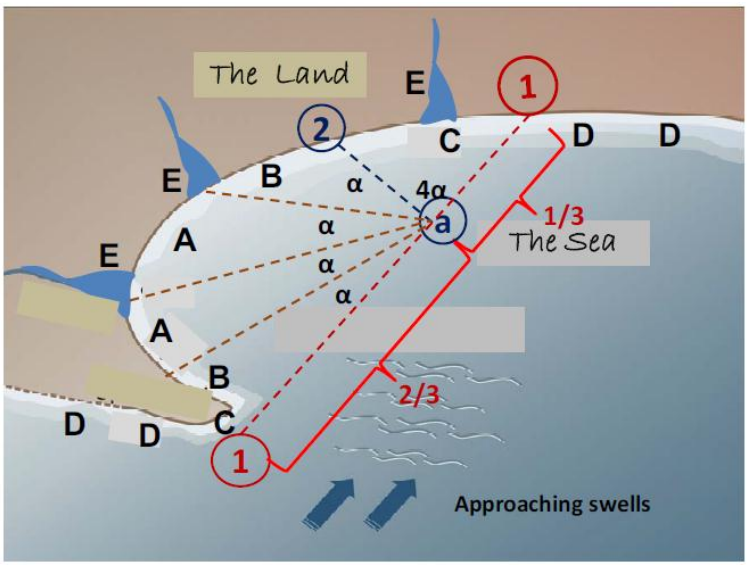

Figure 5.11: Distribution of wave height in a headland-bay beach (Barwell, 2011)

To further investigate the effect of the wind on the south-westerly wave conditions, the corresponding wave spectra are considered. Figures 5.13 and 5.14 are one-dimensional spectra for Conditions 1 and 2 in Table 5.6, respectively. For each condition the spectra are drawn for a number of output locations along the 10m depth contour inside the bay, with Location 1 located in the south-western corner and Location 18 at the eastern end of the bay. These locations are indicated on a map in Figure 5.12.

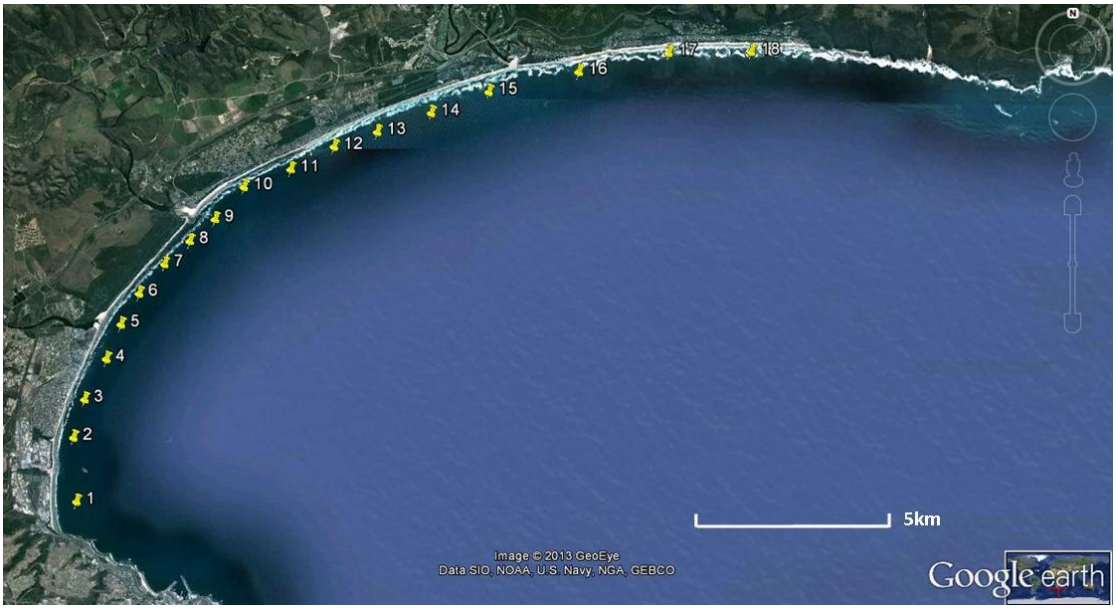

Figure 5.12: Locations of wave model output (Google Earth)

The first observation to be made is the difference in the height of the spectral peak along the bay. It can be seen from both cases that the amount of wave energy in the shadow area is much lower than the more exposed coast. The second important observation is the presence of a secondary peak for Condition 1. The secondary peak is located at a higher frequency and is generated by the easterly wind. The height of this peak is approximately the same for all positions along the bay, except at Location 1 where the energy is most likely dissipated through bottom friction. However, no secondary peak is observed in Condition 2. For the westerly wind, the fetch of the locally generated waves is extremely limited and the resulting energy is negligible.

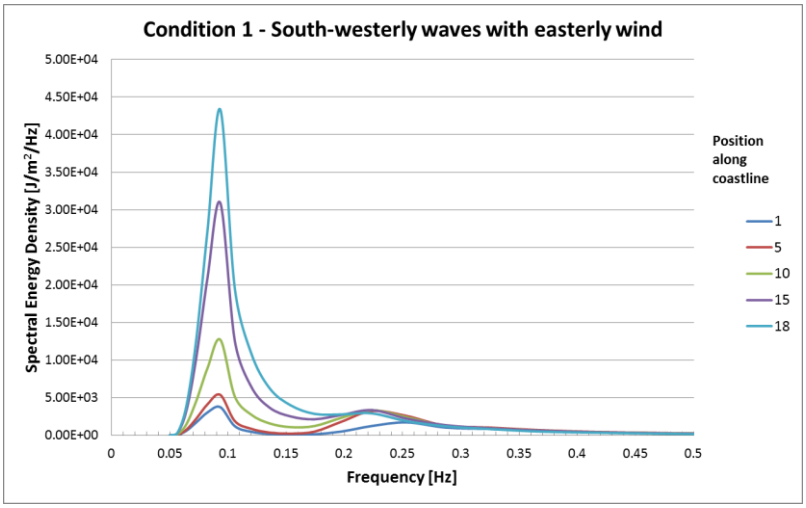

Figure 5.13: Ouput wave spectrum for Condition 1

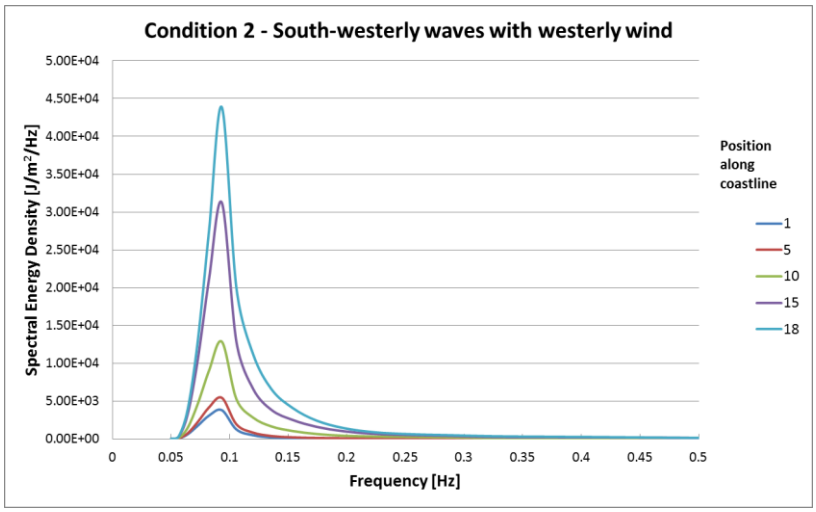

Figure 5.14: Output wave spectrum for Condition 2

As input, UNIBEST requires the local wave height, period and direction of each wave condition in the climate. The output generated by SWAN for wave height is H_{m0}, which is representative of the energy in the entire spectrum, irrespective of the directions of the wave components. The inclusion of the wind will therefore always increase the value of H_{m0}, even though the locally generated waves

may be propagating in a much different direction than the swell waves. The SWAN output direction is then calculated as the weighted mean direction of the energy in the spectrum. The inclusion of wind therefore also affects the input direction specified in UNIBEST. At every location, the input parameters received by UNIBEST are thus:

- H_{m0} representing the wave energy;
- T_P representing the frequency of said energy; and
- A mean direction representing the balance between the wind and wave energy

The effect of this schematisation is further addressed in Chapter 5.5.2.

5.5.1 Sea-level rise

In order to investigate the effect of sea-level rise on the refraction of waves, the changes to the nearshore angles are considered. Before the results are presented, it is useful to assess what could be expected from the model.

The primary hypothesis is that, since wave refraction is caused by water depth, a risen sea-level will affect the angle of the waves as they refract towards the shoreline. A higher water level implies a greater water depth and therefore a smaller change in wave angle. An important consideration is the different refraction patterns for waves originating from different directions. From the wave data presented in Chapter 4.2.2, the offshore wave climate primarily contains waves from two directional sectors – the south-west and the east. These are also the wave conditions considered in the model results above. The effect of a risen sea-level on these two wave directions will therefore be considered next.

In Figure 5.15, the nearshore bathymetry is reproduced. The red arrows indicate the refracted route travelled by waves originating from the south-western quadrant, while the green arrows represent the easterly waves. Since the figure only displays the nearshore bathymetry, some refraction has already taken place in deeper waters.

In the nautical convention, the south-westerly waves will have an offshore wave direction of roughly 225°. By the time the waves have reached the shore, the refracted wave direction is in the order of 90° in the western corner and 180° in the eastern end of the bay, causing a decreased wave angle in the nearshore. For the easterly waves, the refraction is reversed. Along the largest part of the bay periphery, the refracted wave angle is larger than the offshore angle. In the westernmost corner, however, the refraction caused by the nearshore bathymetry leads to a locally decreased wave angle.

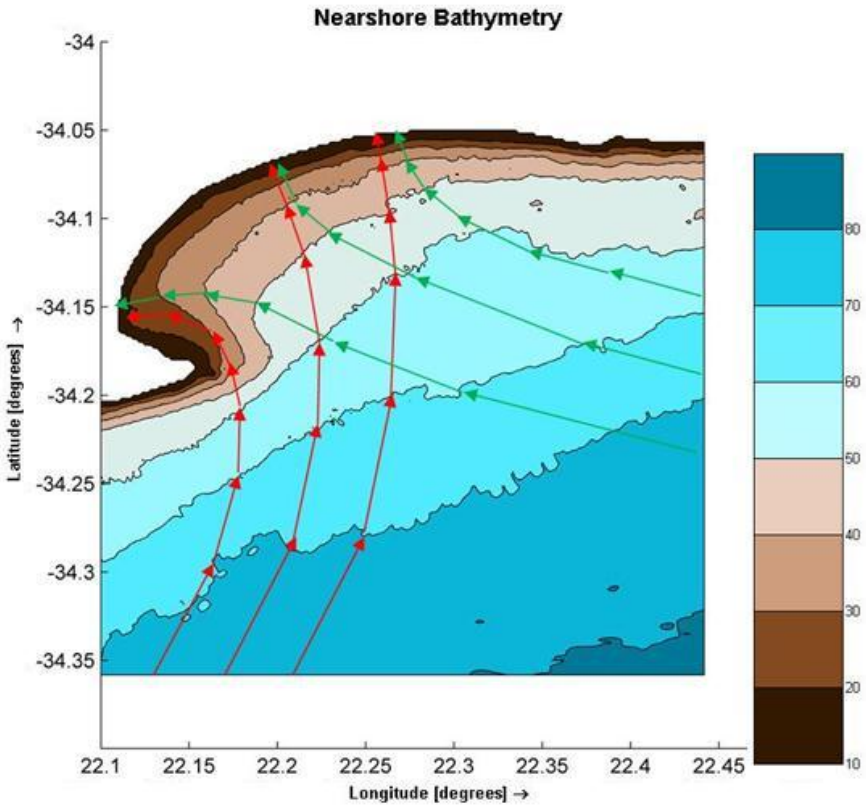

Figure 5.15: Nearshore refraction patterns for south-westerly and easterly waves

According to Snell's law (see Equation 2.8), the extent of refraction experienced by a wave is dependent on the water depth. An increased water depth should reduce the amount of refraction experienced by a wave propagating towards the shore. From Figure 5.15, a reduction in the refraction of south-westerly waves should cause a clockwise rotation of the nearshore wave angle along the entire periphery. Conversely, the refracted angle of easterly waves will experience an anti-clockwise shift, increasing the westerly sediment transport. This is true along the entire shoreline except in the westernmost corner, where refraction of easterly waves is reversed. Here, the refracted easterly wave angle should shift clockwise. In the south-western corner of Mossel Bay, a risen sea-level should therefore cause a clockwise rotation of nearshore wave angles for both the easterly and south-westerly wave conditions. Along the rest of the bay, the effects on the two components should act against each other.

Table 5.7 presents the average difference in computed nearshore wave direction for the easterly and south-westerly waves for the three sea-level rise scenarios. The average change in direction was calculated as the weighted mean (in terms of occurrence) of the directions from the two wind conditions for each wave condition. The positions one to eighteen are the positions indicated in Figure 5.12.

For the south-westerly waves, an increase in wave angle (clockwise rotation) can be seen along the entire coastline. This is consistent with the logical arguments presented above. The easterly waves are seen to experience a decrease in wave angle (counter-clockwise rotation) along most of the periphery. In the western corner (Locations 1-4) the effect is reversed, as expected. The magnitude of all the rotations varies with the extent of sea-level rise, with the largest rise causing the biggest rotations. This result supports the hypothesis that sea-level rise will affect the nearshore wave climates. The investigation of the effect of the changed nearshore wave climate is presented in Chapter 6.

Table 5.7: Relative change in nearshore wave direction resulting from 3 sea-level rise scenarios. Locations 1 to 18 are along the 10m depth contour as presented in Figure 5.12. Values are in degrees.

	0.5m SLR		1.0m SLR		2.0m SLR	
Location	**SW**	**E**	**SW**	**E**	**SW**	**E**
1	0.54	0.69	1.29	1.43	2.83	2.78
2	0.34	0.32	0.94	0.66	2.19	1.27
3	0.10	0.09	0.62	0.22	1.63	0.48
4	0.13	-0.02	0.50	0.03	1.19	0.10
5	0.19	-0.01	0.64	0.01	1.42	0.02
6	0.14	-0.20	0.46	-0.38	1.03	-0.68
7	0.08	-0.29	0.36	-0.52	0.93	-0.96
8	0.20	-0.32	0.47	-0.62	1.02	-1.19
9	0.12	-0.38	0.34	-0.72	0.75	-1.34
10	0.18	-0.41	0.37	-0.83	0.79	-1.62
11	0.15	-0.48	0.33	-0.92	0.69	-1.74
12	0.10	-0.69	0.20	-1.36	0.42	-2.52
13	0.12	-0.74	0.26	-1.46	0.60	-2.69
14	0.31	-0.59	0.59	-1.18	1.16	-2.22
15	0.25	-0.50	0.51	-1.01	1.01	-1.91
16	0.22	-0.69	0.42	-1.40	0.82	-2.61
17	0.11	-0.80	0.23	-1.55	0.48	-3.07
18	0.09	-1.00	0.18	-1.93	0.37	-3.72

5.5.2 Increased wave height

In the wave model, the output wave direction is calculated as a weighted mean of the energy in the directional wave spectrum. The output direction therefore reflects the balance between the swell and locally generated wind sea. The mean spectral wave direction is graphically illustrated in Figure 5.16a, which contains a south-westerly offshore wave condition coupled with a westerly wind.

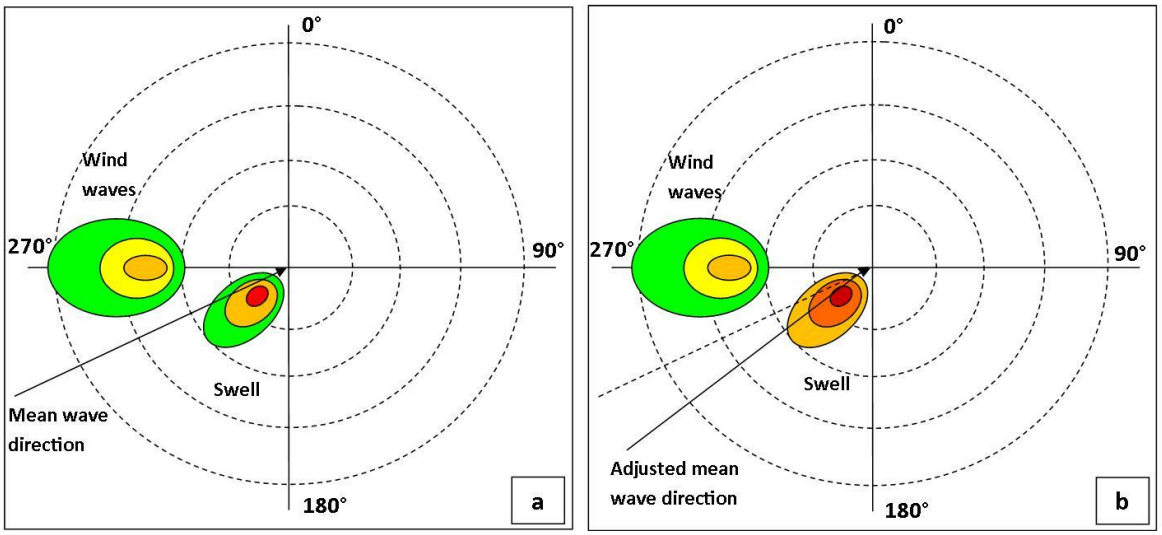

Figure 5.16: Calculation of mean spectral wave direction

An increase in the offshore wave height implies an increase in the wave energy at the spectral peak, while the energy generated by the wind remains constant. This implies that the mean wave direction is shifted towards the incidence angle of the swell waves, as indicated in Figure 5.16b.

The combination of wave and wind conditions with the highest occurrence is that of the south-westerly wave coupled with a westerly wind, which is the case presented in Figure 5.16. For this condition, the effect of increasing the offshore wave height is therefore not only to propagate more energy into the bay, but also to shift the mean direction counter-clockwise and increase the eastward directed sediment transport caused by south-westerly waves. This is contrary to the increase in eastward-directed transports which should result from higher south-westerly waves.

The turning effect caused by the inclusion of wind therefore does not represent the actual case of an increased wave direction. The modelling approach used in this study is therefore not suitable for the investigation of the increased wave height scenario.

5.5.3 Southward rotation in offshore wave directions

The southward rotation of offshore wave directions was modelled as a shift of all wave angles towards 180°, as discussed in Chapters 2.6 and 4.1. Easterly waves therefore experience an increase in offshore wave direction, while south-westerly waves experience a decrease. These rotations are expected to be seen in the nearshore wave angles, but to a smaller extent.

A comparison of the nearshore wave angles for two wave conditions is presented in Table 5.8 for both the 1° and 2° rotations. The values in the table indicate the relative change in nearshore wave direction with a clockwise rotation positive. The wave conditions are the same as those used for the sea-level rise results.

The results indicate a decreased nearshore wave angle for south-westerly waves and an increased angle for easterly waves. This is consistent with the expectations outlined above.

Table 5.8: Relative change in nearshore wave directions resulting from southward rotation of offshore wave directions. Locations 1 to 18 are along the 10m depth contour as presented in Figure 5.12. Values are in degrees.

	SW		E	
Location	**1°**	**2°**	**1°**	**2°**
1	-0.55	-0.59	0.40	0.28
2	-0.53	-0.49	0.48	0.27
3	-0.58	-0.64	0.62	0.53
4	-0.46	-0.73	0.72	0.61
5	-0.46	-0.63	0.79	0.65
6	-0.42	-0.52	0.66	0.61
7	-0.43	-0.53	0.58	0.64
8	-0.45	-0.50	0.56	0.73
9	-0.49	-0.48	0.71	0.89
10	-0.44	-0.43	0.71	0.94
11	-0.46	-0.49	0.67	0.96
12	-0.38	-0.47	0.59	0.90
13	-0.39	-0.52	0.51	0.91
14	-0.43	-0.58	0.52	0.90
15	-0.39	-0.61	0.53	0.89
16	-0.42	-0.64	0.41	0.95
17	-0.32	-0.61	0.39	0.87
18	-0.29	-0.61	0.17	0.88

5.5.4 Summary

Based on the results of the wave transformation, the following observations are made:

- The results have indicated that sea-level rise affects the refraction of waves into the nearshore
- Due to the method of wave and wind schematisation, the wave transformation model is unable to accurately predict the effect of an increased offshore wave height on the nearshore wave climates
- The southward rotation of offshore wave directions affects the angles of waves in the nearshore

In the next chapter, the affected nearshore climates are used in a shoreline model to investigate the impact of these effects on the longshore transport in Mossel Bay.

6 Coastline modelling

6.1 Model description

UNIBEST (UNIform BEach Sediment Transport) is a software package developed as an engineering tool for the simulation and study of sediment transport and coastline stability (WL|Delft Hydraulics, 2005).

The package used in this study consists of:

- UNIBEST-LT – a module for the calculation of longshore sediment transport, and
- UNIBEST-CL – a module for the simulation of coastline dynamics.

UNIBEST-LT calculates the longshore sediment transport based on a wave climate specified at the offshore boundary[6]. For each wave condition, the wave transformation to the shore is computed by a wave propagation and decay model which includes the processes of refraction, shoaling, bottom friction and wave breaking. The longshore current is calculated according to the momentum equation (discussed in Chapter 2.3) and takes into account the effects of bottom friction, the gradient in radiation stress and the tidal surface slope[7]. From the longshore and tidal currents, the longshore sediment transport can be calculated by one of the following formulations:

- CERC (1984)
- Bijker (1968)
- Van Rijn (van Rijn & Kroon (1992), as discussed in Chapter 2.4)
- Van der Meer-Pilarczyk, for gravel beaches

By including the individual contributions of all wave conditions in the climate, UNIBEST-LT derives an equilibrium coast angle (θ_e) for which the combined annual longshore transport is zero. The magnitude of the transport is based on the closure depth and active height of the profile, the specified sediment transport formulation and the local sediment properties. The equilibrium angle thus specifies the equilibrium state, while the magnitude of the transport determines the time needed for equilibrium to be reached.

Deviation from the equilibrium coast angle leads to a net annual longshore transport. The magnitude of this transport is schematised in the following function (WL|Delft-Hydraulics, 2005):

[6] This offshore boundary is usually located near the closure depth which is in the order of ten meters deep. It should not be confused with the offshore boundary used in the wave transformation model which is in the order of hundreds of meters water depth.
[7] Since the model is applied over the extreme long term, the effects of tide are assumed to be averaged out.

$$Q_s^a = c_1 \theta_r e^{-(c_2 \theta_r)^2} \tag{7.1}$$

where Q_s^a is the annual sediment transport, c_1 and c_2 are constants determined by the method of least squares, and the relative coastline angle is determined as:

$$\theta_r = \theta - \theta_e \tag{7.2}$$

This function is graphically presented by the so-called S-Phi (S-ϕ) curve, which relates the coast angle to the transport magnitude and direction. Figure 6.1 is an example of such a curve.

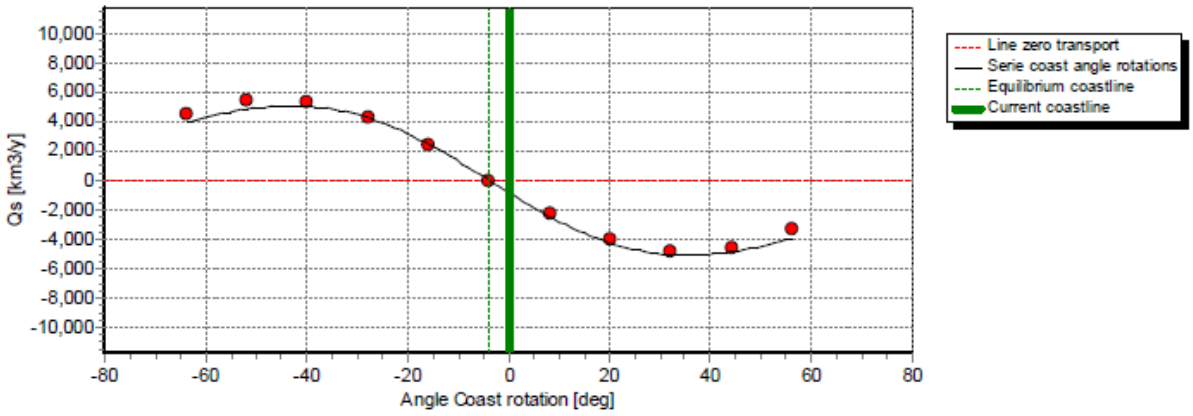

Figure 6.1: The S-Phi curve as calculated in UNIBEST-LT (WL|Delft-Hydraulics, 2005)

The result of the UNIBEST-LT calculation is thus a set of S-ϕ curves representing the longshore sediment transport potential at various positions along the coastline. The curves, together with parameters describing the cross-shore distribution of the longshore transport, then serve as input to the coastline model in the form of *.RAY files.

UNIBEST-CL calculates the coastline position based on the longshore gradients in sediment transport, according to the one-line approach discussed in Chapter 2.8. At every grid point, a local sediment balance leads to accretion or erosion, shifting the profile forwards or backwards while maintaining its shape. The rate of transport is dependent on the coastline angle at the current time step and is obtained from the S-Phi curve calculated by UNIBEST-LT. After every time step, the model recalculates the coast angle at every grid point and adjusts the sediment transport accordingly.

The coastline at the start of the simulation is defined by the basic grid. A number of grid points are specified on a line some distance inland of the actual coastline. This line does not follow small variations in the coastline, rather a smooth trend. The actual coastline is then specified by the cross-shore distance to the shore at every grid point.

At the lateral model boundaries, one of three conditions can be specified. These are:

- Constant coast angle
- Constant sediment transport
- Fixed coastline position

UNIBEST-CL is also able to account for groynes, revetments, offshore breakwaters and sources and sinks within the model domain.

6.2 Model set-up

In order to set up the UNIBEST-LT model, the following input data groups are required:

- The nearshore wave climate,
- the local beach profile,
- the closure depth and active height of the profile,
- the sediment parameters and the transport formulation to be used, and
- the wave breaking parameters

As outlined in Chapter 5, the nearshore wave climate was determined from the wave transformation model. The climates were extracted at 18 positions along the 10m depth contour as indicated in Figure 6.2.

Figure 6.2: Locations of local wave climates (1 to 18) and of cross-shore profiles (P1 to P8) (Google Earth).

Cross-shore profiles were compiled from the available bathymetric data supplied by the SANHO at eight positions along the coastline where the survey reached sufficiently shallow depths. From the landside, cross-shore profiles were obtained from previous surveys at Voorbaai (AR Wijnberg Inc., 1995) and Pansy Beach (CSIR, 1988). The positions of the profiles are also indicated in Figure 6.2.

In addition to data mined from previous projects, a survey of the cross-shore beach profiles at the eight aforementioned locations was carried out as part of this thesis to supplement the profiles with accurate data landward of the surf zone. A Trimple GeoExplorer 6000 handheld GNSS receiver was used for elevation measurements from the top of the dune ridge (where possible) to the maximum possible depth allowed by the splash-proof instrument (-1.4m MSL). In order to maximise the depths reached, measurements were taken during low water at spring tide. After differential correction, 97% of the measurements were accurate to within 15-30cm. Figure 6.3 is an example of one such constructed profile. Figure 6.4 is a photograph of the author conducting the surveys.

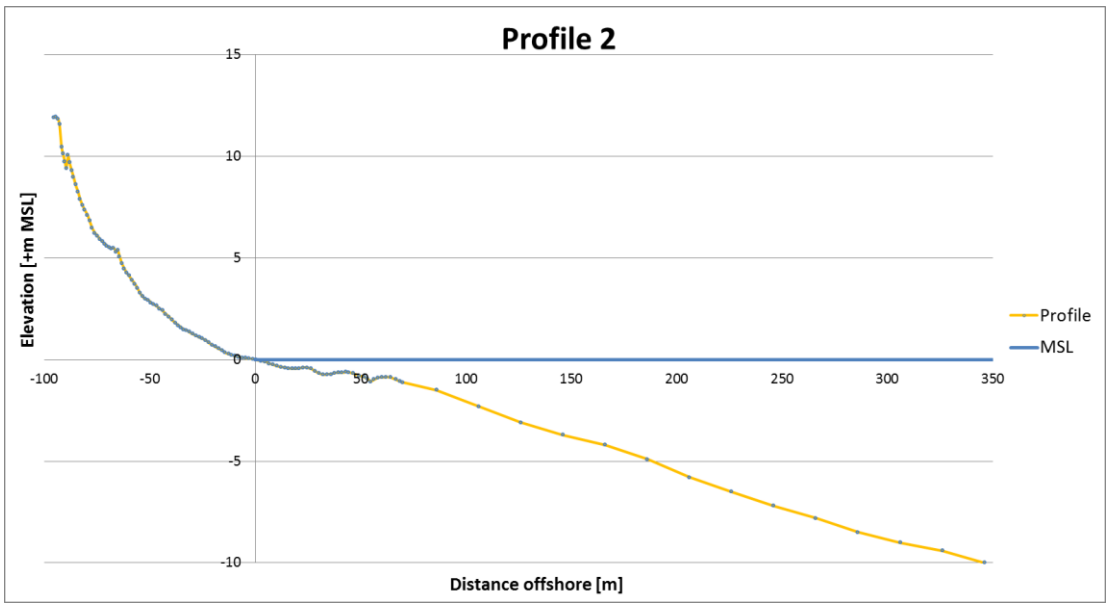

Figure 6.3: Cross-shore profile at survey site 2

For the base condition in this study, UNIBEST receives a set of wave climates at the 10m depth contour from the wave transformation model. However, the climates produced from the sea-level rise runs are no longer at 10m water depth, rather at slightly greater depths. In order to compensate for the mismatch of water levels, the profiles in UNIBEST were extended seaward to the correct depth.

Figure 6.4: Author conducting cross-shore beach survey at Glentana (site 8)

The closure depth for each profile was calculated according to the equations of Hallermeier (1981) and Birkermeier (1985), as presented in Chapter 2.4. The resulting closure depths were in the range of 6m in the lee of Cape St. Blaize and 12m at the exposed coast at Glentana. The active profile height should be chosen to reflect the height to which the profile takes part in the sediment transport, while taking into account the time scale of the model. In this study, the active height was chosen at the foot of the first dune. This is assumed to be a reasonable assumption since this point usually varies with seasons, rather than days or tidal cycles. Furthermore, no vegetation exists seaward of this point, indicating a dynamic interaction with the sediment system. The average over the eight profiles resulted in an active height of 4m above mean sea level.

Sediment samples were also collected for this thesis at the eight aforementioned profile locations. Sieve analyses were carried out to calculate the median (D_{50}) and 90th percentile (D_{90}) particle diameters. Unfortunately, a low number of sieves smaller 1mm resulted in a sediment grading of poor resolution. The poor resolution analyses could therefore not be used for the precise calculation of the necessary parameters. The analyses could, however, be used for an estimation of the range of the median and 90th percentile particle diameters.

In addition to the sieve analyses, a visual analysis was undertaken with a grading tool used to estimate the size of the average particle. A comparison of the results of the two methods is shown in Figure 6.5.

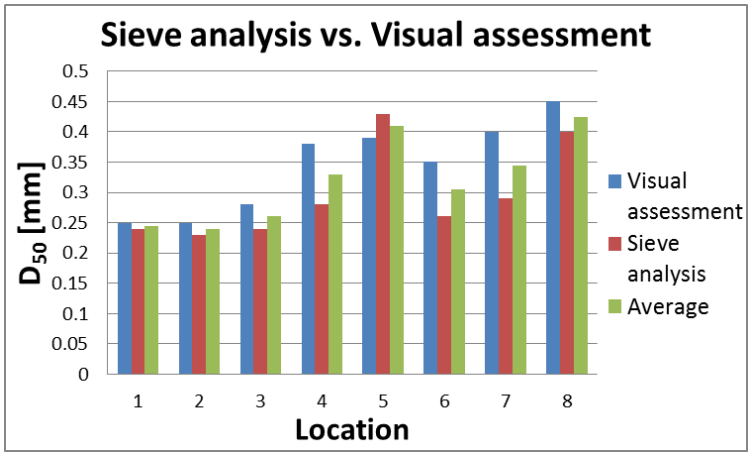

Figure 6.5: Comparison of sieve analysis and visual assessment

From the comparison, it can be seen that the median grain size determined from the visual assessment falls well within the range calculated from the sieve analyses. It was therefore assumed that the visual assessment was sufficiently accurate.

In this study it was decided to use a detailed transport formulation, rather than a bulk transport formula. The two formulae applicable to the study site were therefore those of Bijker (1968) and van Rijn (as cited by van Rijn & Kroon, 1992). In a study comparing predictions by longshore transport formulas with field measurements, Bayram et al. (2001) found the van Rijn formulation to yield the most reliable predictions when applied over a range of swell and storm conditions. The formula of Bijker was found to over-estimate the magnitude of transport. The formula of van Rijn was therefore used in this study.

The default parameters for the coefficients for wave breaking and bottom roughness were used. Since local cross-shore profiles and sediment properties were not available at every location where the local wave climate was known, the data closest to each climate position was specified to calculate the local RAY file. Furthermore, RAY files were not specified at every grid point, but were interpolated by the model to surrounding grid points. All RAY files shared the same wave breaking parameters.

The basic model contained a total of 54 grid points along the bay periphery of 26km. Between each basic grid point, a further four points were generated resulting in a total number of 212 grid points and an average grid spacing of roughly 120m. The coastline was defined by specifying the cross-

shore distance to the vegetation line at every grid point. Since the coastline is used for the calculation of the coast angle and hence the longshore transport capacity, it is important that the specified coastline accurately reflects the coast angle experienced by the waves. It is then logical that the coastline must be more or less parallel to the nearshore bottom contours, which reflect the actual angle felt by the waves. However, in the far western corner of Mossel Bay, the bottom contours deviate significantly from the vegetation line. In this area, the definition of the coastline was slightly adjusted to compensate for this effect.

At the western boundary, a zero sediment transport condition was specified. This is consistent with the sediment budget for Mossel Bay, discussed in Chapter 4.2.5. Due to the presence of rocky cliffs at Glentana, the eastern boundary was assumed to be stable in the long term. Hence, the position of the coastline was fixed at the eastern boundary. The model was set to run with 120 time steps per year, leading to a time step of roughly 3 days. Output was generated at every 20th time step, or every two months.

The sediment sources from the Hartenbos, Klein Brak and Groot Brak rivers were included as point sources at their respective locations. The volume of sediment entering the model through each estuary was chosen according to the sediment budget, while taking into account the construction of dams.

A limitation of UNIBEST was found in the modelling of the intertidal reefs present along a significant section of the bay. As discussed in Chapter 4.1, the presence of the reefs causes a partial protection of the upper beach face which results in a fixed coast angle. In UNIBEST, the coast angle cannot be specified within the model domain. The only two options to approximate this effect are to represent the reefs by an offshore breakwater or a revetment.

An offshore breakwater is included by manually reducing the longshore transport capacity to approximate the reduced wave energy behind the breakwater. The effect of the reefs is to protect a section of the profile, and not to decrease the longshore sediment transport capacity.

In UNIBEST, any erosion behind a revetment is prohibited, while accretion and by-passing is allowed. Including a revetment in the model will therefore fix the coastline position without tampering with the longshore transport potential. This set-up seems to be consistent with the current state of the bay. Under a rising sea-level, however, the effect of the reefs will become less prominent and erosion should be permitted. Unfortunately, the reduced protection of the reefs cannot be modelled gradually. At a certain water level the effect of the reefs should be assumed to be no longer significant and the revetments should be removed from the model. Due to the complex effect of the

reefs on the sediment transport, this water level cannot be simply related to the wave breaking depth. A range of possible scenarios should therefore be tested in the model to allow for the uncertainty regarding the future importance of the reefs under the effect of sea-level rise.

6.3 Model calibration

Since field measurements of sediment transport are very difficult and expensive to conduct, accurate sediment transport rates are almost never available. The only way to calibrate the results of the longshore transport model is therefore to compare the output of the coastline model with observed trends in the coastline position.

In order to assess the stability of the Mossel Bay coastline, a set of imagery data covering the past 30 years was analysed. Two sets of aerial imagery from 1980 and 1991 were obtained from National Geo-spatial Information, a division of the Department of Rural Development and Land Reform. Satellite images were also available through Google Earth for 2004/2005 and 2010.

The stability was assessed by plotting the cross-shore distance from a fixed point to the vegetation line at a set of locations along the bay periphery. The vegetation line was used rather than mean sea level since the tide level could not be calculated without knowing the time at which each image was taken. Moreover, the high contrast between the colours of vegetation and sand allowed for more accurate measurements to be taken. Points in close proximity to estuary mouths were either moved or skipped since varying river flows and river mouth dynamics interfere with the vegetation line. At certain points along the coastline where the vegetation is tall or the profile is very steep, the 1980 position is over-estimated due to southward-oriented shadows. The shadows were clearly visible next to tall structures. Using the 1980 positions as the baseline, the relative variation from the coastline at every location for each image set is presented in Figure 6.6.

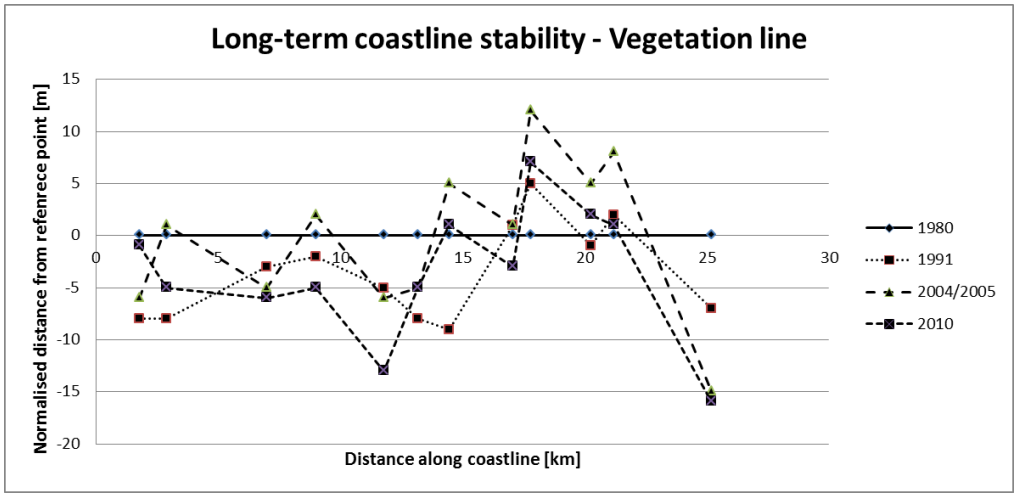

Figure 6.6: Coastline stability assessment

The normalised cross-shore measurements display a variability of mostly less than 15m without any trend or correlation. These variances do not carry sufficient significance to be accepted as a coastline trend and are attributed to inaccuracies in measurements due to low picture quality. Some measurements could also reflect seasonal variances or the short-term effects of storm impacts. The Mossel Bay coastline is therefore assumed to be reasonably stable for the last 30 years.

To test the accuracy of the coastline model, the period from 1980 to 2010 was simulated to compare with the stability assessment. In this model, the revetments were left out in order to investigate the stability of the current bay shape without the effect of the reefs. The result is presented in Figure 6.7 as a plot of the change in cross-shore position along the coastline. The distance along the coast is measured from the western corner. Positive values for coastline change indicate accretion. The positions marked A and B are the locations of the kinks described in Chapter 3.1. The red numbers indicate the positions one to eighteen presented in Figure 6.2.

The model output indicates significant rotation at the positions of the kinks. Moreover, apart from the rotation, the majority of the coastline seems to be in a state of erosion, contrary to the conclusion of the stability assessment.

The rotation at locations A, B and C serve as an indication that the prescribed bay shape does not match the equilibrium bay shape forced by the prescribed wave climate. The model therefore has the tendency to smooth out the kinks in the current shoreline. In reality, the reefs in the bay are maintaining the coast angle where they are present. It was therefore decided to include revetments as an approximation of this effect. The model output for the same period, but with the revetments included, is presented in Figure 6.8.

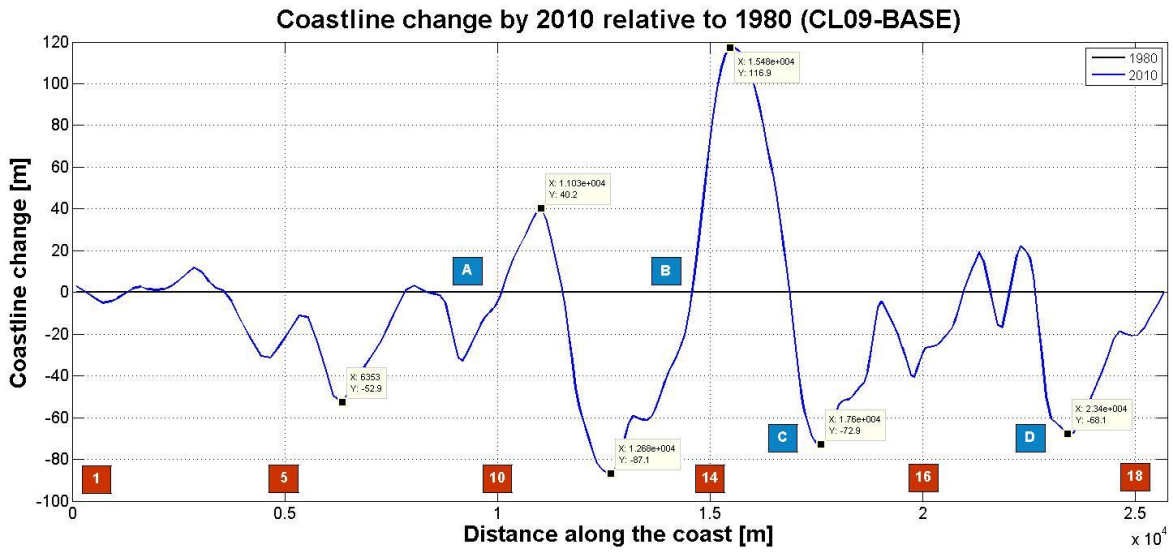

Figure 6.7: Coastline change by 2010 relative to 1980 (no revetments)

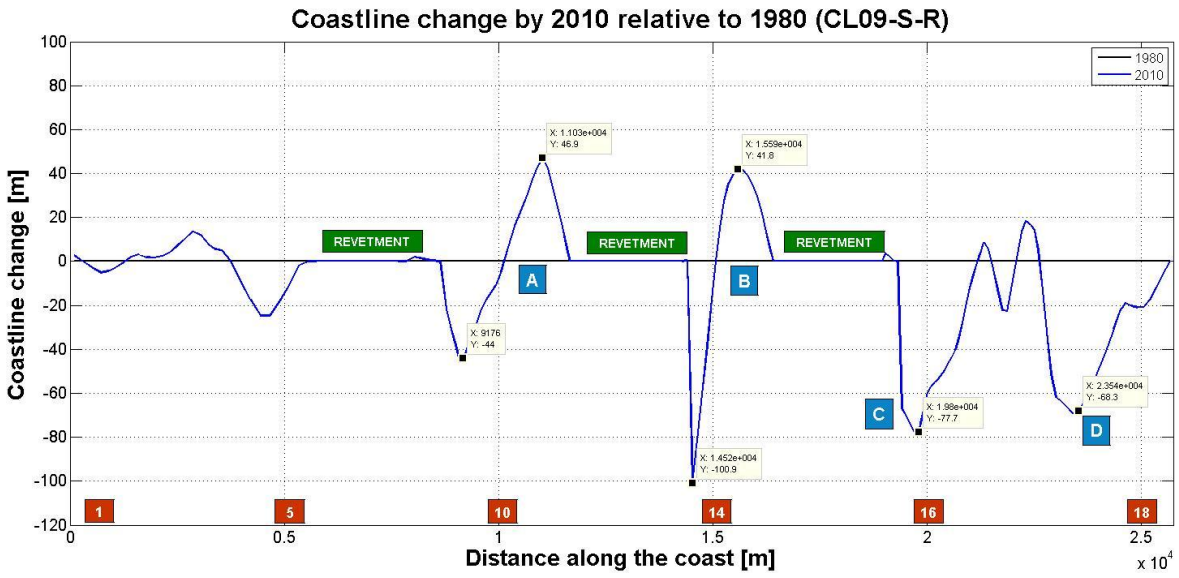

Figure 6.8: Coastline change by 2010 relative to 1980 (revetments included)

From Figure 6.8, it can be seen that the revetments prohibit erosion where the reefs are located and confine the smoothing effect to locations A, B and C – the areas between and adjacent to the revetments. The sharp erosion peaks at locations B and C are exacerbated by boundary effects of the revetments. At the edge of each revetment, the coast angle creates a high sediment transport potential, since the coast cannot adapt to the equilibrium angle required by the local wave climate. At the revetments, no erosion can occur and sediment is taken from the shoreline directly downdrift, leading to sharp erosion peaks.

In order to assess the long-term stability of the coastline as predicted by the model, the above case was run for a further 100 years until 2110. The plot in Figure 6.9 presents the coastline positions up to 2110 relative to the position in 2010. In Figure 6.10, the corresponding sediment transport rate is presented with a positive transport directed westward.

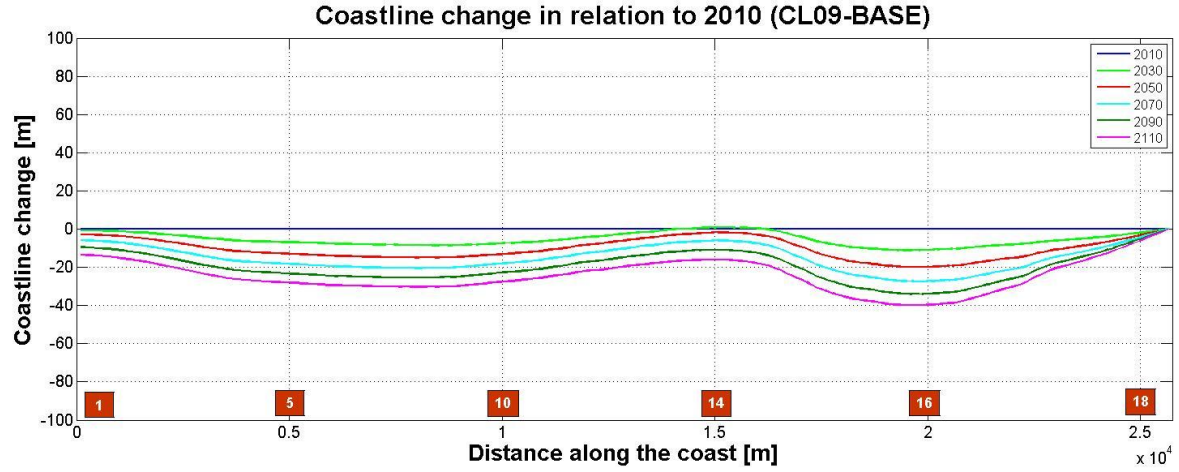

Figure 6.9: Coastline change relative to 2010 (no revetments)

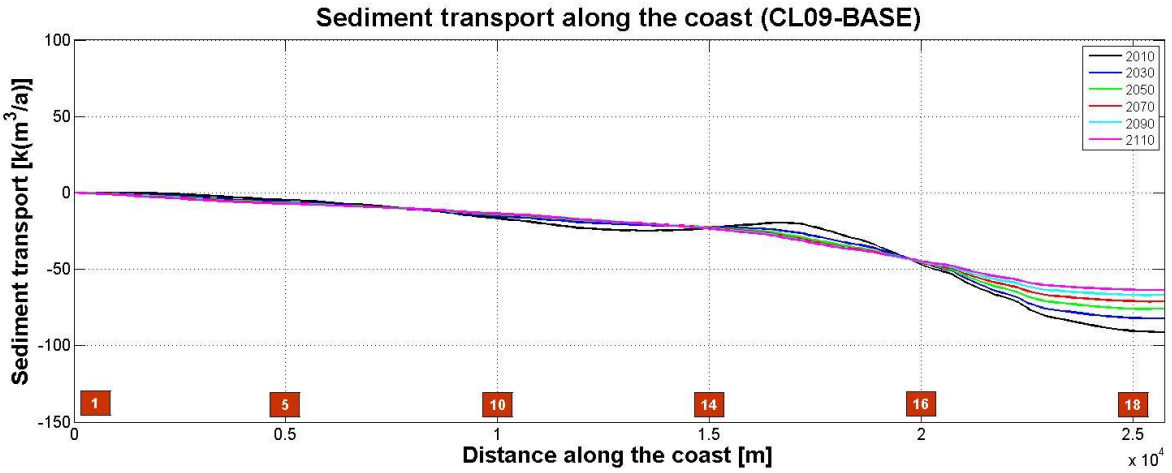

Figure 6.10: Sediment transport along the coast (no revetments)

From Figure 6.9 it can be seen that a continuous erosive trend is present along the entire coastline. Since there is no flow of sediment into the bay from the west, the erosion is caused by the eastward directed transport indicated in Figure 6.10. The model has therefore not reached a state of equilibrium. From the coastline stability assessment, however, there was no clear evidence of an erosive trend.

It is hypothesised that the eastward transport of sediment is caused by an underestimation of the easterly component of the wave climate. In Chapter 5.2 it was explained that the offshore wave conditions only represent the dominant wave component at each time step, which is most often the SW swell. This leads to an underestimation of the easterly wave components at the offshore boundary.

According to the output of the coastline model, the schematisation method used for the wind and waves is not able to reproduce the actual wave climates within the bay. The approach was therefore modified to enhance the contribution of the easterly wave components.

The wind speeds applied to the schematisation are from the local dataset recorded at Seal Island. The average speed from the local dataset is significantly lower than the hindcast wind data at the offshore point. Since the wind wave generation occurs over the whole model domain, the wind speed measured inside the bay may not be representative of the actual wind conditions. In order to attempt a better representation of the local wave climate, the average speed of the easterly winds was increased up to roughly the same average speed of the offshore wind data. The long-term stability of the model resulting from the new approach is presented in Figures 6.11 and 6.12 for the relative coastline position and sediment transport, respectively.

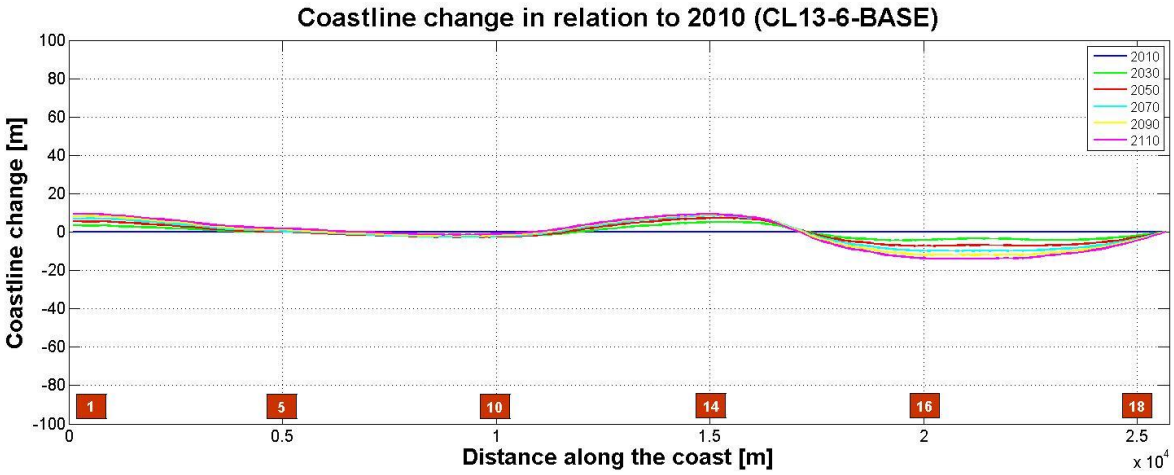

Figure 6.11: Coastline change relative to 2010 (no revetments, modified approach)

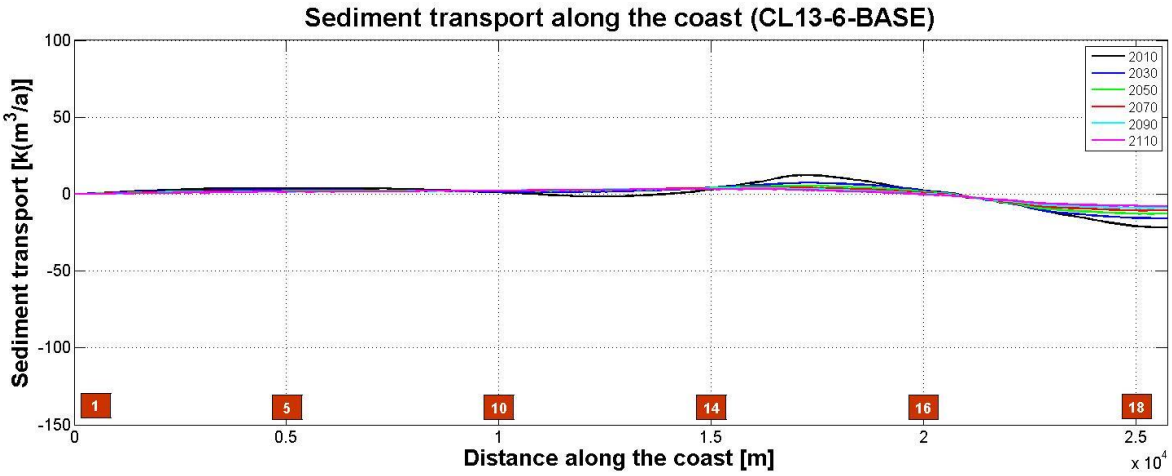

Figure 6.12: Sediment transport along the coast (no revetments, modified approach)

The results from the new approach indicate a much higher overall stability of the model. The sediment transport rates are extremely low by the end of the modelling period, indicating that the model is close to reaching a state of equilibrium. The trends in coastline position are very small – 0.2m per year at most – and are within acceptable limits. It is therefore assumed that the wave climate from the new approach better represents the actual wave climate inside the bay.

To compare the new approach to the coastline stability assessment, the output for the period of 1980 to 2010 is presented in Figure 6.13.

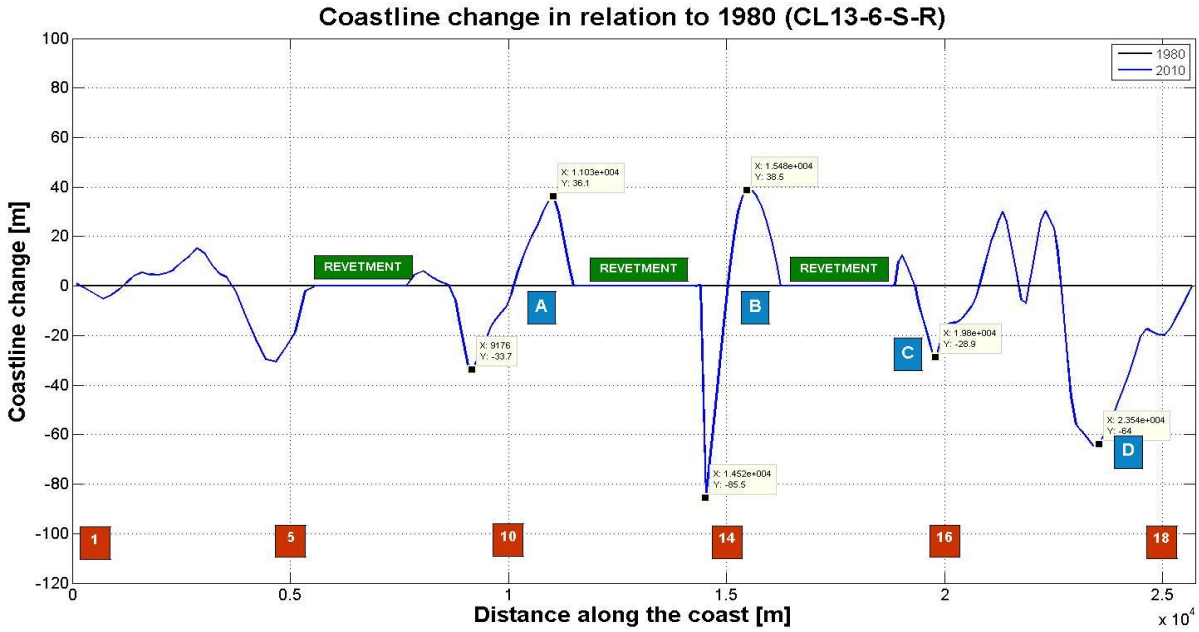

Figure 6.13: Coastline change relative to 1980 (with revetments, modified approach)

From Figure 6.13, it can be seen that all erosive and accretive peaks are lower. The erosive peak at position C has also showed significant improvement. However, the shoreline remains unstable at positions A, B, and D.

At position 4 there are no reefs visible in the intertidal zone. The model prediction of erosion in this area is therefore the result of a discrepancy between the equilibrium angle determined by the prescribed wave climate and the actual equilibrium angle of that section of coast. It is assumed to be caused by a local error in the wave transformation model which could be caused by the sparse bathymetry data in that area or the schematisation of the wave climate.

Since the locations of the kinks coincide with the positions of estuaries, it is difficult to assess whether the rotation predicted by the model is in fact occurring to some extent. At the estuaries, the stability of the coastline is subject not only to the longshore transport, but to a range of effects related to river mouth dynamics. The trend predicted by the model may therefore be hidden in the noise of opening and closing river mouths, storm impacts and floods. Moreover, the aerial images provide only a snapshot view of this dynamic area. These complex interactions cannot be accurately included in a one-dimensional shoreline model.

From the calibration exercise, the following primary observations are made regarding the accuracy of the model:

- During the calibration period, the shoreline is unstable at positions 1 and 2 located between the reefs and in close proximity to estuaries.

- After the initial smoothing of the coastline from 1980 to 2010, the model is very stable and fits the conclusion from the coastline stability assessment.
- The equilibrium coastline required by the local wave climate at position 4 does not agree with the stability assessment.

The primary objective of the coastline model is to investigate the long-term impacts of some climate change effects. Although the model has some areas of instability during the calibration period, acceptable stability is reached by 2010 and maintained for the duration of the projections. The results of the climate change simulations will therefore be based on the coastline predicted by the model at 2010, and not the input coastline at 2010. The results will also not be quantitative predictions of the future coastline position, rather qualitative assessments of the relative impacts of the various climate change effects considered.

The base case against which the results of the various climate change scenarios will be measured is presented in Figure 6.14. The base case considers the development of the coastline from 2010 to 2110 under the current wave climate and with the revetments present.

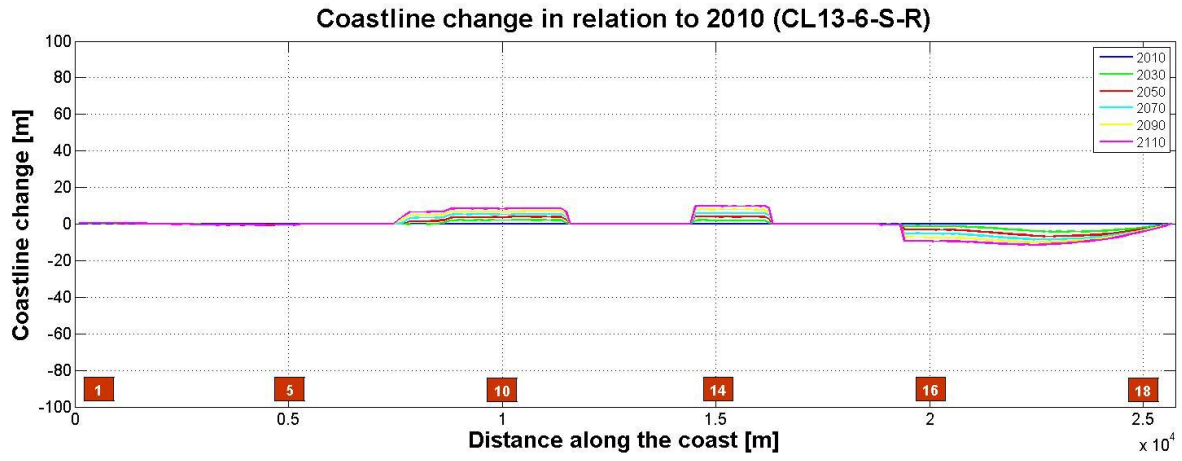

Figure 6.14: Coastline change relative to 2010 (Base case scenario)

6.4 Model sensitivity

The sensitivity of the coastline model to the following parameters was tested:

- Sediment particles (size +/- 20%)
- Sediment transport formulation (Bijker)

The transport formulation of Bijker (1968), like the van Rijn formula, describes the transport of sediment in detail by calculating the bed and suspended loads separately. In Figure 6.15, the sediment transport rates along the bay as calculated with the Bijker sediment transport formulation

are presented. Under the same conditions, the direction and shape of the sediment transport trend agree well with those obtained with the van Rijn formulation (see Figure 6.12). However, the magnitude of the transport is somewhat higher at 25 000 m^3/a vs. the 10 000 m^3/a obtained with the van Rijn formulation (see Figure 6.12). The model results are therefore rather sensitive to the choice of the transport formulation.

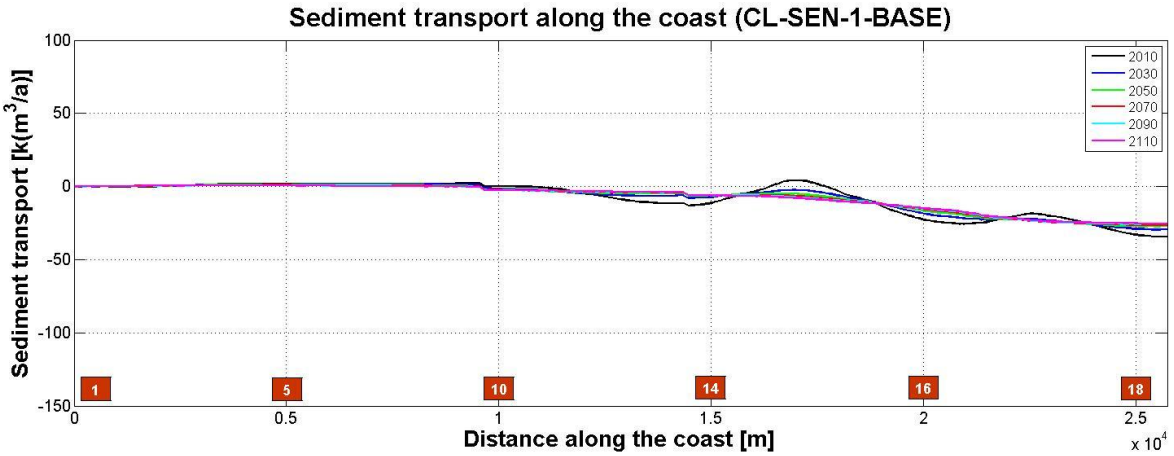

Figure 6.15: Sediment transport along the coast (Bijker formulation)

Generally, it is accepted that not all transport formulations are universally applicable and that once a formulation is chosen, it needs to be calibrated to fit the specific case. The base case selected in the calibration stage was observed to be sufficiently stable with the van Rijn formulation and default parameters. It is therefore assumed that the selected parameters for the van Rijn formulation are acceptable for this study. The higher transport rate from the Bijker formulation is consistent with the aforementioned findings of Bayram et al. (2001), that the Bijker formula over-estimates the magnitude of transport. The van Rijn formulation was considered the best choice for use in this study.

The magnitude of sediment transport is also a function of the sediment particle size. Smaller particles are transported more easily and should lead to higher transport rates. Since the particle size was not accurately measured, the model sensitivity to this parameter was also tested. The effect of the 20% smaller sediment particles is indicated in Figure 6.16 to increase the sediment transport rate by at least 100% when compared with the base case (Figure 6.12). The model is therefore sensitive to the particle size. The estimated distribution of median particle size is considered acceptable since sufficient agreement is found with results from previous studies (mentioned in Chapter 6.2).

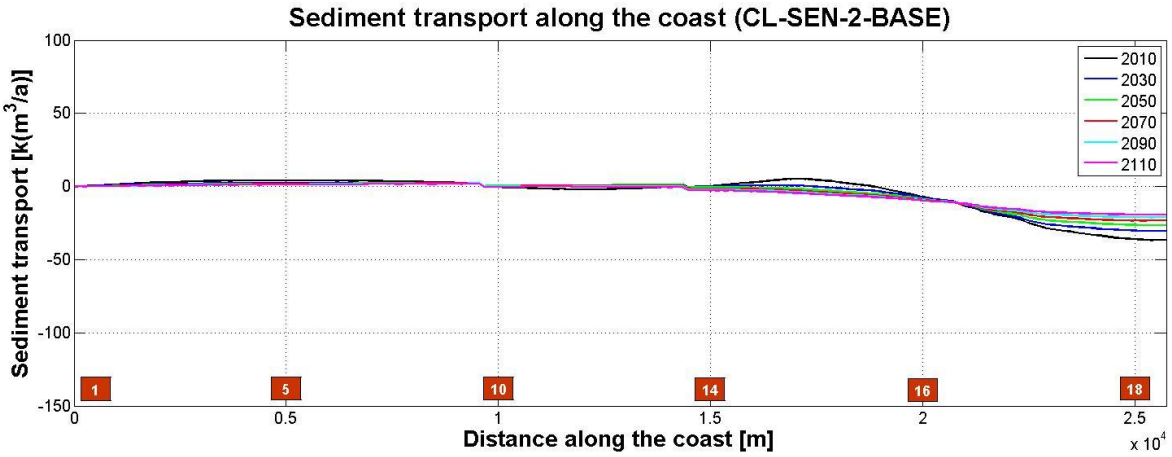

Figure 6.16: Sediment transport along the coast (20% smaller particle size)

6.5 Model runs

The set of selected climate change scenarios is presented in Table 6.1. The scenarios of sea-level rise were further modified to include some possible scenarios of when the reefs were to become less important. These scenarios are presented in Table 6.2.

In order to best present the impacts of the various climate change scenarios, the results are plotted relative to the base case scenario as discussed in Chapter 6.3. The model results are presented in the next chapter and are also discussed therein.

Table 6.1: Summary of Climate Change scenarios

Scenario	Description
SCN1	A linearly increasing sea-level from +0m MSL to +0.5m MSL
SCN2	A linearly increasing sea-level from +0m MSL to +1.0m MSL
SCN3	A linearly increasing sea-level from +0m MSL to +2.0m MSL
SCN4	A wave height increase of 10% from 2010 onwards
SCN5	A 1° southward shift of wave angles
SCN6	A 2° southward shift of wave angles

Table 6.2: Summary of sea-level rise computations

Scenario	Full Revetment	Revetment removed at:			
		+0.4m MSL	+0.8m MSL	+1.2m MSL	+1.6m MSL
SCN1	SCN1-FR	-	-	-	-
SCN2	SCN2-FR	SCN2-PR1	SCN2-PR2	-	-
SCN3	SCN3-FR	SCN3-PR1	SCN3-PR2	SCN3-PR3	SCN3-PR4

7 Results and discussion

7.1 Sea-level rise

Before interpreting the model results, it is valuable to assess what could be expected from the model. From the results of the wave transformation model, the following changes to the nearshore wave climate have been observed:

- A *clockwise* rotation of nearshore wave angles from south-westerly wave conditions along the entire bay periphery
- A *clockwise* rotation of the nearshore wave angles from easterly wave conditions in the western corner of the bay
- An *counter-clockwise* rotation of nearshore wave angles from easterly wave conditions along the rest of the bay periphery

The refracted nearshore wave angles of south-westerly waves are generally such that the consequent sediment transport is directed eastward. The supposed effect of the clockwise rotation of these nearshore angles is then to increase the obliquity with which the waves approach the coast, leading to an increase in easterly sediment transport.

In the areas where the nearshore angles from easterly waves experience a counter-clockwise rotation the effect is the same, but opposite, such that the westerly transport is increased. In the corner of the bay, the nearshore angles from easterly waves experience a clockwise rotation. Depending on the final angle with which these waves reach the shore, this rotation will either reduce the westerly transport or enhance the easterly transport.

By superimposing the above, the expected effect of sea-level rise is to cause a net eastward shift in the transport magnitude in the lee of the headland. Along the rest of the bay, the effects on the easterly and south-westerly waves are expected to counteract, but not necessarily cancel out one another.

The model results for the sea-level rise scenarios are presented in Figures 7.1 to 7.3. In this set of results, the revetments were present for the entire duration of the run. For each of the sea-level rise scenarios, the effects on the stability of the bay can be confined to three main areas.

- The sharp rotation in the south-western corner of the bay,
- the small rotation in the eastern end of the bay, and
- the negligible rotations in the centre of the bay between the revetments

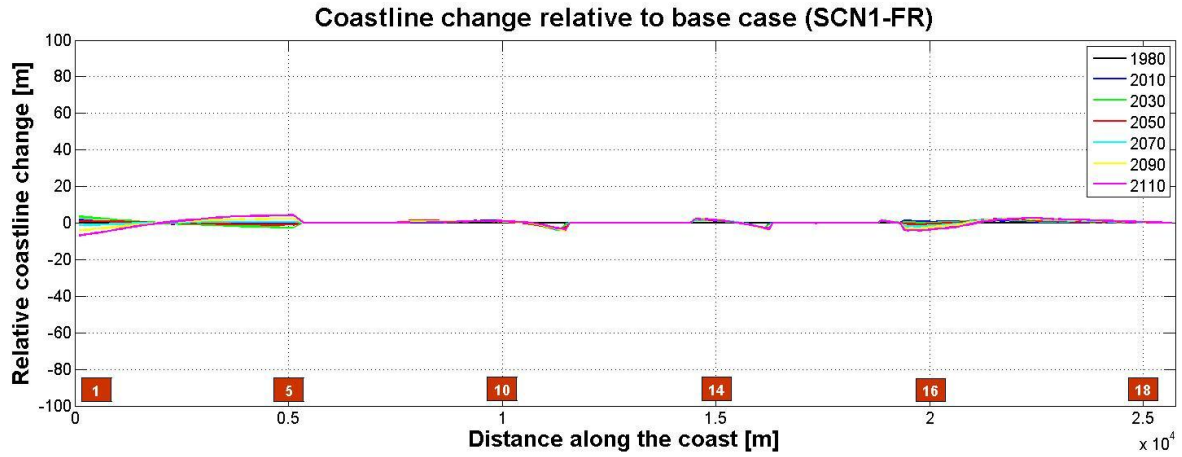

Figure 7.1: Coastline change relative to base case: SCN1 (0.5m SLR, with revetments)

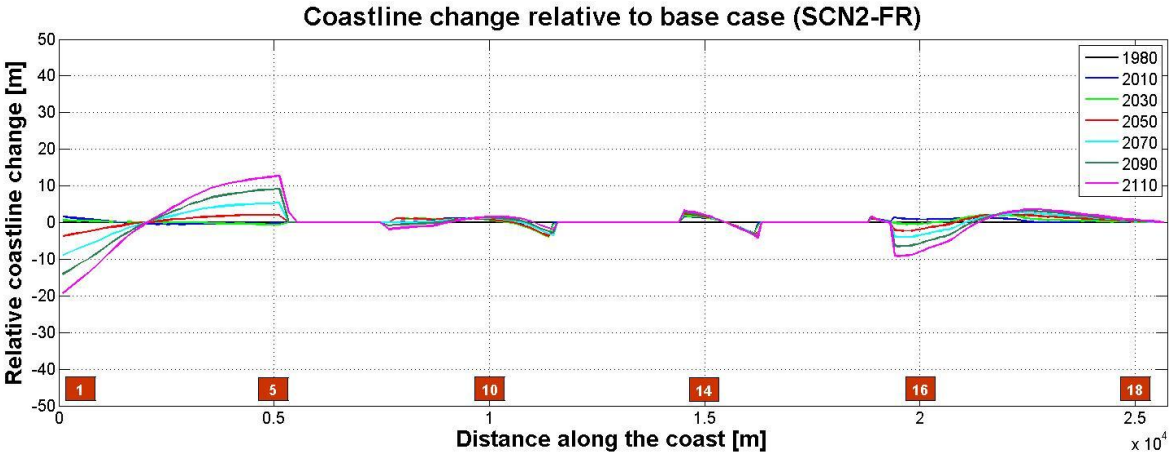

Figure 7.2: Coastline change relative to base case: SCN2 (1.0m SLR, with revetments)

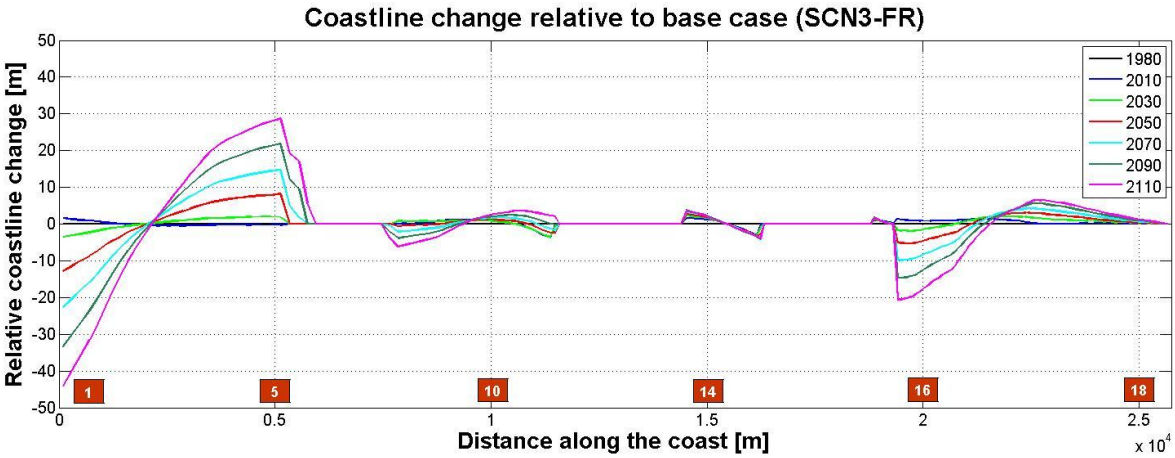

Figure 7.3: Coastline change relative to base case: SCN3 (2.0m SLR, with revetments)

In the south-western corner, the rotation is caused by an eastward movement of sediment – as expected due to the influence of the risen sea-level on wave refraction. At the eastern end, the same rotation is observed, but to a smaller extent. This rotation is also caused by an eastward directed transport. Here, the effect of sea-level rise on the two primary wave directions was expected to

counteract one another. When taking into account the far higher occurrence of the south-westerly waves, however, the net dominance of the eastward transport is logical.

Although the rotations seen as a result of a risen sea-level are noticeable in the plots presented, the displacements of the coastline are small – even for the extreme case of a 2.0m rise in the next 100 years. However, it should be kept in mind that the coastline change predicted by the model only reflects the effect of sea-level rise on the longshore sediment transport in Mossel Bay. Inundation and cross-shore erosion (such as that predicted by the Bruun rule) are not considered.

The three scenarios considered thus far have all neglected the fact that the intertidal reefs will become less influential under rising water levels. Scenarios SCN2-PR1 and SCN2-PR2, where the revetments are removed at +0.4m and +0.8m, respectively, are considered next. The results are presented in Figures 7.4 and 7.5.

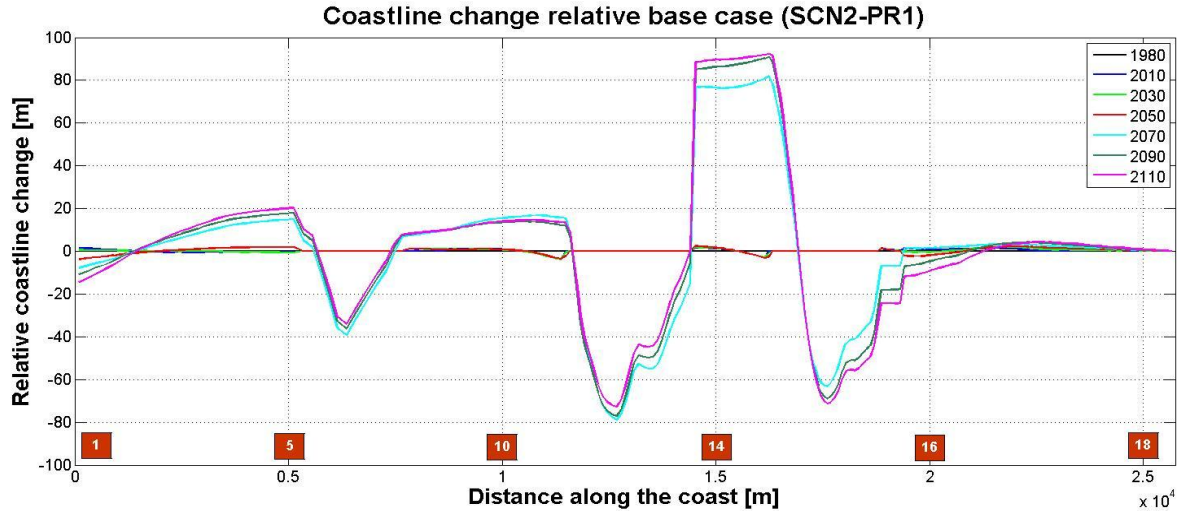

Figure 7.4: Coastline change relative to base case: SCN2-PR1 (1.0m SLR, revetments removed at +0.4m)

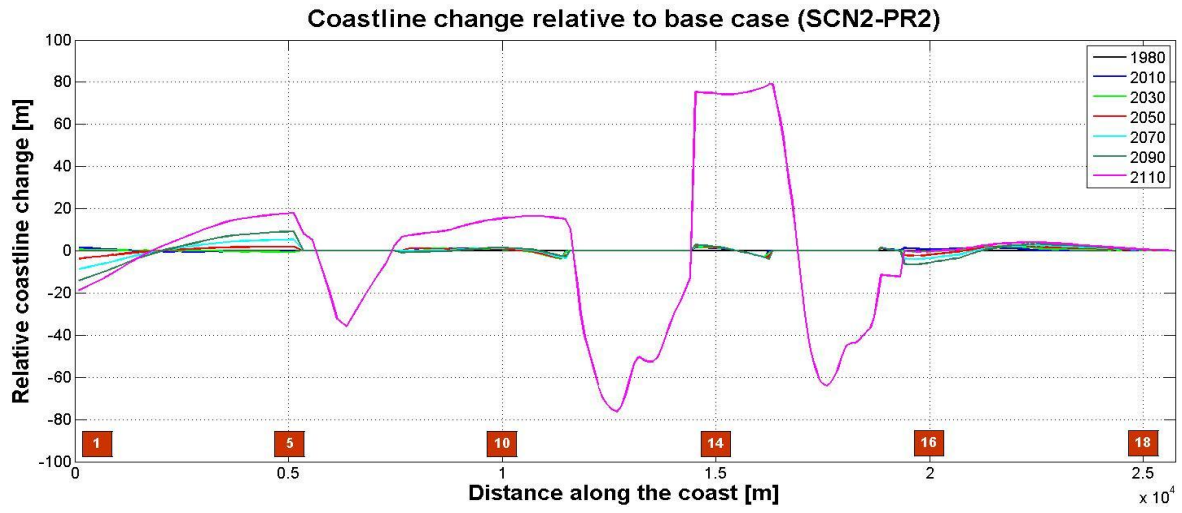

Figure 7.5: Coastline change relative to base case: SCN2-PR2 (1.0m SLR, revetments removed at +0.8m)

A significant redistribution of sediment is observed as soon as the revetments are removed. This observation reinforces the hypothesis that the reefs are very important to the current stability of the bay. Except for the timing of when the redistribution takes place, there is little difference between the end results of the two scenarios. In both cases, the redistribution is shown to result in areas of erosion in the order of 80m. The rotations at the two ends of the bay are still present, but are insignificant when compared to the other changes.

In Figures 7.6 and 7.7, the locations where the significant erosion is expected to take place are indicated. The two locations are directly south and north of Klein Brak, respectively.

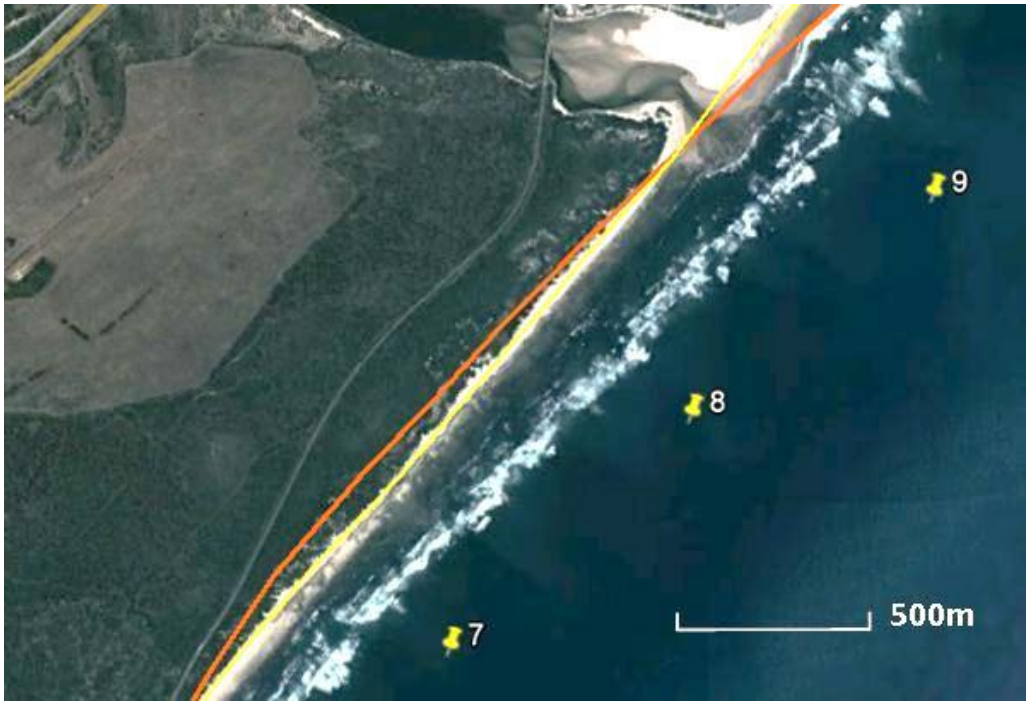

Figure 7.6: Erosion south of Klein Brak

The erosion seen in Figure 7.6 occurs on undeveloped land, and does not reach the railroad located further landward. As stated earlier, the coastline displacements presented in this study do not reflect the full extent of the possible erosion caused by sea-level rise. The line is drawn through large vegetated dunes. If these dunes are eroded, a significant amount of sediment previously stabilised by vegetation may be introduced into the sediment budget. However, the redistribution of sediment is a slow process and according to the model predictions, the sediment will be transported eastwards past Glentana and out of Mossel Bay.

Figure 7.7: Erosion north of Klein Brak

The area of erosion north of Klein Brak occurs in a developed area. Valuable holiday and residential houses are located in this area, on top of the primary dune behind the reefs. Unless this section of coastline is protected, the model results indicate that the dunes on which the houses are built will be eroded under the effect of sea-level rise.

7.2 Increased wave height

The longshore transport equations in Chapter 2.4 have displayed a higher-order relation between the wave height causing the transport and the magnitude of the transport. For each wave condition, an increase in wave height would therefore lead to a nonlinear increase in transport magnitude. If the same increase is applied to all wave conditions, the sum of the increased transports should therefore not necessarily equate to zero. Since the occurrence of south-westerly waves is much higher than that of easterly waves, the net effect is expected to be dominated by the south-westerly conditions. The expected net effect is therefore an increase in easterly transport.

In Chapter 5.5.2, it was concluded that the schematisation of waves and wind the wave transformation model did not allow for an accurate prediction of the effect of an increased wave height. The effect of this scenario was therefore not modelled in UNIBEST. Following the arguments presented above, an increase in the net westward transport is expected throughout the bay, leading to erosion along the entire periphery.

7.3 Southward rotation in offshore wave directions

Waves from the easterly sector have their biggest impact somewhere close to the western corner of the bay, since this is the route where the least refraction takes place. The angle of approach of easterly waves dictates that the consequent longshore transport will be directed westward. From the wave transformation model, we know that when the offshore angle is increased, the waves reach the shore at a slightly less oblique angle. Consequently, the magnitude of the transport away from the centre of the bay should be smaller. Conversely, the south-westerly waves have their biggest impact at the eastern end of the bay and cause an eastward transport. When their angle of approach is decreased, the magnitude of transport should be affected in the same way.

The model result for the case of a 1° poleward shift of wave directions is presented in Figure 7.8. For this case, the revetments were not included in the model.

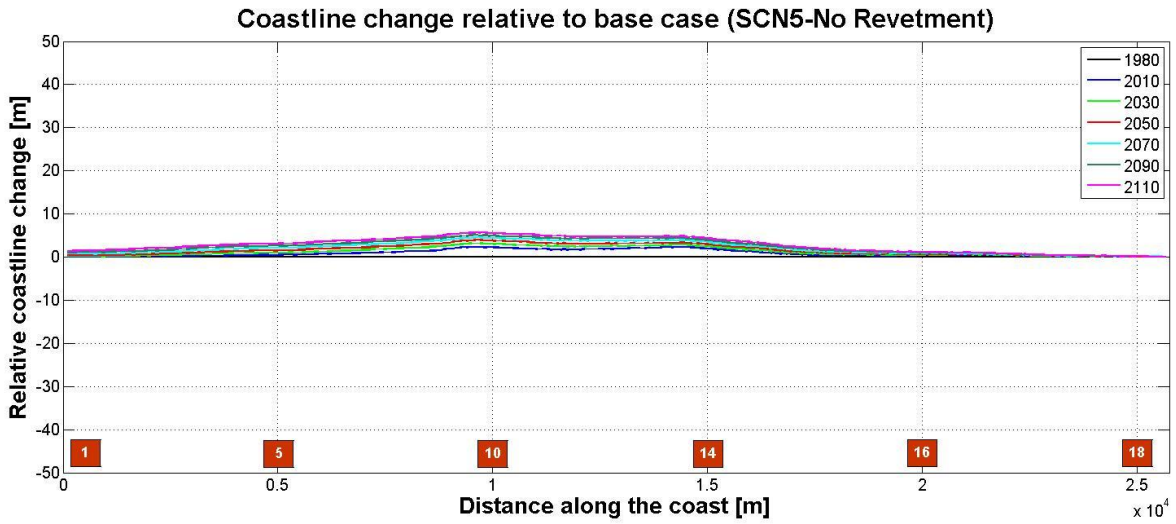

Figure 7.8: Coastline change relative to base case: SCN5 (1° rotation, no revetments)

The results indicate a very small relative accretion in the centre of the bay. This result is consistent with the logical arguments presented above. The southward angle shift has reduced the outward transport in the bay and has led to a small accretion in the centre of the bay, relative to the base case scenario. This relative accretion is so small, however, that when the revetments are kept in the model, no net effect can be observed.

The model results for the case of a 2° southward shift are presented in Figure 7.9. Once again, the case without the revetments is presented first. It is observed that the increased change in wave angle has moved the accretion further towards the eastern end of the bay and increased its magnitude. A negligible erosive trend is found in the western corner. Moreover, sediment is no

longer being transported eastward, rather westward as indicated by the small positive transport in Figure 7.10.

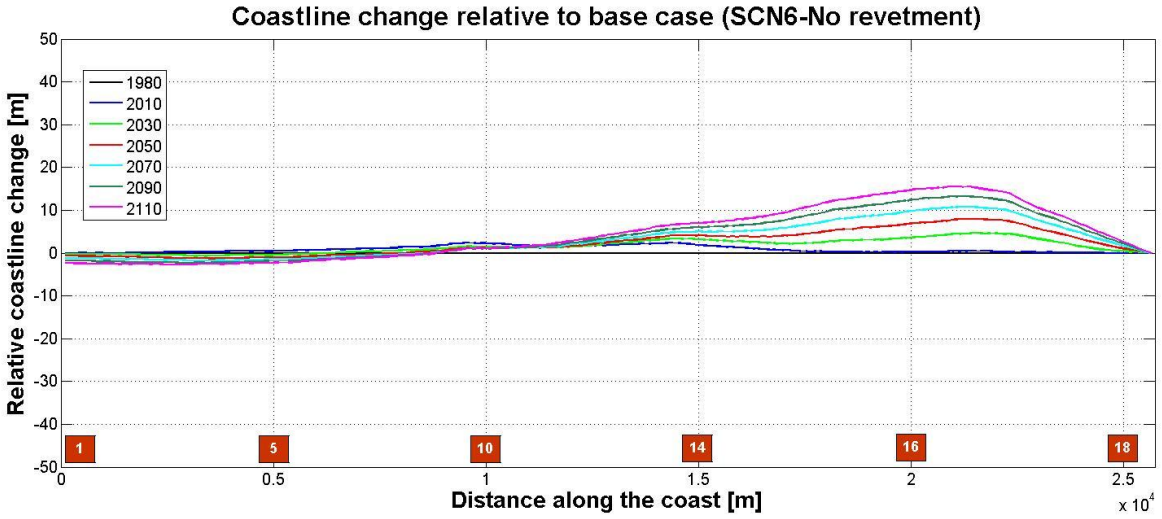

Figure 7.9: Coastline change relative to base case: SCN6 (2° rotation, no revetments)

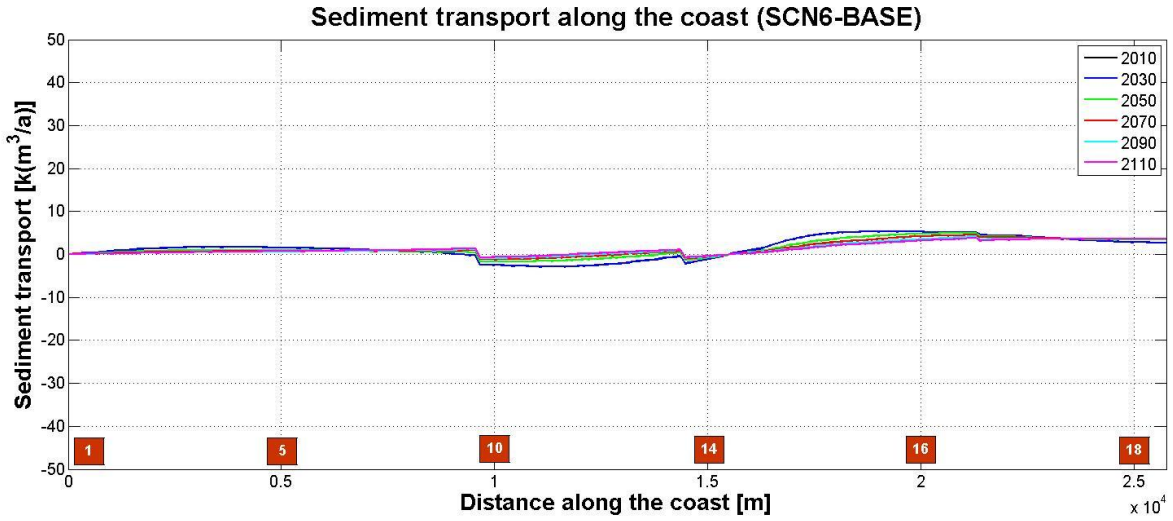

Figure 7.10: Sediment transport along the coast: SCN6 (2° rotation, no revetments)

It is probable that the change of transport direction is caused by the dominance of the south-westerly waves. Since the waves coming from the south-west have a far higher occurrence, the net effect of the changed wave angle is more pronounced on waves from this sector. For the 2 degree rotation, the effect of the increased wave angle has reduced the eastward directed transport sufficiently that the balance between eastward and westward transport has been reversed. The result is a net westward transport and an accretion throughout the bay.

When revetments are included in the model, the same overall rotational effect is observed. The coastline accretes at the eastern end and minor rotations are present between the revetments. The relative coastline change for the case of a 2 degree shift with revetments is presented in Figure 7.11.

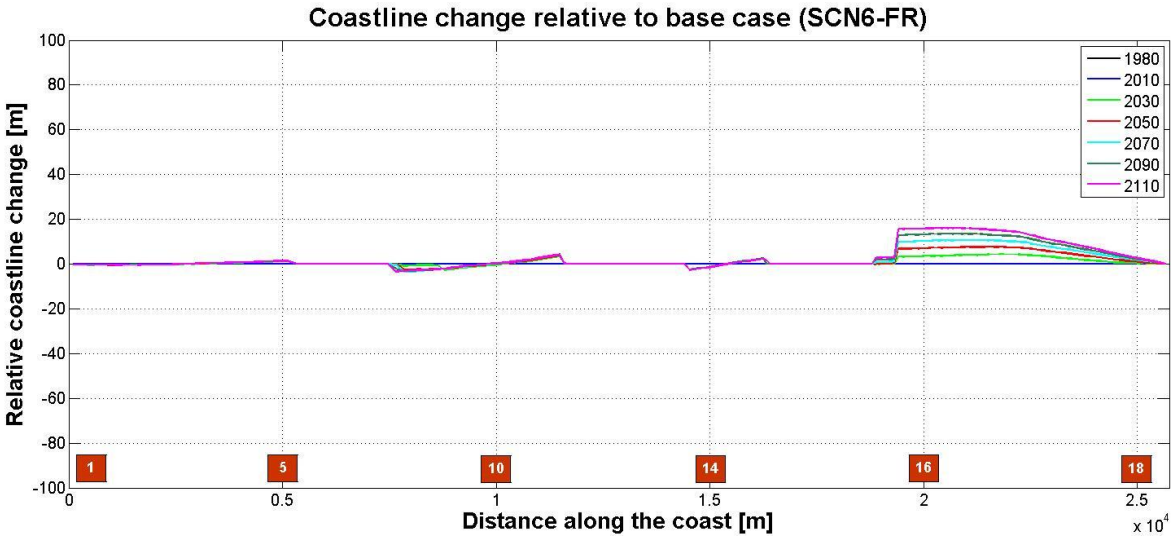

Figure 7.11: Coastline change relative to base case: SCN6 (2° rotation, with revetments)

Although the model predicts a net westward movement of sediment, the fact needs to be considered that the coastline east of Mossel Bay is a rocky stretch of roughly 20km without much available sediment. For this case, the boundary condition of a fixed coastline position does not represent the actual conditions, since there is no limit on the sediment transport into the bay from the east. In order to accurately investigate the impact of a 2 degree shift on Mossel Bay, the sediment dynamics of the adjacent coastlines need to be considered in a much larger model.

8 Conclusions and recommendations

Climate change and its associated consequences are a cause for concern. In order to enable long-term management decisions, it is necessary to gain an understanding of the possible erosive effects of climate change on coastlines. Much work has been done on the linear setback caused by a rise in sea-level through models such as the Bruun Model. In order to comprehend the broader effect of climate change, the secondary effects of sea-level rise on local wave climates need to be considered. Furthermore, the increased wave heights and possible southward rotation of wave directions also need to be considered.

The objective of this study was to investigate the impact of some consequences of climate change on the stability of a typical headland-bay beach on the southern coast of South Africa. The three main climate change effects considered were:

- Sea-level rise
- An increased wave height
- A southward rotation of offshore wave directions

The impacts were assessed through numerical modelling. The main conclusions obtained through the modelling approach are presented in this chapter.

8.1 Sea-level rise

The hypothesis that a rise in sea-level would affect the refraction of the waves has been confirmed. The changes in incident wave angles have caused the following significant trends in the bay periphery:

- A sharp rotation in the south-western corner of the bay
- A small rotation in the eastern end of the bay

The magnitude of the rotations varies with the extent of the rise in sea-level, with the biggest rotations caused by the largest increase in water level. In addition to the effect of the risen sea-level on the refraction of waves, the importance of the intertidal reefs to the current stability of Mossel Bay has been discovered. Under the effect of sea-level rise, the stabilising effect of these reefs will become less significant such that a redistribution of sediment is expected to take place.

The coastline changes predicted by this study do not represent the total effect of sea-level rise, but rather the effect of sea-level rise on the longshore transport regime in Mossel Bay. Significant setback may arise due to inundation and cross-shore erosion as suggested by equations such as the Bruun Rule.

8.2 Increased wave height

The model results for the increased wave height were inconclusive. The wave transformation model was found to be unsuitable for the simulation of the scenario of an increased wave height due to the approach of wind and wave schematisation.

8.3 Southward rotation of offshore wave directions

The rotation of offshore wave directions causes a reduction in the outward directed transports at both ends of the bay. The net effect is observed as an accretion in the centre of the bay. For the case of a 1° southward rotation in wave angle, the observed accretion is small (~5m by 2110). For the case of a 2° rotation, the accretion is located further eastward and is somewhat larger (~15m by 2110). The eastward shift is due to the dominance of south-westerly waves in the offshore wave climate.

8.4 Summary of findings

The findings of this study can be summarised as:

- Sea-level rise will cause changes to the nearshore wave climate in Mossel Bay such that counter-clockwise rotations causing erosion in the order of 20m could occur by 2110 for a 1m rise in sea level. These rotations represent only the effect of SLR on the nearshore wave climates and associated longshore transport and not the effects of inundation or erosion due to SLR.
- A rising sea level will cause the intertidal reefs to become less prominent. If a sufficiently high water level is reached, a significant redistribution of sediment is expected, causing erosion in the order of 80m.
- A southward rotation of offshore wave directions larger than 1° is expected to cause a noticeable accretion in the eastern part of the bay by 2110.

8.5 Limitations of the modelling approach

The modelling approach used in this study employed two numerical models. A wave transformation model was used to transform an offshore wave climate into the bay. The nearshore wave climate was then used in a coastline model to calculate the longshore transport and the stability of the bay. This modelling approach had some limitations:

- The schematisation of the offshore wave and wind conditions
- The representation of the reefs in the coastline model

The ideal approach to obtain a nearshore wave climate would be to construct it directly from a time series of nearshore measurements. Such a time series is obviously not available at all nearshore locations in the bay, but a long-term time series is available offshore. The second best approach is therefore to transform the entire offshore time series into the bay and construct the nearshore climates from the results. However, this approach is too computationally intensive since the 10-year dataset contains over 30 000 data points. The approach used in this study was therefore to construct an offshore wave climate, and to transform the limited number of conditions into the bay. A total of 150 offshore wave conditions each with its own probability of occurrence were therefore chosen to represent the annual wave climate.

The offshore wave conditions mostly only represent swell waves, while sediment is also moved by locally generated waves. The importance of the wind waves was well noted in both the calibration of the wave and coastline models. The inclusion of the wind in the wave model was therefore found to be very important. In this study, one of two wind conditions was statistically coupled to each wave condition. This crude approach was calibrated by increasing the mean wind speed of the easterly winds to account for the lack of easterly wave energy. Although the model was found to be sufficiently calibrated for the sea-level rise scenarios, the model could not accurately model the effects of an increased wave height under this approach.

The second limitation in the modelling approach is the representation of the intertidal reefs. UNIBEST is a one-dimensional model which only considers longshore sediment transport. The complex cross-shore hydrodynamic sediment transport can therefore not be accurately reflected. Moreover, the diminishing of the dissipative and protective effects of the reefs due to sea-level rise cannot be modelled gradually. Therefore, the model can only predict the result when the reefs are totally insignificant and no intermediate observations can be made.

8.6 Recommendations

In order to enable long-term management decisions, it is recommended that the findings of this study be superimposed on the cross-shore erosion caused by sea-level rise. The combined coastline trends can then be used for the planning of coastal protection works or beach nourishment strategies. It is also recommended that the undeveloped dune area between Klein Brak and Hartenbos remain undeveloped, since the model predictions indicate the possibility of significant erosion in this area. Vulnerable areas such as this should be monitored (beach profiles, etc.).

In order to investigate the effects of an increase in the average offshore wave height, it is recommended that a different approach toward the wind and wave schematisation be considered. It

is suggested that the occurrence of offshore wave conditions and wind conditions be considered separately. The data should be binned into a number of wave conditions and wind conditions. These conditions should then be transformed into the bay and their duration scaled down to one year. These resulting climates can then be fed to UNIBEST which will calculate the sediment transport as a result of the swell waves and wind waves separately. In this way, the height of the offshore waves can be increased without the mean spectral direction being affected.

Lastly, it is recommended that the complex hydrodynamic sediment interaction with the intertidal reefs be examined in more detail. Through a full 3D morphodynamic model such as XBeach, the effect of the reefs on the cross-shore and longshore transports can be better understood. Moreover, the sea-level at which these reefs become insignificant should be determined.

9 Bibliography

AR Wijnberg Inc., 1995. Mossel Bay Municipality. Voorbaai marine outfall: Site investigations interim progress report.

Allison, I. et al., 2009. *The Copenhagen Diagnosis: Updating the World on the Latest Climate Science*, Sydney, Australia: The University of New South Wales Climate Change Research Centre (CCRC).

Barwell, L., 2011. Integrity assessment procedure for buffer dune systems on the Cape south coast, South Africa. Master's Thesis, University of Stellenbosch, Stellenbosch, South Africa.

Bayram, A. et al., 2001. Cross-shore distribution of longshore sediment transport: comparison between predictive formulas and field measurements. *Coastal Engineering*, 44, 79 - 99.

Bijker, E.W., 1968. Littoral drift as a function of waves and current. In *11th Conference on Coastal Engineering*. London, U.K., pp. 415-435.

Bindoff, N.L. et al., 2007. *Observations: Oceanic Climate Change and Sea Level. In: Climate Change 2007: The Physical Science Basis. Contribution of Working Group I to the Fourth Assessment Report of the Intergovernmental Panel on Climate Change*. S. Solomon et al., Cambridge, United Kingdom and New York, NY, USA: Cambridge University Press.

Birkemeier, B.W., 1985. Field data on seaward limit of profile change. *Journal of Waterway, Port, Coastal and Ocean Engineering*, 111(3), 598-602.

Booij, N., Ris, R.C. & Holthuijsen, L.H., 1999. A third-generation wave model for coastal regions. 1: Model description and validation. *Journal of Geophysical Research*, 104, 7649 -7666.

Bosboom, J. & Stive, M.J., 2012. *Coastal Dynamics I* 0.3., Delft, the Netherlands: VSSD.

Brunel, C. & Sabatier, F., 2009. Potential influence of sea-level rise in controlling shoreline position on the French Mediterranean Coast. *Geomorphology*, 107(1-2), 47-57. Available at: http://linkinghub.elsevier.com/retrieve/pii/S0169555X08004984.

CEM, 2003. *Coastal Engineering Manual*, US Army Corps of Engineers.

CERC, 1984. *Shore Protection Manual* 4th ed., Washington, DC: U.S. Army Corps of Engineers. U.S Government Printing Office.

CSIR, 1988. Bathymetric and geophysical survey - Mossel Bay. CSIR Report EMA-C8871.

CSIR, 2003. Sediment transport regime and location of dredge dumpsite at the Port of Mossel Bay. CSIR Report ENV-S-C2004-069. March 2003.

CSIR, 2000. South Africa Estuaries: Data report on Topographical Surveys for Selected Estuaries: 1985-1999. Volume 1: Northern Cape and Western Cape.

Chadwick, A., Morfett, J. & Borthwick, M., 2004. *Hydraulics in Civil and Environmental Engineering* 4th ed., Abingdon: Spon Press.

Cooper, J. & Pilkey, O., 2004. Sea-level rise and shoreline retreat: time to abandon the Bruun Rule. *Global and Planetary Change*, 43, 157-171. Available at: http://linkinghub.elsevier.com/retrieve/pii/S0921818104001195.

Corbella, S. & Stretch, D.D., 2012. Decadal trends in beach morphology on the east coast of South Africa and likely causative factors. *Natural Hazards and Earth System Sciences*, 12(8), 2515-2527.

DEFRA, 2006. Flood and Coastal Defence Appraisal Guidance FCDPAG3 Economic Appraisal Supplementary Note to Operating Authorities – Climate Change Impacts.

Davidson-Arnott, R.G., 2005. Conceptual Model of the Effects of Sea Level Rise on Sandy Coasts. *Coastal Research*, 21(6), 1166-1173.

Dean, R.G. & Dalrymple, R.A., 2002. *Coastal Processes with Engineering Applications*, Cambridge: Cambridge University Press.

Deltares, 2010. *Delft3D-WAVE Simulation of short-crested waves with SWAN. User Manual* 3.04., Delft, The Netherlands: Deltares.

Dronkers, J., 2005. *Dynamics of Coastal Systems*, Singapore: World Scientific Publishing Co. Pte. Ltd.

Fredsoe, J. & Deigaard, R., 1992. *Mechanics of coastal sediment transport* First Edit., Singapore: World Scientific Publishing Co. Pte. Ltd.

González, M. & Medina, R., 2001. On the application of static equilibrium bay formulations to natural and man-made beaches. *Coastal Engineering*, 43, 209-225.

Hallermeier, R.J., 1981. A profile zonation for seasonal sand beaches from wave climate. *Coastal Engineering*, 4, 253-277.

Hanson, H. & Kraus, N.C., 2011. Long-term evolution of a long-term evolution model. Journal of Coastal Research, (50), 118-129.

Hanson, H., 1989. Genesis: A generalised shoreline change numerical model. J*ournal of Coastal Research*, 5(1), 1-27.

Hasselmann, K. et al., 1973. Measurements of wind-wave growth and swell decay during the Joint North Sea Wave Project (JONSWAP). *Erganzungsheft zur Deutschen Hydrographischen Zeitschrift*, A8(12).

Holthuijsen, L.H., 2007. *Waves in Oceanic and Coastal Waters*, New York: Cambridge University Press.

Hsu, J.R. & Evans, C., 1989. Parabolic bay shapes and applications. In *Proceedings of the Institution of Civil Engineers, Part 2*. pp. 557-570.

Hsu, J.R. et al., 2010. Static bay beach concept for scientists and engineers: A review. *Coastal Engineering,* 57, 76-91. Available at: http://dx.doi.org/10.1016/j.coastaleng.2009.09.004.

IPCC, 2007. Summary for Policymakers. *In: Climate Change 2007: The Physical Science Basis. Contribution of Working Group I to the Fourth Assessment Report of the Intergovernmental Panel on Climate Change.* M. T. Solomon, S., D. Qin, M. Manning, Z. Chen, M. Marquis, K.B. Averyt, Cambridge, United Kingdom and New York, NY, USA: Cambridge University Press.

Kapp Prestedge & Retief, 1988. Model investigations of possible extensions to Mossel Bay Harbour.

Komar, P.D., 1998. *Beach Processes and Sedimentation* 2nd ed., New Jersey: Prentice-Hall.

Lausman, R., Klein, A.H. & Stive, M.J., 2010. Uncertainty in the application of the Parabolic Bay Shape Equation : Part 1. *Coastal Engineering*, 57, 132-141. Available at: http://dx.doi.org/10.1016/j.coastaleng.2009.09.009.

Lausman, R., Klein, A.H. & Stive, M.J., 2010. Uncertainty in the application of the parabolic bay shape equation: Part 2. *Coastal Engineering*, 57, 142-151. Available at: http://linkinghub.elsevier.com/retrieve/pii/S0378383909001392.

Longuet-Higgins, M., 1970. Currents Generated by Obliquely Incident Sea Waves. *Geophysical Research,* 75(33), 6778-6789.

Mather, A.A. & Stretch, D.D., 2012. A Perspective on Sea Level Rise and Coastal Storm Surge from Southern and Eastern Africa: A Case Study Near Durban, South Africa. *Water*, 237-259.

Mather, A.A., Garland, G. & Stretch, D., 2009. Southern African sea levels: corrections, influences and trends. African Journal of Marine Science, 31(2), 145-156.

Mather, A.A., 2008. Sea-level rise for the east coast of South Africa. In *COPEDEC VII*. Paper no M-04. Dubai, UAE.

Mavume, A.F. et al., 2009. Climatology and Landfall of Tropical Cyclones in the South-West Indian Ocean. *Journal of Maritime Science*, 8(1), 15-36.

Melis & Du Plessis, 1990. Report on the marine geotechnical study for the product export pipeline route and SPM site at Voorbaai, Mossel Bay. , A3-A5.

Moreno, L.J. & Kraus, N.C., 1999. Equilibrium shape of headland-bay beaches for engineering design. In *Coastal Sediments*. pp. 860 - 875.

Mori, N. et al., 2010. Projection of Extreme Wave Climate Change under Global Warming. *Hydrological Research Letters*, 4, 15-19.

PRDW, 2010. Global Climate Change: Consequences for coastal engineering design. Position paper. Report No. 939/1/001.

PRDW, 2001. Mossel Bay port study. Wind, wave and current data report 3.

Pierson, W.J. & Moskowitz, L., 1963. A proposed spectral form for fully developed wind seas based on the similarity theory of S.A. Kitaigorodskii. New York University. Department of Meteorology and Oceanography. *Geophysical Sciences Laboratory Report* 63-12. October.

Rooseboom, A., 1975. Sedimentproduksiekaart vir Suid-Afrika. Technical Report No. 61, DWA.

Rossouw, J., 1989. Design waves for the South African coastline. Master's Thesis, University of Stellenbosch, Stellenbosch, South Africa.

Rossouw, M. & Theron, A.K., 2009. Investigating the potential Climate Change impacts on maritime operations around the South African coast. In *Sustainable Transport: 28th Annual Southern African Transport Conference (SATC) 2009*, Pretoria, South Africa.

SANHO, 2012. South African Tide Tables.

Schoonees, J.S. & Theron, A.K., 1996. Improvement of the most accurate longshore transport formula. In *Proceedings of the 25th Conference on Coastal Engineering*. Orlando, Florida: ASCE, pp. 3652-3665.

Schoonees, J.S. & Theron, A.K., 1993. Review of the field-data base for longshore sediment transport. *Coastal Engineering*, 19, 1-25.

Schoonees, J.S., 1996. Longshore sediment transport in terms of the applied wave power concept. Master's Thesis, University of Stellenbosch, Stellenbosch, South Africa.

Schwartz, M.L., 2005. *Encyclopaedia of Coastal Science*. Dordrecht: Springer, pp. 510-511.

Schwartz, M.L., 1967. The Bruun Theory of Sea-Level Rise as a Cause of Shore Erosion. *Journal of Geology*, 75(1), 76-92. Available at: http://www.jstor.org/stable/30084988 .

Silvester, R. & Ho, S., 1980. Use of crenulate shaped bays to stabilize coasts. In *17th International Conference on Coastal Engineering*. Sydney, Australia: ASCE, pp. 1306-1319.

Silvester, R., Tsuchiya, Y. & Shibano, Y., 1972. Zeta bays, pocket beaches and headland control. In *13th International Conference on Coastal Engineering*. Vancouver, Canada: ASCE, pp. 1347-1365.

Singleton, A. & Reason, C.J., 2007. A Numerical Model Study of an Intense Cutoff Low Pressure System over. *Monthly Weather Review*, 135(3), 1128-1150.

Theron, A.K. et al., 2012. Coastal Planning and Adaptation to Mitigate Climate Change Impacts - Responding to Climate Change in Mozambique (Phase II, Theme 2). Report prepared for National Institute for Disaster Management (INGC) by CSIR, CSIR Stellenbosch, South Africa.

Theron, A.K., 1994. Sea level rise impacts and the use of Bruun's erosion rule. *SAICE Journal*, (4)

van Rijn, L.C. & Kroon, A., 1992. Sediment transport by currents and waves. In *23rd International Conference of Coastal Engineering*. Venice, Italy.

van Rijn, L.C., 1998. *Principles of Coastal Morphology* 1 ed., Amsterdam, The Netherlands: Aqua Publications.

WL|Delft-Hydraulics, 2005. *UNIBEST CL+ 6.0 User and Theoretical Manual*.

Yasso, W.E., 1965. Plan Geometry of Headland-Bay Beaches. *Journal of Geology*, 73(5), 702-714.

Zhang, K., Douglas, B.C. & Leatherman, S.P., 2004. Global Warming and Coastal Erosion. *Climatic Change*, 64, 41-58. Available at: http://www.springerlink.com/openurl.asp?id=doi:10.1023/B:CLIM.0000024690.32682.48.

Appendix A: SWAN

In this section, some aspects of the numerical scheme as well as the most important formulations used in SWAN will be explained.

For most wave transformation models where calculations are made in explicit schemes, stability is determined by the Courant criterion which states that the wave energy may not propagate more than one grid cell in geographical space in one time-step, such that (Holthuijsen, 2007):

$$\Delta t < \begin{cases} \Delta x / c_{g,x} \\ \Delta y / c_{g,y} \end{cases} \tag{B.1}$$

where c_g is the wave group velocity[8] in the x- and y-directions and Δx and Δy are the grid cell dimensions. In deep water with a coarse grid resolution this criterion is acceptable, but in order to resolve wave processes in shallow water a much finer grid is needed. This results in very short time steps which cause models to become too computationally intensive. In SWAN, calculations are therefore done in implicit numerical schemes which are fundamentally stable.

For the propagation of wave energy, SWAN uses the Eulerian approach (Booij et al., 1999). As opposed to the Lagrangian approach where the computation follows the wave ray while accounting for changes in wave energy, the Eulerian approach allows for finite-difference computations to balance the local energy at every grid point. For deep water, Holthuijsen (2007) schematises this approach as:

$$change\ of\ energy\ in\ cell = net\ import\ of\ energy + local\ generation\ of\ energy \tag{B.2}$$

where:

$$change\ of\ energy\ in\ a\ cell = \frac{\partial E(f,\theta;x,y,t)}{\delta t} \tag{B.3}$$

$$net\ import\ of\ energy\ in\ the\ x-direction = -\frac{\partial c_{g,x} E(f,\theta;x,y,t)}{\delta x}\Delta x\Delta y\Delta t \tag{B.4}$$

$$net\ import\ of\ energy\ in\ the\ y-direction = -\frac{\partial c_{g,y} E(f,\theta;x,y,t)}{\delta y}\Delta x\Delta y\Delta t \tag{B.5}$$

$$local\ generation\ of\ energy\ (source\ term) = S(f,\theta;x,y,t) \tag{B.6}$$

and thus:

[8] Outside the surf-zone, wave energy propagates at the wave group velocity, c_g

$$\frac{\partial E(f,\theta;x,y,t)}{\delta t} + \frac{\partial c_{g,x} E(f,\theta;x,y,t)}{\delta x} + \frac{\partial c_{g,y} E(f,\theta;x,y,t)}{\delta y} = S(f,\theta;x,y,t) \quad \text{(B.7)}$$

In deep water, the net import of energy (or energy propagation) is the finite difference between the energy import and export for both the x- and y-directions. In the nearshore, however, the effects of refraction, shoaling and diffraction are also included. The processes of refraction and diffraction cause a further propagation of wave energy from one directional sector to another. To represent this turning effect, the following term[9] is added to the left-hand side of the energy balance equation to move energy from one directional sector to another (Holthuijsen, 2007):

$$net\ import\ of\ energy = -\frac{\partial c_\theta E(f,\theta;x,y,t)}{\delta \theta} \Delta\theta \Delta x \Delta y \Delta t \quad \text{(B.8)}$$

The local generation of energy is summarised in the source term (the right-hand side of Equation B.6) as the sum of wind generation (S_{in}), nonlinear wave–wave interactions (S_{nl}) and dissipation (S_{diss}):

$$S = S_{in} + S_{nl} + S_{diss} \quad \text{(B.9)}$$

The dissipation term includes the effects of white-capping, bottom friction and depth-induced breaking as discussed in Chapter 2. In SWAN, white-capping is added as an energy sink applied over the whole model in a quasi-linear formulation related to the overall steepness of the wave spectrum. The maximum wave height for the modelling of depth-induced breaking is determined from the breaker parameter:

$$\gamma = H_{max}/D \quad \text{(B.10)}$$

with a default value of 0.73.

SWAN is also able to include the effects of wave–current interactions. In order to include this process, the Energy Balance Equation (Equation B.7) is modified to the Action Balance Equation (Holthuijsen, 2007).

[9] This term is also derived from a finite-difference approach. The import of energy is schematised as the finite difference between the energy entering and leaving a directional bin.

Appendix B: Offshore wave conditions used in SWAN

Number	Significant wave height [H_{m0}]	Peak period [T_P]	Direction [°N]	Occurrence [%]
1	1.65	5.14	82.13	0.18
2	1.71	5.20	100.01	0.25
3	1.53	5.35	125.04	0.10
4	1.72	5.50	215.00	0.02
5	1.71	4.99	240.60	0.08
6	1.78	4.88	263.45	0.14
7	1.77	7.06	83.48	0.12
8	1.78	7.09	98.58	0.58
9	1.67	7.25	141.32	0.29
10	1.69	7.50	195.35	0.10
11	1.68	7.39	213.19	0.16
12	1.50	7.26	235.98	0.13
13	1.69	6.79	256.65	0.05
14	1.77	8.75	84.58	0.06
15	1.77	8.70	101.11	0.52
16	1.73	8.97	147.52	0.97
17	1.75	9.29	193.57	0.77
18	1.74	9.39	215.76	2.51
19	1.66	9.34	231.05	0.98
20	1.42	8.71	254.43	0.03
21	1.76	10.51	102.43	0.03
22	1.77	10.30	156.10	0.17
23	1.75	10.66	196.26	0.49
24	1.81	10.72	215.04	3.71
25	1.79	10.71	230.46	1.04
26	1.53	10.06	248.95	0.00
27	1.62	12.67	161.73	0.02
28	1.74	12.25	195.76	0.06
29	1.81	12.68	216.67	0.47
30	1.82	12.43	231.70	0.08
31	1.83	14.32	163.76	0.00
32	1.88	14.39	200.71	0.01
33	1.87	14.92	217.37	0.06
34	1.82	15.25	229.63	0.02
35	2.40	5.56	82.55	0.47
36	2.37	5.60	98.73	0.64
37	2.33	5.62	132.35	0.08
38	2.04	5.84	191.08	0.01
39	2.06	5.60	213.66	0.01
40	2.30	5.63	241.42	0.14

Number	Significant wave height [H_{m0}]	Peak period [T_P]	Direction [°N]	Occurrence [%]
41	2.38	5.51	262.82	0.42
42	2.57	6.94	85.75	1.45
43	2.50	6.98	96.77	2.13
44	2.50	7.22	139.97	0.66
45	2.34	7.50	193.63	0.11
46	2.39	7.33	214.56	0.22
47	2.57	6.91	238.49	0.53
48	2.66	6.67	258.60	0.73
49	2.49	8.62	87.02	0.43
50	2.43	8.81	99.46	1.55
51	2.39	9.08	147.59	1.74
52	2.40	9.22	193.48	1.02
53	2.38	9.49	214.33	3.77
54	2.39	9.30	232.17	1.33
55	2.60	8.88	253.14	0.08
56	2.51	10.51	86.41	0.03
57	2.34	10.48	102.57	0.13
58	2.52	10.66	157.27	0.87
59	2.49	10.83	195.34	2.18
60	2.45	11.02	214.51	17.82
61	2.40	10.92	229.66	2.60
62	2.24	12.28	159.44	0.07
63	2.58	12.64	198.09	0.31
64	2.57	12.65	215.20	7.69
65	2.49	12.70	228.18	1.00
66	2.64	14.54	198.36	0.05
67	2.61	14.59	215.08	0.64
68	2.46	14.57	228.38	0.11
69	2.79	16.67	199.86	0.01
70	2.60	16.70	216.52	0.04
71	2.08	16.07	225.81	0.00
72	3.18	5.86	84.77	0.03
73	3.14	5.78	95.45	0.02
74	3.32	5.79	281.33	0.01
75	3.33	7.16	85.36	0.78
76	3.33	7.11	96.15	0.82
77	3.35	7.30	135.73	0.29
78	3.24	7.37	194.82	0.02
79	3.40	7.44	216.80	0.04
80	3.36	7.34	240.24	0.31

Number	Significant wave height [H_{m0}]	Peak period [T_P]	Direction [°N]	Occurrence [%]
81	3.39	7.22	261.58	0.68
82	3.42	8.54	86.81	0.41
83	3.33	8.73	97.64	0.40
84	3.43	9.07	152.42	0.58
85	3.34	9.31	191.58	0.32
86	3.31	9.45	216.43	0.76
87	3.49	9.11	235.08	0.79
88	3.63	8.57	257.18	0.22
89	3.38	10.87	86.39	0.01
90	3.30	10.44	105.07	0.04
91	3.48	10.88	148.81	0.45
92	3.39	11.09	195.55	0.67
93	3.39	11.18	215.04	6.29
94	3.46	10.99	229.75	1.04
95	3.67	10.40	247.85	0.00
96	3.42	12.67	100.64	0.01
97	3.41	12.17	142.31	0.04
98	3.35	12.69	197.85	0.39
99	3.43	12.75	214.41	6.26
100	3.52	12.65	229.23	0.65
101	3.46	14.52	199.12	0.07
102	3.44	14.61	215.12	0.64
103	3.49	14.56	228.60	0.10
104	3.73	17.27	199.51	0.00
105	3.42	16.56	213.75	0.05
106	4.08	7.55	88.15	0.03
107	4.32	7.61	98.05	0.04
108	4.14	7.41	134.90	0.02
109	4.05	7.90	216.34	0.00
110	4.24	7.79	240.06	0.01
111	4.20	7.68	262.82	0.08
112	4.16	8.48	86.21	0.06
113	4.41	8.68	96.81	0.08
114	4.33	9.20	150.94	0.10
115	4.48	9.62	192.63	0.04
116	4.53	9.48	215.36	0.11
117	4.41	9.33	237.58	0.51
118	4.39	8.81	254.55	0.28
119	4.54	10.66	87.98	0.01
120	4.66	10.84	97.65	0.02

Number	Significant wave height [H_{m0}]	Peak period [T_P]	Direction [°N]	Occurrence [%]
121	4.52	10.72	160.66	0.19
122	4.38	11.00	193.47	0.28
123	4.40	11.23	216.09	1.80
124	4.50	10.81	232.09	0.73
125	4.49	10.18	251.67	0.03
126	4.39	12.64	103.22	0.02
127	4.67	12.06	130.88	0.01
128	4.40	12.78	198.19	0.10
129	4.41	12.83	213.98	2.48
130	4.39	12.86	229.24	0.34
131	4.33	15.40	201.04	0.01
132	4.43	14.67	212.95	0.38
133	4.37	14.59	227.55	0.05
134	4.14	16.34	202.25	0.01
135	4.37	16.11	214.92	0.01
136	5.47	9.45	91.32	0.03
137	5.40	10.12	173.04	0.10
138	5.28	10.64	216.54	0.06
139	5.47	10.24	236.33	0.37
140	5.60	9.80	254.22	0.12
141	5.65	13.37	99.91	0.03
142	5.64	11.56	185.95	0.14
143	5.59	12.58	215.22	1.61
144	5.80	12.06	230.97	0.58
145	5.71	11.28	248.48	0.01
146	5.49	15.29	200.28	0.02
147	5.66	14.81	215.63	0.31
148	5.91	14.57	226.47	0.03
149	7.33	11.78	232.06	0.07
150	7.69	13.99	219.72	0.17